STUDY OF STRUCTURAL AND MAGNETIC PROPERTIES OF NANOCRYSTALLINE $(Fe_{0.95}Co_{0.05})_{73.5}Cu_1Nb_3Si_{13.5}B_9$ ALLOY

By

Ratan Krishna Howlader
Roll No: 0955551
Session: July-2009

A THESIS SUBMITED TO THE DEPARTMENT OF PHYSICS, KHULNA UNIVERSITY OF ENGINEERING & TECHNOLOGY, KHULNA- 9203 IN PARTIAL FULFILMENT OF THE REQUIRMENT FOR THE DEGREE OF MASTER OF PHILOSOPHY
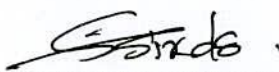
DEPARTMENT OF PHYSICS
KHULNA UNIVERSITY OF ENGINEERING & TECHNOLOGY
KHULNA - 9203, BANGLADESH
SEPTEMBER- 2013

DECLARATION

This is to certify that the thesis work entitled as **"Study of Structural and Magnetic Properties of Nanocrystalline $(Fe_{0.95}Co_{0.05})_{73.5}Cu_1Nb_3Si_{13.5}B_9$ Alloy"** has been carried out in partial fulfillment of the requirement for M. Phil. Degree in the Department of Physics, Khulna University of Engineering & Technology, Khulna-9203, Bangladesh. The above research work or any part of this work has not been submitted to anywhere for the award of any degree or diploma. No other person's work has been used without due acknowledgement.
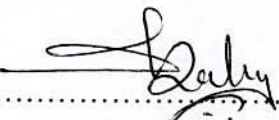
1. Supervisor

Candidate

....

....

Prof. Dr. Shibendra Shekher Sikder

Ratan Krishna Howlader

2. Co-supervisor

....

Dr. Dilip Kumar Saha

KHULNA UNIVERSITY OF ENGINEERING & TECHNOLOGY
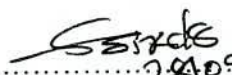**DEPARTMENT OF PHYSICS**

Approval

This is to certify that the thesis work submitted by *Ratan Krishna Howlader* entitled *"Study of Structural and Magnetic Properties of Nanocrystalline $(Fe_{0.95}Co_{0.05})_{73.5}Cu_1Nb_3Si_{13.5}B_9$ Alloy"* has been accepted by the board of examiners for the partial fulfillment of the requirements for the degree of *Master of Philosophy* in the Department of *Physics*, Khulna University of Engineering & Technology, Khulna, Bangladesh in 28 September 2013.

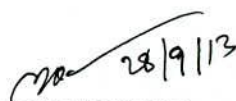**Board of Examiners**

Sl. No.	Name, Designation & Address	
1.	Prof Dr. Shibendra Shekher Sikder Department of Physics Khulna University of Engineering & Technology	Chairman & Supervisor
2.	Dr. Dilip Kumar Saha Chief Scientific Officer Materials Science Division Atomic Energy Centre, Shahbag Dhaka -1000, Bangladesh	Co-Supervisor & Member
3.	Head Department of Physics Khulna University of Engineering & Technology Khulna 9203	Member
4.	Prof Dr. Md. Abdullah Elias Akhter Department of Physics Khulna University of Engineering & Technology Khulna 9203	Member
5.	Prof. Dr.Md. Abu Hashan Bhuiyan Department of Physics Bangladesh University of Engineering & Technology Dhaka -1000	Member (External)

To

My PARENTS

Acknowledgements

ABSTRACT

This thesis is based on the experimental investigation of nanocrystal formation from FINEMET type of amorphous ribbons subjected to controlled thermal treatment and evolution of unique soft magnetic properties that are microstructure dependent. Amorphous ribbon of composition $(Fe_{0.95}Co_{0.05})_{73.5}Cu_1Nb_3Si_{13.5}B_9$ was prepared by rapid quenching method at wheel speed of 25m/s in an Ar atmosphere. The alloy has been annealed in a controlled way in the temperature range of $550°C$ to $750°C$ for 30 minutes. Crystallization onset temperature for FeCo(Si) phase was found around $550°C$. Thermal analysis experiment and from the obtained data, the activation energy was calculated to be 2.40eV. Nanocrystalline state was evaluated by X-ray diffraction. In the range of optimizing annealing temperature $550°C$ to $750°C$ the grain size has been obtained in the range of 9 – 26nm. Temperature and frequency dependence of permeability of amorphous and devitrified toroid shaped samples have been measured. The initial permeability for the optimum annealed samples has been found to 5.8×10^3 and the highest value of quality factor is found for the sample annealed at $550°C$; which also indicates the best heat treatment temperature to obtain the highest value of quality factor.

It is notable that the addition of Co has significant effects on enhancement of Curie temperature (T_c). In the as-prepared condition the T_c has been found to be $422°C$, which is quite high compared to the T_c of conventional FINEMET (i.e. sample without Co), which is $354°C$. As the nanocrystalline phase appeared, it was found that at and above the crystallization temperature, T_c of the residual amorphous phase gradually decreases with the increase of annealing temperature. This is because the amorphous matrix is depleted with Fe and relative amount of Nb in the amorphous matrix increases, which weakens the exchange interaction resulting in reduction of T_c. The high permeability of the optimum nanocrystallized sample has been achieved due to drastic of effective anisotropy resulting from nanometric grain size effect and strong magnetic coupling. The results show that amounts of Cu and Nb are very important for the soft magnetic properties of FINEMET alloys.

List of Symbols

a_0	=	Lattice parameter
B	=	Magnetic induction
D_g	=	Grain size
DTA	=	Differential Thermal Analysis
DSC	=	Differential Scanning Calorimetry
d	=	Average diameter
FWHM	=	Full Width at Half Maximum
H	=	Magnetic field
H_c	=	Coercivity
H_a	=	Applied magnetic field
[hkl]	=	Miller Indices
k	=	Magnetic hardness parameter
K_{eff}	=	Effective magnetic anisotropy constant
L	=	Self inductance of the sample core
L_0	=	Inductance of the winding coil without sample
L_{ex}	=	Ferromagnetic exchange length
M	=	Magnetization
M_s	=	Saturation magnetization
nm	=	nano meter
NM	=	Nobel metal
RAM	=	Random anisotropy model
TTT	=	Temperature, time & transformation
T_a	=	Annealing temperature
T_c	=	Curie temperature
T_g	=	Glass transition temperature
T_x	=	Crystallization temperature
T_m	=	Melting point
T_{x_1}	=	Primary crystallization temperature

T_{x_2}	=	Secondary crystallization temperature
T_{p_1}	=	Primary crystallization peak temperature
T_{p_2}	=	Secondary crystallization peak temperature
$\tan\delta$	=	Loss factor or loss tangent
VSM	=	Vibrating Sample Magnetometer
XRD	=	X-ray diffraction
μ	=	Permeability
μ_i	=	Initial permeability
μ'	=	Real part of the complex permeability
μ''	=	Imaginary part of the complex permeability
μ_m	=	Maximum permeability
μ_o	=	Vacuum magnetic permeability
λ	=	Wave length
θ	=	Scattering angle
t_o	=	Time constant
β	=	Heating rate
ρ	=	Electric Resistivity
ω	=	Frequency
σ	=	Effective stress
Q	=	$1/\tan\delta$ (quality factor)
$\mu'*Q$	=	Relative quality factor
$<K>$	=	Average anisotropy
T_c^{am}	=	Curie temperature of residual amorphous matrix
$|Y|$	=	Absolute value of admittance
$|Z|$	=	Absolute value of impedance
ΔH	=	Enthalpy of crystallization

Contents

CHAPTER-I   INTRODUCTION

CHAPTER-II   PREPARATION OF NANOCRYSTALLINE ALLOY

CHAPTER-III   THEORETICAL BACKGROUND

CHAPTER-IV   EXPERIMENTAL DETAILS

CHAPTER-V   **RESULTS AND DISCUSSION**

List of Figures

CHAPTER- V

List of Tables

CHAPTER - I
Introduction

Chapter –I Introduction

1.1   Introduction

Magnetic materials played a prominent role in the discovery of new civilizations and also development of modern technology. Over the past several decades, amorphous and more recently nanocrystalline materials have been investigated for applications in magnetic devices requiring magnetically soft materials such as transformer, inductive devices, etc. Most recently, research interest in nanocrystalline soft magnetic alloys has dramatically increased. Soft magnetic materials face demanding requirements from new, high performance electronic and power distribution systems. The new systems must operate in high temperature and high frequency regions that are inaccessible to conventional crystalline and amorphous magnetic materials. The need for increased energy efficiency requires reduced power loss from inductive component. All magnetic elements in the pure form are soft; whereas magnetic solid solutions and compounds can be either soft or hard. The distinguishing characteristic of the first type is high permeability which as usual, is accompanied by low coercivity. It is flux multiplying power of the magnetically soft materials that fits them for their jobs in machine and devices.

Nanocrystalline materials designate a novel type of interface controlled solids that are characterized by a structural modulation on the length scale of several nanometers. Nowadays, the attempts to understand different properties of materials on a smaller an smaller length scale are making footsteps for development of research in many areas of materials science. With the reduction of size into nanometer range, the materials exhibit interesting properties including physical, chemical, mechanical, magnetic and electrical, comparing to conventional coarse grained counterparts. This new field based on nano materials has been named as 'Nanotechnology' and emerged as a new branch of science and technology. Research interest in the study of soft magnetic nano structured materials synthesis and characterization techniques and the realization that these materials exhibit may unique and interesting physical, optical, magnetic and chemical properties with a number of potential technological applications [1.1-1.6]. Nanocrystalline soft magnetic

materials were first reported in 1988 by Yoshizawa et. al. [1.7] through controlled crystallization of Fe-Si-B amorphous alloys with the addition of Copper(Cu) and Niobium (Nb). The material was cast as an amorphous ribbon by rapid solidification. Exploitation of this novel material in practical applications started shortly after the discovery and manufactured by Hitachi Co. Ltd. under the trade names FINEMET [1.8] and VITROPERM [1.9]. The originally proposed composition was $Fe_{73.5}Cu_1Nb_3Si_{13.5}B_9$.

The development of nanocrystalline Fe-Si-B-Nb-Cu alloys [1.7] commercially known as FINEMET, established a new approach to develop soft magnetic materials with high magnetic flux density, that is magnetocrystalline anisotropy can be reduced by refining the grain is less than few tense of nanometers [1.10-1.11]. The nanocrystalline state is achieved by subsequent heat treatment from their as cast amorphous precursor above the primary crystallization temperature. It is characterized by a homogeneous ultra fine grain structure of bcc Fe-Si with grain sizes, D_g of typically 10 to 15 nm and random orientation, embedded in an amorphous minority matrix.

Nanocrystalline soft magnetic materials constitute a new class of condensed matter having interesting properties, which are mostly microstructure dependent. These materials are first formed into amorphous ribbons and than annealed above the crystallization temperature to form the nanocrystalline microstructure that consists of bcc Fe(Si) nano grains embedded on amorphous matrix. Excellent soft magnetic properties can be found in these nanocrystalline materials obtained by the controlled crystallization of Fe-Si-B amorphous ribbons containing Cu and Nb. The addition of Cu and Nb results in the formation of an ultra fine grain structure. Cu is used as nucleating agent for the growth of nanocrystals while Nb for inhibiting their growth. Therefore, the appropriate amount of Cu and Nb are very important for controlling the crystallization behavior of FINEMET type amorphous alloys. Instead of Nb other refractory elements such as Ta, Mo may be used [1.12], while Au and Ag can be used for Cu [1.13-1.14]. Crystallization behavior and grain size are very much correlated with the magnetic properties.

Hakim et. al. [1.13] and Manjura Hoque et. al. [1.15] found that magnetic initial permeability and naocrystalline/amorphous ribbon strongly depends on annealing temperature and exhibits super ferromagnetic behavior at $T > T_c^{am}$, when $T > T_c^{am}$ the grain coupling is largely but no completely interrupted above T_c^{am} and still persists to higher value of permeability compared to annealed temperature at $T > T_c^{am}$ exhibiting the magnetic coupling between particles is significant. The precise coupling mechanism for this type of behavior at $T > T_c^{am}$ may be explained in terms of exchange penetration through thin paramagnetic inter granular layer and /or dipolar interaction. Crystallization behavior and grain size are very much correlated with the magnetic properties. The soft magnetic properties of nanomaterials are connected with size, distribution of the nano metric grains, their composition, inter faces of constituent phases vanishing magnetic anisotropy ($\langle k \rangle \approx 0$), vanishing magnetostriction ($\langle \lambda \rangle \approx 0$), strong inter grain magnetic coupling and reduced magneto elastic energy. The theoretical understanding of the nano metric grain with magnetic softness has been consolidating in the light of Random Anisotropy Model (RAM) proposed by Albens et. al. [1.16] and subsequently developed by Herzer [1.12].

Continuing efforts to improve the soft magnetic properties of FINEMET alloy have been made of modifying the alloy compositions. M. Ohnuma et. al [1.17] reported that the substitution of Fe by Co decreases the saturation magnetostriction in FINEMET type amorphous alloys. The magneto crystalline anisotropy of the small randomly oriented grains is averaged out of exchange interaction. To investigate the effect of Cu and Co on the micro structural evolution from (FeCo)-Si-B-Nb-Cu amorphous alloys to optimize the nano crystalline micro structure for obtaining good soft magnetic properties in Co containing FINEMET type alloys. The aim of the present work is to study of low coercivity in Co replaced FINEMET type alloys to improve the high frequency performance of Fe-based nanocrystalline soft magnetic materials. To investigate the micro structural evolution by the crystallization $(Fe_{0.95}Co_{0.05})_{73.5}Cu_1Nb_3Si_{13.5}B_9$ melt spun amorphous ribbons. In this work to understand the mechanism of the formation of

3

nanocrystals, size of the nanocrystals their volume fraction along with the effect on the magnetic properties through controlled thermal treatment.

1.2   The Aim and Objectives of the Present Work

The main objective of the present work is to study of the evaluation of the nanocrystallite by heat treatment and the concomitant development of microstructural and magnetic properties of $(Fe_{0.95}Co_{0.05})_{73.5}Cu_1Nb_3Si_{13.5}B_9$ amorphous alloy.

The objectives of the research works are as follows:

- Synthesis of the FINEMET alloys in the form of the ribbon with varying amount of Cu and Nb in the amorphous state rapid solidification technique.
- Growth of nano crystals on amorphous matrix by thermal treatment.
- Characterization of nano structured phases such as the size of the nanograins, composition of the nanograins and the volume of the nanograin.
- Correlation of the evaluation of nanograins with the magnetic properties.
- Optimization of annealing temperature corresponding to the good magnetic properties.
- Explain the results using existing theoretical models in the literature.

1.3   Experimental reason for Choosing this Research Work

In the present work, soft magnetic amorphous FINEMET type alloy nominal compositions of $(Fe_{0.95}Co_{0.05})_{73.5}Cu_1Nb_3Si_{13.5}B_9$ synthesized by a melt spinning technique is reported.

To improve the magnetic properties of these amorphous ribbons, microstructure is an important parameter that can be controlled by heat treatment condition. Also one effective way of preparing nanocryastalline alloy via the amorphous state of material is

4

an appropriate heat treatment that has been found leading to two phase crystallization. The nanostructures arte often obtained primary crystallization. As a consequence, the aim of current evolution as a function of heat treatment temperature.

As the composition of a primary crystal differs from that of an amorphous matrix, the process of crystal growth becomes diffusion controlled. In order to control the growth process of nanostructured alloys, it is important to investigate the kinetics of crystallization. The crystallization of these metallic glasses enables the study of both nucleation and growth process. Thus the main ambition of this thesis is to present techniques and models to observe and describe the kinetics of solid phase transformation taking place on the nano scale, i.e., a study of nanocrystallization which promotes the evolution of superior soft magnetic properties in the studied composition.

In this research work the kinetics of crystallization of amorphous FINEMET type alloys were investigated by the use of Differential Thermal Analysis (DTA) and X-ray diffraction (XRD) techniques. The combination of these two techniques is necessary for the complete description of the processes occurring during the nanocrystallization from amorphous precursors as well as microstructural evolution in FINEMET type alloys in its crystalline state. Results will aid in interpreting the effect of heat treatment on magnetic properties and application of this type of alloys. Optimum annealing temperature would be ascertained through isothermal annealing over a wide range of temperature. All the annealing heat treatments would be performed in evaluated quartz tube in conjunction with a microprocessor controlled muffle furnace. Finally, magnetic properties were studied by using an Impedance Analyzer.

The Curie temperature has been determined by permeability versus temperature measurement with the help of a oven using a LCR meter. Permeability, magnetic loss factor and relative quality factor as a function of frequency and annealed temperature has been determined using an impedance analyzer. Hysteresis parameters have been determined by B-H loop tracer. Magnetization of the samples has been measured as a function of field and temperature using Vibration Sample Magnetometer (VSM).

5

It can be observed that in this composition Fe has been partially replaced by Co as comparing to original FINEMET alloy of the composition $(Fe_{0.95}Co_{0.05})_{73.5}Cu_1Nb_3Si_{13.5}B_9$. Co is well known for its anisotropy effect which would play an important role on both structural and magnetic phase transition temperature. It may be mentioned that magnetocrystalline anisotropy constant k_1 of Co is $4.3 \times 10^5 J/m^3$ whereas that of Fe as $-4.5 \times 10^3 J/m^3$. Higher value of magnetocrystalline anisotropy constant of Co shows that the presence of Co in the alloy system would give rise to frequency stability of permeability compared to original FINEMET which will increase the resonance frequency to higher value. Further, Curie temperature of Fe and Co is 770^0C and 1127^0C, respectively. Replacement of Co for Fe would enhance the Curie temperature because of the much higher magnetocrystalline anisotropy of Co which increases thermal stability of this type of alloy from application point of view.

The main study of the present work are the synthesis Fe-based nanocrystalline alloys of the above mentioned composition in the amorphous states by using rapid solidification technique and their magnetic properties with the evolution of different phases by varying annealing conditions. Finally it is shown how this material of this kind may be realized technologically and that its magnetic behavior corresponds entirely to the prediction of the theory.

1.4   Review of Researches on FINEMET

This review is intended to summarize recent developments in the synthesis, structural characterization, properties and applications of nanocrystalline and amorphous magnets. The term "Nanocrystalline alloy" will be used for these alloys that have a majority of grain diameters in the typical range form $\approx$ 1-50nm. This term will include alloys made by rapid solidification, deposition and solid state reaction methods where the initial materials may be in the amorphous state and subsequently crystallized. We consider processing routes and method to control chemistry and microstructural morphology on increasing smaller length scales and various developing experimental techniques which allow more accurate and quantitative probes of structure including

6

magnetic domain structure on smaller length scales. The impact of microstructural control on the development of state of the art soft magnetic materials.

The Extended X-ray Absorption Fine Structure (EXAFS) technique has been successfully used to support the role of Cu as nucleation sites in the nanocrystallization process in FINEMET alloys. Early papers by Yoshizawa et. al. [1.7] cited the reduction of the crystallization temperature of the α-FeB phase due to the Cu addition, but failed to show direct evidence of their hypothesis that the Cu provided heterogeneous nucleation sites. Later, Hono et. al. [1.18] showed by atom probe field in microscopy that Cu clusters formed in these alloys at very short annealing times, and concluded that the Fe-based nanocrystals formed in the regions away from the Cu rich clusters. Although the technique started to show the early development of the nanocrystalline microstructure, the probe of the local short range order of Cu-rich nanoparticle was only possible with the EXAFS technique. EXAFS was first used by Kim et. al. [1.19] to discover that Cu-rich particle, were FCC and formed at temperature much lower than the crystallization of the α-FeSi phase. Another effort by Ayers et. al. [1.20] showed the formation of the Cu-rich phase during the early stages of the heat treatment and evidence of FCC Cu formation in the as spun alloy. These studies were followed by a set of experiments performed by Ayers et. al. [1.21] that led to the development of a model, for the formation of the nanocrystalline microstructure in the FINEMET alloys.

A new class of Fe-based alloys was introduced by Yoshizawa, Orgume and Yamauchi, 1988 which exhibited superior soft magnetic behavior. The material was produced by crystallization of an amorphous Fe-Si-B alloy with small addition of Cu and Nb. The identifying characteristics of the new material are its ultrafine microstructure of BCC Fe-Si withgrain sizes of 10-15 nm from which their soft magnetic properties emerge. These include coercivities of 0.01Oe and permeabilities of $\approx 10^5$. The pioneer alloy composition $Fe_{73.5}Cu_1Nb_3Si_{13.5}B_9$ known as FINEMET, has been thoroughly studied due to its novel magnetic properties. Yoshizawa et. al. [1.22] and Noh et. al. [1.23 – 1.24], studied the effect of Cu on the crystallization behavior in $Fe_{74.5-x}Cu_xNb_3Si_{13.5}B_9$ for x = 0 and x = 1. The crystallization behavior of this x = 0 alloy is quite different and leads to a severe degradation of the soft magnetic properties compared to the original

amorphous state. They also found that the average grain size just after the onset of crystallization is relatively large up to about 60 nm with a broad scatter and show a distinct variation with the annealing temperature. This indicates the significantly lower nucleation rate than in the Cu-doped alloy whose finer grain size is almost constant in a wide range of annealing temperature [1.25].

One the important features of FINEMET system is that one can play with different compositions, annealing temperatures and time to control the grain size and their distribution upon which the magnetic properties of these new materials strongly depend. In choosing the composition one has to consider the magnetic components like Fe, Co, Ni etc., the crystallization component eg. Cu and the component Nb for stabilizing the nanocrystal growth by inhibiting the grain growth and glass forming materials like Si, C, B etc. Amorphous ferromagnetic material based on Fe-Si-B show good magnetic properties when they are heat treated below their crystallization temperature while the Fe-Cu-Nb-Si-B alloys exhibit extraordinary high permeability, two orders of magnitude higher than their conventional Fe-Si-B alloys due to heat treatment just above the crystallization temperature for a specific time. The great scope of technical applications this material $Fe_{73.5}Cu_1Nb_3Si_{13.5}B_9$ arise from this freedom of tailoring the magnetic properties [1.26-1.29]

Miller et. al. [1.30] showed that like Nb, the atomic volume of refractory elements (group V or VI elements Cr, V, Mo, W or Ta) are larger than that of Fe that reduces diffusion co-efficient and thus, stabilizes the amorphous matrix and shows down the kinetics of grain coarsening. The efficiency of these elements for grain size refinement increases in the order of their atomic volumes i.e. Cr < V < Mo ≈ W < Nb ≈ Ta. Thus, finest grain structures and superior magnetic properties require a certain amounts of elements Nb and Ta. Inoue et. al. [1.31] observed that group IVa to Via transition metals extends the glass forming range a low Si or B contents. The glass forming range is the widest for if containing alloys and decreases in the order Zr > Nb ≈ Ta > Mo ≈ W > V > Cr. According to Suzuki et. al. [1.32-1.33] the glass forming ability is considerably improved with the addition of Hf or Zr.

8

Alben et. al.[1.32] and Sava et. al. [1.33] worked on the relation of grain size and domain wall width. If grain size exceeds the domain wall width, domains can be formed within the grains and the coercive field, H_c is found to depend on the grain size, D_g as $H_c \propto D_g^6$. Butinno et. al. [1.35] studied the effect of annealing temperature on H_c. Due to stress produced during the quenching process the as-quenched metallic glasses always have anisotropy. Anisotropy is averaged out after annealing because annealing can relative stress and causes reduction of H_c. Hence annealing makes the amorphous ferromagnet a magnetically soft material.

Herzer [1.36] studied on Curie temperature and permeability of nanocrystalline material. According to his when measuring temperature approaches the Curie point of the inter granular amorphous phase, the exchange coupling between the crystallites is largely reduced. As a result, the initial permeability drops down. As reported by Hakim et. al. [1.13] magnetic initial permeability of nanocrystalline amorphous ribbon strongly depends on annealing temperature and exhibits super paramagnetic behavior at $T > T_c$. Iranco et. al. [1.37] also studied the super paramagnetic relaxation in FINEMET type of alloy Fe-CU-Nb-Si-B without adding any extra refractory element and they have demonstrated that this behavior is a general characteristics of this nanocrystalline alloys provided the volume fraction of crystallites are very low. If the size of the nanocrystals is small enough and inter granular amorphous matrix is sufficiently thick to minimize the magnetic interactions between them, the super paramagnetic behavior of the nanocrystalline particles is expected.

There have been done so many researches on various effect of replacement of Co for Fe as late transitional metal element. The research on Co substituted Fe-Nb-Ta-Mo-B amorphous alloys [1.38] showed that Co substitution increased saturation magnetization and Curie temperature of the amorphous phase and decreased coercivity. The desire for large magnetic induction typically limits choices to alloys of Fe and Co (the elemental transition metal magnets with the largest atomic dipole moments). Curie temperatures are also largest for elemental Fe(770^0C) and Co(1100^0C), suggesting the use of Fe or Co (or Fe-Co) alloys especially in high temperature applications. Many important soft magnetic alloy systems have zero crossing of the magnetocrystalline anisotropy or

magnetostriction coefficients, which can be exploited in the development of soft magnetic materials. The development of advanced and newer magnetic materials with enhanced properties is closely related to the fundamental understanding and exploitation of influence of microstructures on the extrinsic magnetic properties.

1.5   Organization of the Thesis

The Thesis has been divided into five chapter:

Chapter-I presents a brief introduction of Ni-Cu-Zn ferrite and organization of the thesis.

Chapter-II briefly describes the theories necessary to understand the present work.

Chapter-III enunciates with the detail experimental process related to this research work.

Chapter-IV describes the results and discussion about the optimization of Fe deficiency in $(Ni_{0.8} Cu_{0.10}Zn_{0.62}O)(Fe_2O_3)_{1-x}$ ferrites.

Chapter-V contains the concluding remarks.

Finally a complete list of references has been given towards the end of the chapters.

Chapter - II

Preparation of Nanocrystalline Alloy

Chapter-II Preparation of Nanocrystalline Alloy

2.1 Composition of the Nanocrystalline

The study of metallic glasses dates back to the pioneering work of Pol Duwez at Caltech in the 1950s. Duwez employed atomization [2.1] prior to splat quenching [2.2-2.4]. Ferromagnetic amorphous alloy were first reported by Mader and Nowik [2.5]. Soon after, Tsuei and Duwez [2.6] reported splat quenched amorphous ferromagnetic with interesting soft magnetic properties. Generally the optimum and magnetic properties of nanocrystalline soft magnetic materials are obtained for partially crystallized materials. This means that those materials are formed in two phases. In general, nanocrystalline alloys can be described as $TL_{1-x}(TE, M, NM)_x$ where

- TL denotes a late ferromagnetic transition metal element (TL = Co, Ni or Fe).
- TE denotes an early transition metal element (TE = Zr, Nb, Hf, Ta etc.)
- M is a metalloid (M = B, P, Si etc) and
- NM is a noble metal (NM = Cu, Ag, Au etc)

This composition usually has $x < 0.02$ i.e. with as much late ferromagnetic transition metals (TL of Co, Ni or Fe) as possible. The remaining early transition metals (TE = Zr, Nb, Hf, Ta etc) and metalloids (M = B, P, Si etc) are added to promote glass formation in the precursor. The noble metal element (NM = Cu, Ag, Au etc) serve as nucleating agents for the ferromagnetic nanocrystalline phase. The compositions are limited by where glass formation can occur prior to the nanocrystallization route. These alloys may be single phase (Type-I) but are generally two phase materials with a nanocrystalline ferromagnetic phase and a residual amorphous phase at the grain boundaries (Type-II).

The type-II nanocrystalline alloys might have general properties:
- relatively high resistivity (50-80 $\mu\Omega$-cm)
- low magnetocrystalline anisotropy and

11

- increased mechanical strength.

With properties such as these, nanocrystalline alloys have great potential as soft magnetic properties. In the ongoing research we are any interested about the second type.

One the important feature of this magnetic system is that one can play with different compositions, annealing temperature and time to control the grain size and their distribution upon which the magnetic properties of these new materials strongly depend. In choosing the composition, one has to consider the magnetic component like Fe, Co, Ni etc the crystallization component e.g. Cu and the component Nb for stabilizing the nanocrystal growth by inhibiting the grain growth and glass forming material like Si, Cu, B etc.

Nanocrystalline soft magnetic alloys have received considerable attention due to their excellent soft magnetic properties [2.7]. Small addition of Cu and Nb into Fe-Si-B amorphous materials changes considerably their crystallization process, which is executed under appropriately controlled conditions and the specific purpose of these addition are

- The element is used for helping the formation of nuclei of ultra fine grains and
- The element is used to impede the growth of the crystallites.

In this material, the nanocrystalline state is composed of a fine structure of α-Fe(Si) and is usually around 10 nm. For such an average grain size the exchange interaction dominates the magnetic behavior of randomly oriented crystallites guided by random anisotropy [2.8].

2.2   An Overview of Nanocrystalline Materials

Nanocrystalline amorphous ribbon can be considered as an off shoot of amorphous materials. In fact nanocrystalline amorphous ribbon is a composite material where nanocrystals are embedded in an amorphous matrix. Nanocrystalline materials

12

represent one of the most active research areas in recent time for the atomic tailoring of materials with specific properties and property combinations. However, it is still in its infancy since its emergence as potential materials has just began at this stage of development. There have been glimpse of exciting new properties like superplasticity, giant magnetoresistance (GMR), transparency in opaque ceramics, enhanced homogeneity, unusal soft ferromagnetic and giant magnetocaloric effects, possessed by material where reduced to nanometer dimension. In addition to the understanding of the usual properties possessed by nano phase materials there are three other associated areas, which need serious attention:

(i)   Identification and development of suitable preparation methods, especially those which are capable of providing large industrial quantities of nanometer scale materials.

(ii) Development of processing methods for manufacturing these materials into useful size and shapes without losing there desirable nanometer size feature and

(iii) Identification of proper characterization methods, where the nanometer size range of these materials fall just below or at the resolution limit of the conventional tools.

2.3 Alloy Design Issues

Alloy design issues include issues of chemistry and processing designed to (i) optimize one of a number of important intrinsic and or extrinsic magnetic properties as well as to (ii) optimize structural or microstructural features which promote important magnetic properties. The first of these issues concerns the choice of chemistry to impact the intrinsic magnetization of the material. The second issue pertinent to alloy additions designed at aiding formation of an amorphous phase.

As intrinsic properties we take to mean microstructure insensitive properties including the saturation magnetization, Curie temperature, magnetocrystalline anisotropy and magnetostrictive coefficients are all important. Also it includes magnetic dipole

moment and exchange interaction. Extrinsic magnetic properties important in softmagnetic materials include the magnetic permeability and coercivity, which typically have an inverse relationship. Also induced magnetic anisotropy and magnetic coupling through amorphous phases are included to these properties. Magnetic anisotropy and magnetostriction can be considered as extrinsic (microstructure sensitive) in the sense that for a two phase material (in aggregate) they depend on microstructure.
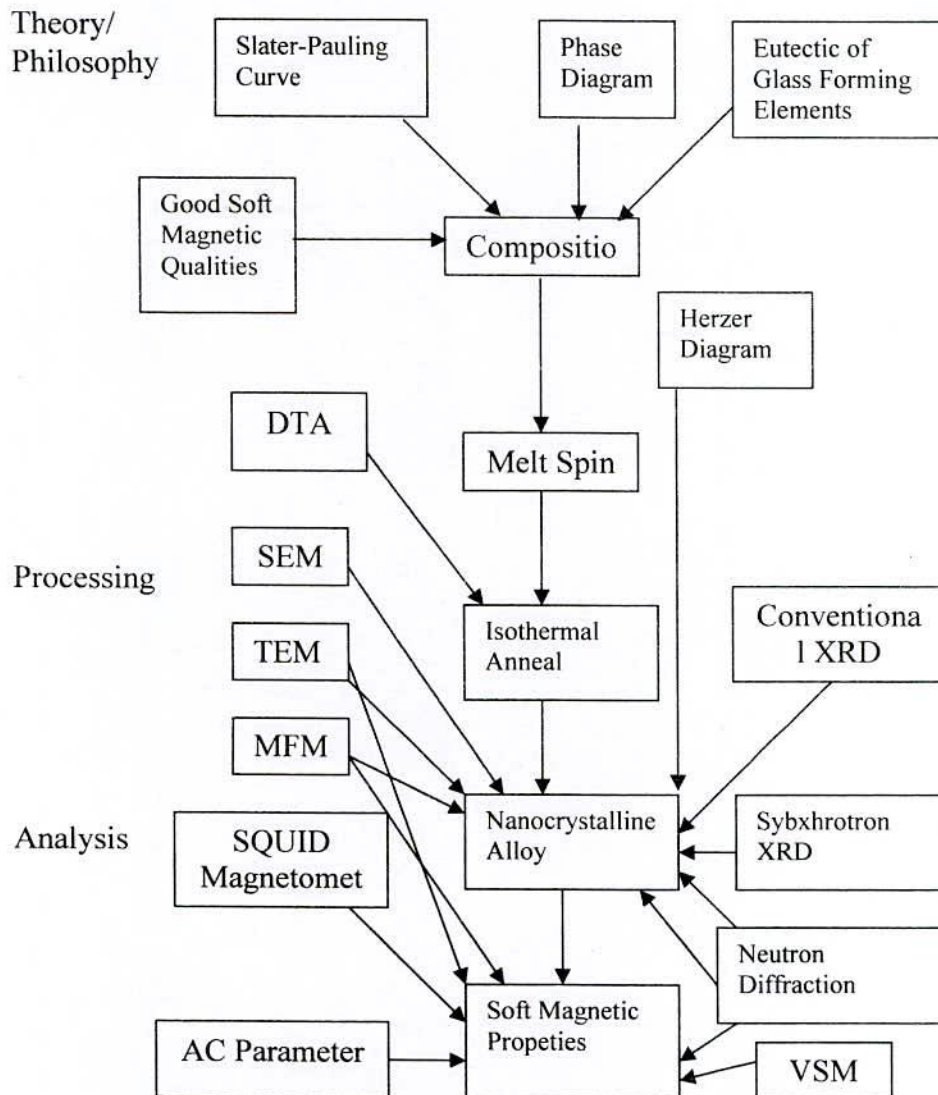
Fig. 2.1 Flow chart for the consideration in designing and developing a nanocrystalline soft magnetic material from an amorphous precursor route

14

Since microstructure of alloy influence extrinsic magnetic properties, the important microstructure features should be recognized including grain size, shape and orientation, defect concentrations, compositional inhomogeneties, magnetic domains and domain walls. The development of soft magnetic materials for applications requires attention to a variety of intrinsic magnetic properties as well as development of extrinsic magnetic properties through an appropriate optimization of the microstructure.

Alloy design issues are in many ways influenced by the processing routes used to achieve desired microstructures. Fig-2.1 illustrates a flowchart for the considerations in designing and developing a nanocrystalline soft magnetic material from an amorphous precursor route as one example of the design process. Here, we consider first the effects of alloy composition on intrinsic magnetic properties. This is followed by consideration of alloying additions necessary to produce an appropriate amorphous precursor. Typical experimental steps used to identify the structure and properties of the resulting materials are also illustrated.

2.4   Stages of Evolution of Microstructure

A typical nanocrystalline structure with good soft magnetic properties occurs if the amorphous state is crystallized provided the primary crystallization of bcc Fe takes place prior to the formation of secondary inter metallic phases like Fe-B. Both an extremely high nucleation rate and slow growth of the crystalline precipitates are needed in order to obtain a nanoscaled microstructure. Such crystallization characteristic seems to be rather an exception case than the conventional rule. Thus, crystallization of conventional metallic glasses optimized for soft magnetic applications usually yield a relatively coarse grained microstructure of several crystalline phases and correspondingly, deteriorates the soft magnetic properties.

It has been established that controlled crystallization of the amorphous alloys in the form of their ribbons prepared by rapid solidification technique using melt-spinning machine appeared to be the most suitable method available until now to synthesize

nanocrystalline alloys with attractive soft magnetic properties. The basic principle for the crystallization method from amorphous solids is to control the crystallization kinetics by optimizing the heat treatment conditions such as annealing temperature and time, heating rate, etc. The nanocrystalline microstructure and the accompanying soft magnetic properties are rather insensitive to the precise annealing conditions within a wide range of annealing temperature $T_a \approx 525\text{-}580^0C$. They develop in a relatively short period of time (about 10-15 minutes) and do not much latter even after prolonged heat treatment of several hours [2.9]. A typical heat treatment like T_a at 540^0C in most cases yields a nanocrystalline microstructure to the the Quasi-equilibrium State and characteristic for the individual alloy composition.

Only annealing at more elevated temperature above about 600°C leads to the precipitations of small fractions of boride compounds like Fe_2B or Fe_3B with typical dimensions of 50 nm to 100 nm, while the ultra fine grain structure of bcc Fe-Si still persists. Further increase of the annealing temperature above about 700°C finally yields grain coarsening. Both the formation of Fe borides and grain coarsening deteriorates the soft magnetic properties significantly. The evolution of microstructure during annealing is depicted schematically in Fig. 2.2 and summarized as follows according to Hono *et al.* [2.10-2.11].

The formation of the particular nanocrystalline structure is essentially related to the combined addition of Cu and Nb (or other group IV or VI elements) and their low solubility in bcc grains while Nb impedes grain coarsening and at the same time, inhibits the formation of boride compounds. The microstructure evolution is schematically illustrated in Fig.-2.2 can be summarized as follows:

Annealing at temperatures in general between about 500°C to 600°C leads to primary crystallization of the bcc Fe. At the initial stage of annealing, before the onset of crystallization, the phase separation tendency between Cu and Fe leads to the formation of Cu-rich clusters, with 5 nm size and probably still amorphous [2.12, 2.10]. The presence of Nb seems to promote the formation of these Cu-rich clusters on a much finer scale than in an Nb free alloy composition [2.13].
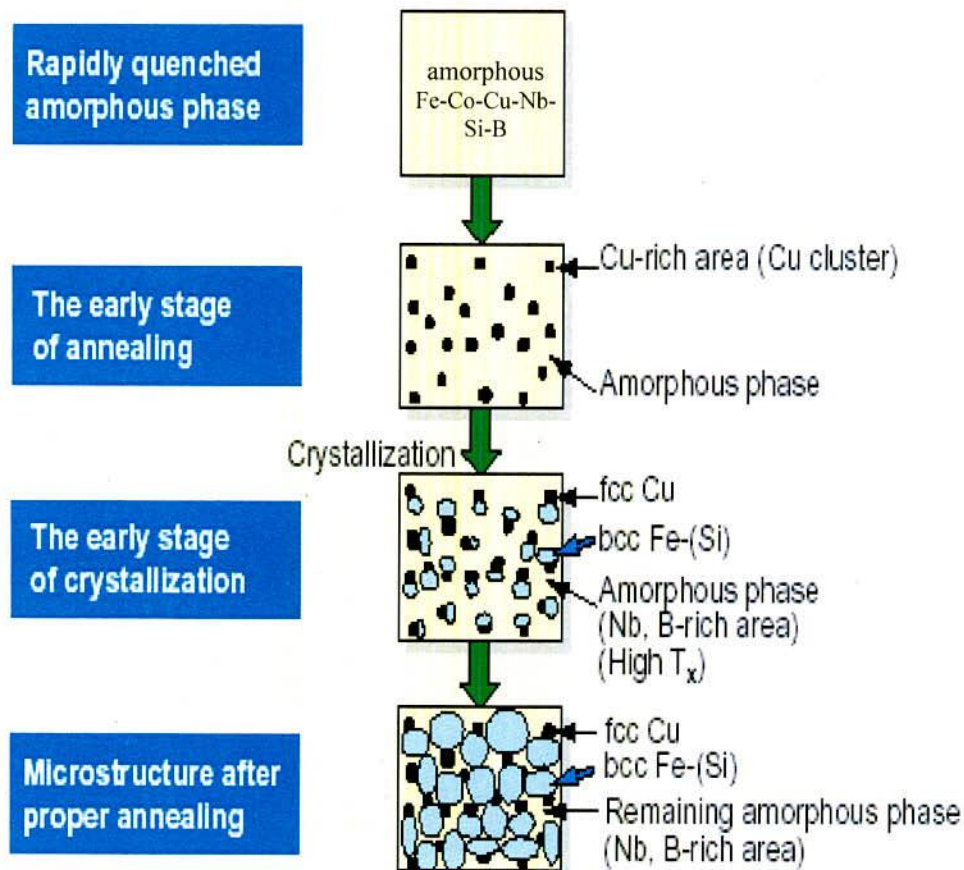
Fig. 2.2 Schematic illustration of the formation of the nanocrystalline structure in Fe-Cu-Nb-Si-B alloys

This is cluster formation cause a concentration fluctuation of Fe, since Cu substitutes for Fe. Thus the regions in between Cu-rich clusters provide a significantly increased density of nucleation sites for the crystallization of bcc Fe. The consequence is an extremely fine nucleation of bcc Fe-Si crystallites at a high rate which subsequently grow in a diffusion controlled process [2.14] as the annealing proceeds further.

17

As the bcc Fe-Si phases forms Nb and B are excluded from the crystallites because of their low solubility in bcc Fe-Si and are enriched in the residual amorphous matrix. At the same time ass Si effectively tends to be partitioned into the bcc Fe-Si phase [2.15, 2.12]. The enrichment with B and in particular, with Nb increasingly stabilizes the residual amorphous matrix and thus hinders coursing of bcc grains. The presence of Nb at the same time inhibits the formation of Fe-B compounds. The transformation finally cases in a metastable two phase microstructure of bcc Fe-Si embedded in an amorphous Fe-Co-Nb-B matrix.

The resulting microstructure is characterized by randomly oriented ultrfine grains of bcc Fe-Si (20at.%) with typical grain sizes of 10-15 nm immersed in a residual amorphous matrix which occupies about 20-30% of the volume and separates crystallites at a distance of about 1-2 nm. These features are basis for the excellent soft magnetic properties indicated by the high values of initial permeability of about 10^5 correspondingly low coercivities of less than 1A/m. A characteristic feature is that nanocrystalline microstructure and the accompanying soft magnetic properties are rather insensitive to the precise annealing conditions within a wide range of annealing temperature, T_a, of about $\Delta T_a \approx 50 - 100°C$.

They develop in a relatively short period of time and do not much alter even after prolonged heat treatment of several hours [2.15]. Only annealing at an elevated temperatures above about 600°C leads to the precipitation of small fraction of boride compounds like Fe_2B or Fe_3B with typical dimensions of 50 -100 nm, while the ultrafine grain structure of bcc Fe-Si still persists. Further increase of annealing temperature above about 700°C, finally yields grain coarsening the formation of Fe borides and grain coarsening deteriorates the soft magnetic properties significantly.

Our present composition is $(Fe_{0.95}Co_{0.05})_{73.5}Cu_1Nb_3Si_{13.5}B_9$, which possess 14.7% Co as a part of ferromagnetic transitional element. For cobalt substituted FINEMET alloy system, Mössbauer spectra and XRD results [2.16] show that α-FeCo is the first crystalline phase that precipitates in this alloy system. Researchers [2.17] found that addition of cobalt causes alteration of disordered DO_3-type structure of Fe-Si grains

nanocrystalline FINEMET, in to bcc (FeCo)Si solid solution of low silicon concentration. In case of Co substituted FINEMET, it has been reported [2.18] that cobalt takes part in the main composition of nanocrystal, i.e. the nanocrystalline part should be $(FeCo)_3Si$.

2.5 Advantages of Soft Nanocrystalline Alloys

Nanocrystalline amorphous ribbons are produced by melt-spinning technique to produce an amorphous metal and then heat-treating this alloy at temperature higher than its crystallization temperature. Choice of soft magnetic materials for applications has been guided by recent developments in the field of soft magnetic materials. Amorphous and nanocrystalline magnetic materials, in terms of combined induction and permeabilities are now competitive with Fe-Si bulk alloys and the Fe-Co alloys.
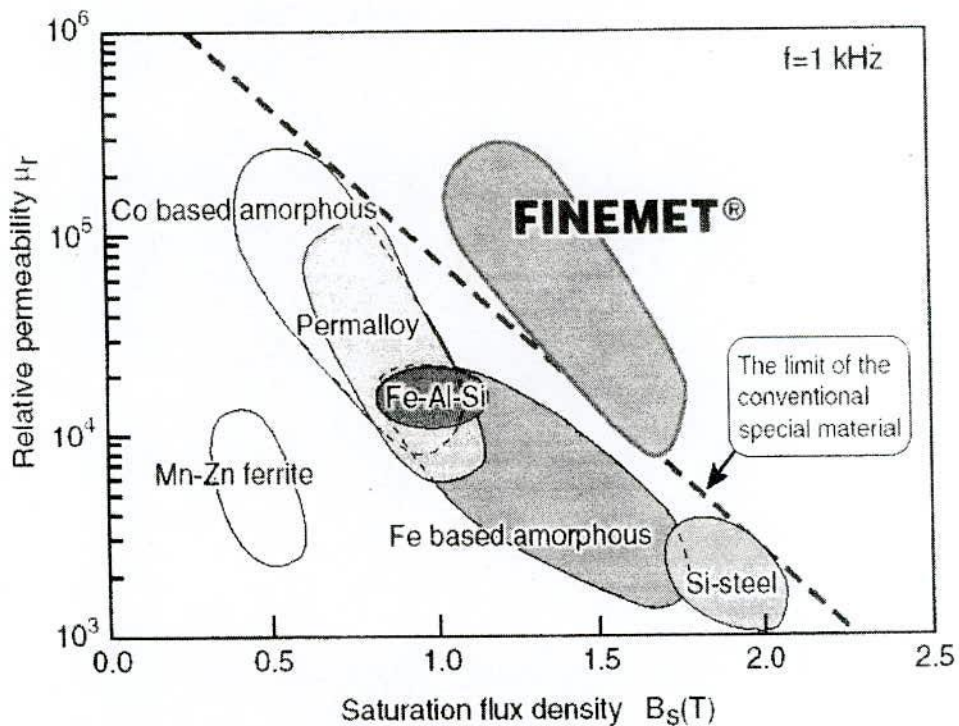
Fig. 2.3 FINEMET is superior compared to conventional materials

19

In Fig. 2.3 [2.19], figures of merit for Fe-based amorphous alloys, Co-based amorphous alloys and nanocrystalline alloys are summarized. Co-based amorphous alloys, Fe-based amorphous alloys and Nanocrystalline alloys have evolved over the past decades with soft magnetic properties which now exceed those of the bulk alloys based on Fe, Co and Fe-Co.

This FINEMET material is still in its immaturity since its emergence, although much research work has been carried out for the potential utility of this unique material. At this stage of development, this material has the following advantages:

- High saturation magnetic flux density, more than 1 Tesla or 10 kOe.
- High permeability over $\mu_i \approx 10,000$ at 100 kHz.
- Excellent temperature characteristics.
- Less affected by mechanical stress.
- Very low audio noise emission, lower magnetostriction significantly reduces audible noise emission when the voltage and current is applied to the core at audible frequency range.
- Flexibility to control magnetic properties, "B-H curve shape" during annealing and three types of B-H curve square ness, high, middle and low remanence ratio, corresponding to various applications.

2.6 Viscosity condition for the Formation of Metallic glass

In terms of viscosity and diffusion co-efficient we find the condition for formation of glass:

1. The metals atomic bonding is metallic; the viscosity is lower than the diffusion co-efficient and mobility is high.
2. In the amorphous state viscosity become high and the diffusion co-efficient decreases. Atomic bonds tend to be covalent as in the case of silicate (SiO_2).

2.7 Conditions for the formation of Nanocrystalline alloys

The essential conditions for preparing nanocrystalline materials are:

(i) The magnetic properties are highly dependent on grain size; if the grain size is larger; the magnetic anisotropy would be very high, which in turn will have diverse effect on the soft magnetic properties specially the permeability.

(ii) There should be nucleation centers initiated for the crystallization process to be distributed throughout the bulk of amorphous matrix.

(iii) There must be a nucleation for stabilizing the crystallites.

(iv) Nanocrystalline materials obtained from crystallization must be controlled so that the crystallites do not grow too big. The grain growth should be controlled so that the grain diameter is within 15-20 nm.

(v) The size of the grains can be limited to nanometer scale by doping group-II metals are

$\rightarrow$ Cu (Au........)

$\rightarrow$ Nb,W, Mo, Cr, Ta etc.

(vi) The stability must be lower and the crystallization must be higher.

2.8 Methods used for Preparation of Nanocrystalline Alloy

There are various techniques in use to produce a metallic alloy in an amorphous state whose the atomic arrangement have no long-range periodicity. The methods are generally classified into two groups

(i) The atomic deposition methods

(ii) The fast cooling of the melt.

As we know, controlled crystallization from the amorphous state is the only method presently available to synthesize nanocrystalline alloys with superior soft magnetic properties. In this thesis work amorphous ribbons have been prepared by fast cooling of the melt.

2.8.1 The Fast Cooling of the Melt

The molten alloy must be cooled through the temperature range from the melting temperature (T_m) to the glass transition temperature (T_g) very fast allowing no time for crystallization. The factors controlling T_g and crystallization are both structural and kinetic. Atomic arrangement, bonding and atomic size effect are related in the structural factors. The structural factors as discussed by Turnbull [2.20] are the nucleation, crystal growth rate and diffusion rate compared to the cooling rate. The methods using the principle of fast cooling of melt techniques are:

(i)   The gun techniques

(ii)   Single roller rapid quenching techniques

(iii)   Double roller rapid quenching techniques

(iv)   Centrifuge and rotary splat quenching techniques

(v)   Torsion catapult techniques

(vi)   Plasma-jet spray techniques

(vii)   Filamentary casting techniques

(viii) Melt extraction techniques

(ix)   Free-jet spinning techniques

(x)   The melt spinning techniques

Among the techniques, the single roller rapid quenching technique is widely used to prepare amorphous ribbons.

2.9   Sample Preparation

2.9.1 Master alloy Preparation

Amorphous ribbons with the nominal composition $(Fe_{0.95}Co_{0.05})_{73.5}Cu_1Nb_3Si_{13.5}B_9$, were prepared in an arc furnace on a water-cooled copper hearth under an atmosphere of pure Ar. Their purity and origin of the constituent elements were Fe (99.9 %), Co (99.9%), Nb (99.9 %), Si (99.9 %), Cu (99.9 %) and B (99.9 %) as obtained from Johnson Mathey (Alfa Aesar Inc.). The required amounts of constituent elements were taken from pure metal bars or flakes, weighed carefully with a sensitive electronic

22

balance and placed on the copper hearth inside the arc furnace. Before melting the furnace chamber was evacuated (10^{-4} torr), and flashed with Ar gas. The process was repeated several times to get rid of residual air and finally the furnace chamber were kept in an Ar atmosphere.

Fig. 2.4 Vacuum arc Melting Machine

A substantial amount of pure Titanium getter, placed inside of the chamber on the side of the copper hearth was melted first in order to absorb any oxygen present in the furnace chamber. The constituent elements were then melted in the shape of buttons. The arc melting facilities used to prepare the samples are installed at the Centre for Materials Science, National University of Hanoi, Vietnam. The arc furnace used in the preparation of master alloy is shown in Fig. 2.4.

2.9.2 Preparation of ribbon by Melt Spinning Technique

Melt-Spinning is a widely used production method for rapidly solidifying materials as well as preparing amorphous metallic ribbon [2.21-2.23]. In order to prepare amorphous of $(Fe_{0.95}Co_{0.05})_{73.5}Cu_1Nb_3Si_{13.5}B_9$ alloys, a melt spinning facilities was used

at the Centre for Materials Science, National University of Hanoi, Vietnam. The arc melted master alloy was crashed into small pieces and put inside the quartz tube crucible for re-melting by induction furnace using a medium frequency generator with a maximum power of 25 kW at a nominal frequency of 10 kHz.
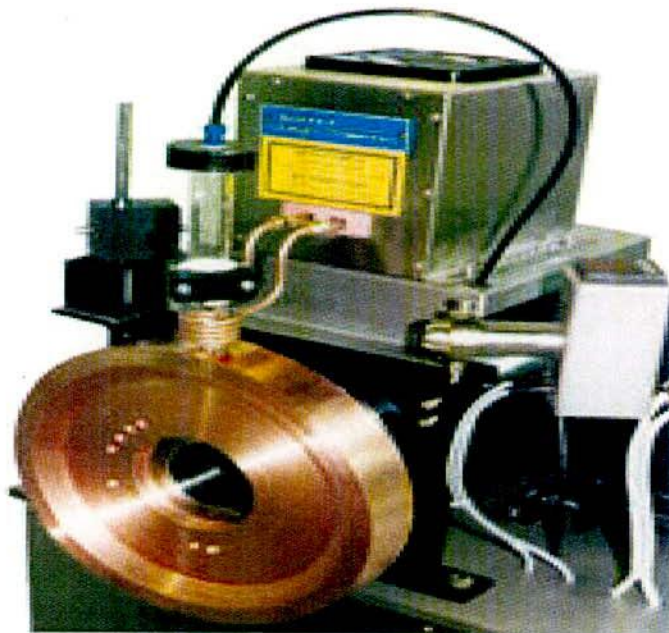
Fig. 2.5 Melt-Spinning Machine

Fig. 2.5 shows the pictorial view of the melt-spinning machine. The quartz crucible has in its bottom part a rectangular nozzle tip of 8 mm length and 0.7 mm width. The position of the nozzle tip can be adjusted with respect to the copper wheel surface, so that the molten alloy was perpendicularly ejected onto the wheel surface from a distance of about 0.3 mm. The small pieces of the master alloy samples were inductively remelted inside the quartz tube crucible followed by ejecting the molten metal with an over pressure of 250 mbar of 99.9 % pure Ar supplied from an external reservior through a nozzle onto a rotating copper wheel with surface velocity of 30 m/sec. The temperature was monitored by an external pyrometer from the upper surface of the molten alloy

24

through a quartz window. The metal alloys were ejected at a temperature of about 150-250 K above the melting point of the alloy. The resulting ribbon samples had thickness of about 20-25 μm and width of ~ 6 mm. Processing parameters such as the thermal conductivity of the rotating quench wheel, wheel speed, ejection pressure, thermal history of the melt before ejection, distance between nozzle of quartz tube and rotating wheel, as well as processing atmosphere have influence on the microstructure and properties of melt-spun ribbons.

The lower pressure of 250 mbar as mentioned above stabilizes the turbulence between melt pull and rotating copper wheel enhancing the heat transfer resulting in a more uniform quenching. As a result, a more uniform ribbon microstructure can be obtained at relatively low wheel speed. With increasing wheel speeds for a given ejection rate, the increasing extraction rate results in thinner ribbons.

2.10 Important Factors to Control the Thickness of Ribbons

    (i)   Rotating speed:

- Angular velocity ω = 2000 rev/min
- Surface velocity V = 20 m/s to 30 m/s

    (ii)   Gap between nozzle and rotating copper drum h = 200 to 30 μm

    (iii)   Oscillations of rotating copper drum both static and dynamic have maximum displacement 1.5 to 5 μm.

    (iv)   Pressure = 0.2 to 0.3 bar argon atmosphere.

    (v)   Temperature of molten metals $T_m \cong 1500°C$; other wise quartz tube would be melted.

    (vi)   A steady flow of the molten metal on the surface of the rotating drum needs to be ensured.

2.11 Confirmation of Amorphousity of Ribbon

The amorphousity of the two ribbons has been checked by X-ray diffraction using Cu-K$_\alpha$ radiation using Philips (PW 3040) X 'Pert PRO XRD System located at Materials Science Division, Atomic Energy Centre, Dhaka (AECD
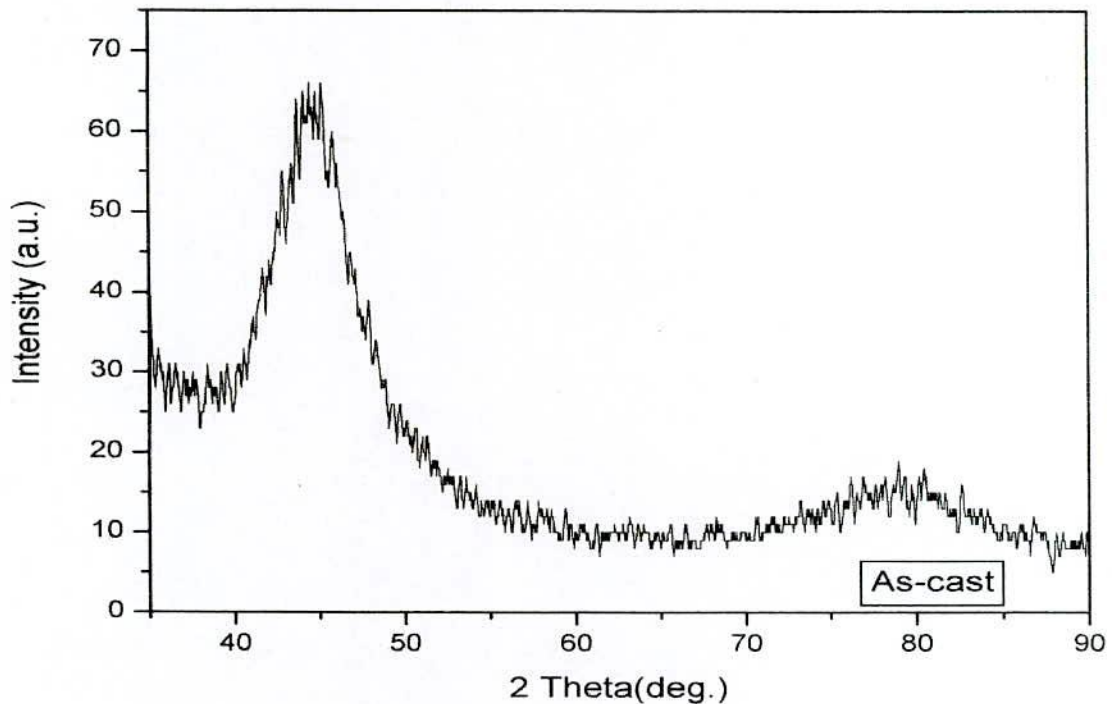
Fig. 2.6 X-ray diffraction of as-cast nanocrystalline amorphous ribbons with composition $(Fe_{0.95}Co_{0.05})_{73.5}Cu_1Nb_3Si_{13.5}B_9$ alloy

From the XRD pattern of the ribbon samples in Fig-3.3, no peaks are observed within the scanning range. Although there is a small hump is shown in diffraction pattern around $2\theta = 45°$, but it cannot be regarded due to the crystalline effects. So from the over all pattern of the X-ray diffraction it is confirmed that both the samples are in amorphous state.

26

Chapter - III
Theoretical Background

Chapter-III Theoretical Background

3.1 Amorphous Alloy or Metallic Glass

In condense matter physics, an amorphous (from the Greek a, without, morphe, shape, form) or non-crystalline solid is a solid that lacks the long-range order characteristic of a crystal.

In part of the older literature, the term has been used synonymously with glass. The local structure in amorphous metallic material is distinct from that of window glass. By analogy, the term 'metallic glass' usually refers to a metallic alloy rapidly quenched in order to "freeze" its structure from the liquid state.

A 'glass' refers to a molten mass that is cooled rapidly to prevent crystallization. The expression 'glass' in its original sense refers to an amorphous or nanocrystalline solid formed by continuous cooling of a liquid [3.1], while a solid is defined somewhat arbitrary as object having a viscosity greater that 10^{14}Pa.s. Glasses have been found in every category of materials and of various bond types: covalent, ionic, Vander Walls, hydrogen and metallic. Different types of amorphous solids include gels, thin films and nanostructured materials.

3.1.1 Nature and Formation of Amorphous Alloys

It is very difficult to get pure metals in the amorphous state. It is necessary to add glass forming materials to pure metals or alloys to get the amorphous state and to bring the cooling rate within a reasonable rate. Usually around 20 % of glass forming materials like B, Si, P, C etc which have atomic radii comparatively small compared to those of metallic atoms and the glass forming atoms occupy the voids left between the bigger atoms of metals when they are closely packed. It can be showed that when there is random close packing of hard spheres, there is about 20% voids created between these atoms. The glass forming materials which have smaller atoms occupy these voids which explain the importance of the glass forming material in the preparation of an amorphous ribbon.

The term "amorphous" defines a non-crystalline body while a "glass" refers to a molten mass that is cooled rapidly to prevent crystallization. By analogy, the term "metallic glass" usually refers to a metallic alloy rapidly quenched in order to "freeze" its structure from the liquid state.

The expression "glass" in its original sense refers to an amorphous or nanocrystalline solid formed by continuous cooling of a liquid while a solid is defined somewhat arbitrary as object having a viscosity grater than 10^{14} Pa.s [3.2]. A glass lacks three- dimensional atomic periodicity beyond a few atomic distances. It is characterized by limited number of diffuse halos in X-ray, electron and neutron diffraction and no sharp diffraction contrast in high- resolution electron microscopy. Glasses have been found in every category of materials and of various bond types: covalent, ionic, Vander Walls, hydrogen and metallic.

Glasses are generally formed if upon cooling of a melt, crystal nucleation and/or growth are avoided. At a temperature called glass transition temperature (T_g) the liquid freezes to a rigid solid, however without crystalline order. Thus, glasses and amorphous solids in general are structurally characterized by the absence of long-range translational order. But a short-range order is still present and may be similar to that found in the crystalline counterpart.

Synthesizing amorphous alloys requires rapid solidification, in order to by-pass the crystallization [3.3]. The metastable structure thus achieved nevertheless may possess a short-range order (SRO) that resembles the equilibrium crystal structure [3.4]. This indicates that the thermodynamic forces that drive crystallization in metals are extremely strong and in most cases, overpowering. Thus the search for alloy systems that allow formation of amorphous structures is of keen technological importance.

Fig-3.1 shows schematically, the time taken for a small amount of crystalline phase to form in an undercooled liquid as a function of temperature. The Temperature-Time-Transformation (TTT) diagram shows a characteristic C curve behavior. At the temperature close to melting point T_m, there is little driving force for crystallization, so that the crystal nucleation and growth rates are small, and the crystallization onset time t_0 is large. As the temperature decreases, the crystallization onset time reaches a minimum

value t_0^* at a temperature T_n, and then increases again as the thermal energy becomes insufficient for atomic motion.
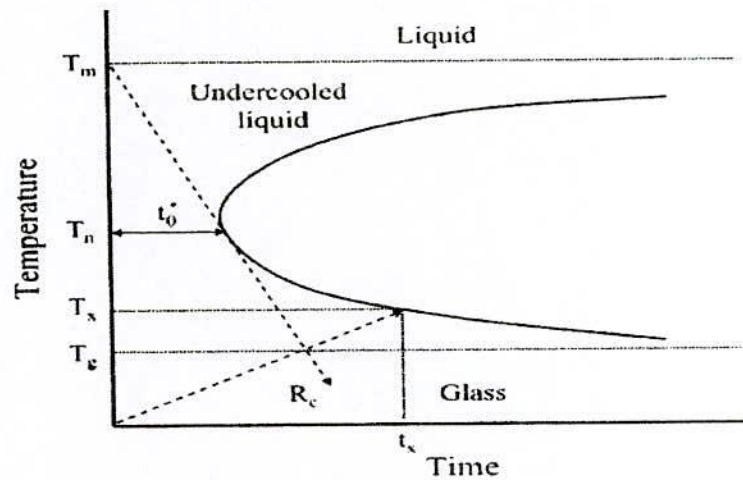
Fig. 3.1 Schematic TTT diagram for the onset of crystallization

Close to the glass transition temperature (T_g) atomic motion is completely suppressed and the amorphous structure is frozen in, so that the crystallization onset time t_o, becomes large. Therefore, critical cooling rate R_c to avoid crystallization is given below:

$$R_c = \frac{T_m - T_n}{t_o^*} \qquad (3.1)$$

3.1.2 Factors Contributing to Glass Formation and Stability

There are three interrelated factors that determine glass forming tendency. These are:

(i)   Thermodynamic conditions that favor the liquid phase relative to crystalline phase.

(ii)   The kinetic conditions that inhibit crystallization and .

(iii)   The process factors that rise due to the experimental conditions.

The thermodynamic factors for glass formation are liquidus temperature ™ at which the alloy melts, the heat of vaporization and the free energy of all phases that arise

or could potentially arise during solidification process. Viscosity of the melt, the glass transition temperature (T_g) and the homogeneous nucleation rate belong the kinetic parameters. Processing parameters are the cooling rate, the heterogeneous nucleation rate and the supercooling temperature interval. The temperature of the glass transition is slightly dependent on the cooling rate. At each cooling rate, the glass will freeze in a different state of internal energy.

A single parameter that express glass forming tendency is the ratio of the glass transition temperature to the melting temperature defined as

$$T = \frac{T_g}{T_m},$$

(3.2)

which is usually mentioned as reduced glass transition temperature or reduced temperature.

Higher values of τ obviously favor glass formation. For metallic glass to be formed by rapid cooling, τ should be greter than 0.45 as mentioned by H. S. Chen [3.5]. Based on alloy composition, there are two major groups that rapidly from glasses. In one of these groups the metal in from Fe, Co, Ni, Pd or Pt and the metalloid is B, C, Si, Ge or P. These metallic glasses constitute soft amorphous magnetic materials.

It is very difficult to get pure metals in the amorphous state. It is necessary to add glass forming materials to pure metals or alloys to get amorphous state and to bring cooling rate with in a reasonable rate. Usually around the 20% of glass forming materials like B, Si, P, C etc. which have atomic radii comparatively small compared to these of metallic atoms, occupy the voids left between the bigger atoms of metals when they are closely packed. It can be showed that when there is random close packing of hard spheres, there is about 20% voids created between these atoms. The glass forming materials also reduces the melting point of the alloys and there by the separation between the glass forming temperature and the crystallization temperature is reduced.

The amorphous alloy composition most favorable for glass formation is near eutectic, i.e. the composition in which the transformation from the liquid state to solid state take place instantaneously without passing through liquid plus solid mixed phase. The deeper the eutectic, the better is the glass formation ability [3.6].

The magnitude of T_g and T_x are very different for amorphous materials and depend strongly on composition. The activation energy ranges typically between 2 and 6eV [3.7].

The crystallization is associated with nucleation and growth process. Since the formation of an amorphous alloy depends on the absence of long range order, change of composition is expected to effect T_g and T_x. This is because the long range ordering of atoms depends on the free energy difference between the crystallite state and amorphous state.

3.2 Structure and Microstructure of Amorphous and Nanocrystalline alloys

An amorphous solids is one in which the atomic positions do not have crystalline periodic order. The amorphous structure is postulated to be that of the frozen liquid. The local structure in amorphous metallic materials is distinct from that of window glass. A periodically spaced atom does not exist in amorphous alloys. Therefore XRD does not show any diffraction pattern. If one performs an X-ray scattering experiment on amorphous material, one does observe one or more broad peaks in the scattered intensity shown in Fig. 3.2 at angles similar to those where one or more diffraction peaks would occur in a crystalline alloy of the same composition.

Scherrer analysis of the breadth of the X-ray scattering peak(s), one would conclude that the 'crystallite size' was on the order of atomic dimensions. This is a good argument for only short-range atomic correlations being present in amorphous metals. Scattering experiments on amorphous alloys can be used to determine the so-called radial distribution function that is derived from an appropriate Fourier transform of a normalized scattered intensity expressed as a function of scattering angle.

The atoms in an amorphous solid are not periodically arranged and therefore the concept of a lattice is not appropriate for describing their positions. Thus in an amorphous solid there is not an equivalent concept to that of a lattice and a basis of region to describe atomic positions in a more probabilistic sense using the concept of a

31

pair correlation function, g(r). The pair correlation function is defined as the probability that two atoms in the structure are separated by a distance, r. To define g(r) further begin by considering N atoms in a volume, Ω, letting R_1, R_2, R_3,...., R_N denote the positions of the N atoms with respect to an arbitrary origin. The distance r denotes the magnitude of the vector connecting two atoms i and j,

$$\text{i. e.} \quad r = R_i - R_j \tag{3.3}$$

Two additional atomic distribution functions related to the pair correlation function are the spatially dependent atomic density, $\rho(r)$, which is defined as;

$$\rho(r) = \frac{Ng(r)}{\Omega}, \tag{3.4}$$

and the radial distribution function, RDF(r), which is defined in terms of the pair correlation function as:

$$RDF(r) = 4\pi r^2 \rho(r) \tag{3.5}$$
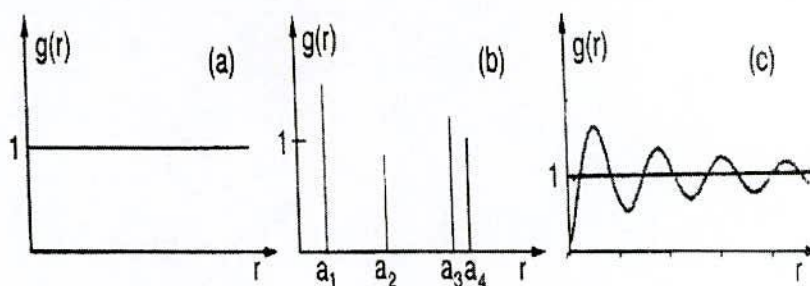
Fig. 3.2 Typical pair correlation function for (a) a completely disordered, (b) a crystalline completely ordered, and (c) an amorphous short-range ordered material

Fig. 3.2 illustrates schematically the distinction between the pair correlation functions for a completely disordered, a crystalline completely ordered and an amorphous short range ordered material. A completely disordered material, like a gas has a uniform

unit probability of finding neighboring atoms at all possible distances which leads to a uniform, featureless g(r). On the other hand, a crystalline solid has a set of discrete distances between atomic positions and therefore the pair correlation function in a set of discrete δ-like functions, the amplitude of which reflects the particular coordination number for nearest neighbor, next nearest neighbor,.......etc. pairs of atoms. This is consistent with Bragg scattering (diffraction). In amorphous alloys g(r) is neither discrete nor featureless; instead broad peaks reflect the short-range order in these materials.

3.3   Stability of the Amorphous Nanocrystalline Materials

Amorphous materials are always in a metastable state, which tend to transform into more stable crystalline phases. There are three kinds of stability of significance for amorphous magnetic alloys:

(i)   Their resistance to the initiation of crystallization

(ii)   Structural relaxation effects and

(iii)   The relaxation or reorientation of directional order.

Actually, Controlled crystallization from the amorphous state seems to be the only method presently available to synthesize nanocrystalline alloys with attractive soft magnetic properties. The formation and resultant stability of amorphous alloys are important topics both theoretically and technologically. The theoretical analyses of the factors controlling the ease of formation and the stability of the resultant amorphous alloys have been extensively reviewed [3.8-4.9]. From the thermodynamic view point [3.10-3.11], the ability of an alloy to be quenched into the glassy state is generally measured by the magnitude of the quantity.

$$\Delta T_g = T_m - T_g,$$
(3.6)

where T_m and T_g are the melting and glass transition temperature respectively. In a similar manner the stability of the glass after formation is generally measured by the magnitude of the quantity.

$$\Delta T_x = T_x - T_g,$$
(3.7)

where T_X is the temperature for the onset of crystallization. As the temperature decreases from T_m the rate of crystallization will increase rapidly and then fall rapidly as the

temperature decreases below T_g. The amorphous alloy composition most favorable for glass formation is near eutectic i.e. the composition in which the transformation from the liquid state to solid state takes place instantaneously without passing through liquid plus solid mixed phase. The deeper the eutectic the better is the glass formation ability [3.12]. There have been three approaches to relating the stability of the glass, i.e., its microstructure:

[i]   Bernal's model of randomly packed hard sphere's [3.13] . The metal atoms are assumed to form a random network of close packed hard spheres and the smaller metalloid atoms fill the holes inherent in such a structure.

[ii] The effect of atomic sizes and interatomic interactions [3.14], i.e. chemical bonding and suggested that it is chemical bonds which are the dominating factors in glass formation and stability.

[iii] The third approach [3.15] is based on the role of the electron gas and showed that under certain circumstances a nearly free electron gas will produce a barrier against crystallization.

The transition to the glassy state and the crystalline state is accompanied by an exothermic heat effect giving rise to a sharp peak in temperature dependence of the heat flow. Therefore, differential thermal analysis (DTA) is a widely used technique to study thermally induced transformations in amorphous alloys and to determine T_g and T_x. The magnitude of T_g and T_x are very different for amorphous materials and depend strongly on composition. The activation energy ranges typically between 2 and 6 eV. [3.16]

3.3.1   Characteristics of the Glass Transition Temperature

Glass transition temperature (T_g) occurs when the timescale of molecular rearrangements are too long for equilibrium to be maintained.

i) T_g means the time scale of the experiment matters.

ii)   A high frequency/short time scale experiment allows less long for equilibrium to be established – even for an identical cooling rate.

iii) So NMR (high frequency technique 10^{15}Hz) always measures a higher T_g than DTA (Differential thermal analysis, 1Hz).

iv)   In the glass itself, entropy is similar to the crystal, and originals in vibrational modes, which are still present.

v)   Long range transnational motions are frozen out. The temperature T_g Configuration freezes out, relaxation (including transnational motion) but vibrational relaxations are still in equilibrium.

vi) T_g decreases as melt cooled more and more slowly.

vii)   When the timescale of the experiment and the configurational relaxation time coincide, begin to see departure from equilibrium.

viii)   The timescale for configuration relaxation will be related to rotational or translational diffusion co-efficient.

ix)   Operational definition of T_g is when the viscosity of the super cooled liquid exceeds 10^{13} NSm^{-2}. Where as in the liquid there is an Arrenhivs type with a Boltzmann factor containing an activation energy.

3.4   Differential Thermal Analysis and its Application

Differential Thermal Analysis (DTA) is a technique to study the structural change occurring both in solid and liquid materials under heat treatment. During this process, the temperature difference between a substance and a reference material is measured as a function of temperature whilst the subject and the reference material are subjected to same controlled temperature program. The transition of an amorphous or glassy state to crystalline state is accompanied by an exothermic heat effect that gives rise to a sharp peak in temperature dependence of the heat flow. To study this thermally induced transformation in amorphous alloys, Differential Thermal Analysis (DTA) is awidely used technique.

Amorphous alloys are in a metastable state and tend to transition into stable crystalline phases. At temperature below the crystallization temperature, structural relaxation effects take place which are are caused by atomic rearrangements.

Differential thermal analysis (DTA) is an important technique for the study of structural change both in solid and liquid materials under heat treatment. The principle of differential thermal analysis is widely used to understand the crystallization nature of amorphous. Differential thermal analysis is a direct and effective technique for analyzing

the kinetics of amorphous materials and stability with respect to crystallization process. The crystallization is associated with the nucleation and growth process. Since the formation of an amorphous alloy depends on the absence of long range atomic order, change of composition is expected to effect T_g and T_x.

This is because long range ordering of atoms depends on the free energy difference between the crystalline state and the amorphous state. The magnitude of T_g and T_x are very different for amorphous materials and depend strongly on composition. Using DTA technique it is possible to determine T_g and T_x. Nanocrystalline amorphous ribbons prepared by rapid quenching method have been subjected to differential thermal analysis (DTA) using a Shima dzu thermal analyzer. Different peaks, crystallization temperatures, crystallization activation energies are obtained from this analysis.

3.4.1 Evaluation of Activation Energy Based on DTA Technique

Based on the work of Murray and White [3.17-3.19] the kinetics of crystallization of materials can be understood by interpretation of DTA patterns of the materials. The dependence of T_x on the heating rate $\beta = \dfrac{dT}{dt}$ can be used to determine the activation energy of crystallization [3.20]. Considering the fraction x of amorphous material transformed into the crystalline state in time t and at temperature T, one obtains for the first- order rate process [3.21-3.22].

$$\left(\frac{\delta x}{\delta t}\right)_T = K(1-x) \qquad (3.8)$$

For thermally activated process, the rate constant K obeys an Arrhenivs type of equations

$$K = K_o e^{-\left(\frac{\Delta E}{RT}\right)} \qquad (3.9)$$

Where K_o is a constant and ΔE is the activation energy. Combining eq^n(3.8) and eq^n(3.9) and using $dx = \left(\dfrac{\delta x}{\delta t}\right)_T dt + \left(\dfrac{\delta x}{\delta t}\right)_t dT$ with $\left(\dfrac{\delta x}{\delta t}\right)dt \cong 0,$ one obtains

$$\frac{dx}{dt} = K_o(1-x)e^{-\left(\Delta E/RT\right)} \qquad (3.10)$$

$$\frac{d^2x}{dt^2} = \frac{d}{dt}\left[K_0(1-x)e^{-\Delta E/RT}\right]$$

$$= -K_0 \frac{dx}{dt}e^{-\Delta E/RT} + K_0(1-x)\frac{d}{dT}\left(e^{-\Delta E/RT}\right)\frac{dT}{dt}$$

$$= -K_0 \frac{dx}{dt}e^{-\Delta E/RT} + \frac{dx}{dt}\left(\frac{\Delta E}{RT^2}\right)\beta$$

At the peak of the exothermic heat, the change of the reaction rate $\frac{d^2x}{dt^2} = 0$, yielding

with $T = T_x$ but $\frac{dx}{dt} \neq 0$

$$K_0 e^{-\left(\frac{\Delta E}{RT_x}\right)} = \left(\frac{\Delta E}{RT_x^2}\right)\beta \tag{3.11}$$

From eq^n(3.11) it is easily seen that

$$\frac{d\left(\ln\frac{\beta}{T_x^2}\right)}{d\left(\frac{1}{T_x}\right)} = -\frac{\Delta E}{R} \tag{3.12}$$

Here $\beta = \frac{dT}{dt}$ the heating rate. ΔT_x for the stability of amorphous alloys as given by eq^n(3.7) and is obtained from DTA. The values of ΔE also appear to correlate well with the number of atomic species in the alloy; the more complex the alloy the greater is ΔE. Similar correlation between thermal stability as measured by ΔT_x and ΔE appears to small.

From the measured data of the heating rate (β) and the respective crystallization temperature (T_x), the activation energy can be deduced from the slope of a plot of $\ln\left(\frac{T_x^2}{\beta}\right)$ versus $\frac{1}{T_x}$. Eq^n(3.12) can be derived from transformation theory, where ΔE is the activation energy for versus flow, and other terms have been omitted because they have an insignificant temperature dependence in this region of temperature. The values of ΔE also appear to correlate well with the number of atomic species in the alloy; the more complex the alloy the greater is ΔE.

3.5   Determination of Nanometric Grain Size by X-ray Diffraction

Nanocrystalline alloys are basically crystalline, and because of their crystallinity they exhibit Bragg scattering peaks in X-ray diffraction experiments. However, due to their small size, significant fine particle broadening is observed in the Bragg peaks. The X-ray scattering from a crystalline solid is given by Bragg's law:

$$2d \sin \theta = n\lambda \qquad\qquad (3.13)$$

This equates the path difference of X-rays scattered from parallel crystalline planes spaced $d = d_{hkl}$ apart to an integral number (n) of X-ray wavelength λ. Here θ is the X-ray angle of incidence (and of diffraction) measured with respect to the crystalline planes. For an infinite crystal Bragg scattering occurs at discrete values of 2θ satisfying the Bragg condition, i.e. Bragg peaks are δ-functions. For finite sized crystals the peaks are broadened over a range of angles as shown in Fig. 3.3
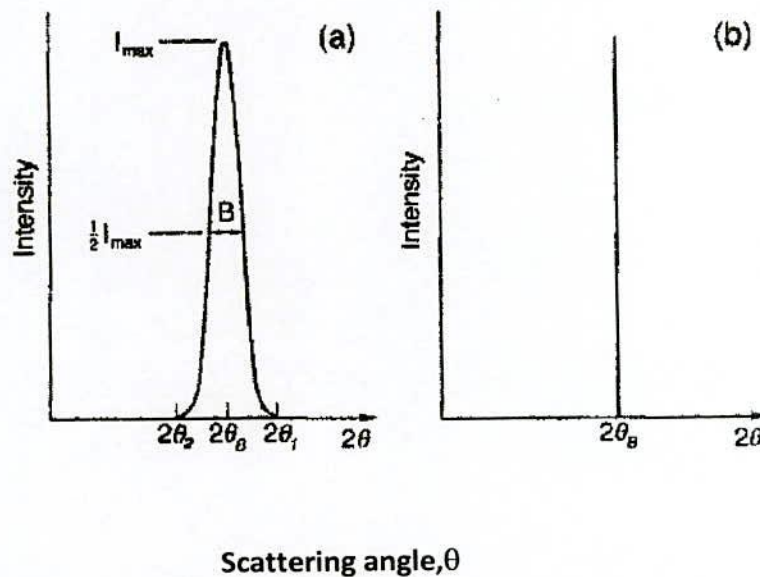
Fig. 3.3 Effect of fine particle broadening in XRD (a) fine particles and (b) perfect crystal

To better understand the phenomenon of fine particle broadening [3.23], we consider a finite crystal of thickness, $D_g = md$, where m is an integer, and d is the distance between crystalline planes, i.e., there are m planes in D_g. Considering Fig. 4.4,

if the broadened Bragg peak begins at an angle $2\theta_2$ and ends at $2\theta_1$, the breadth of the peak or full width at half maximum is given as:

$$\beta = \frac{1}{2}(2\theta_1 - 2\theta_2) = \theta_1 - \theta_2 \qquad (3.14)$$

Now consider the path differences for each of the two angles θ_1 and θ_2, for X-rays traveling through the full thickness of the crystal. The width β is usually measured in radians, an intensity equal to half the maximum intensity. As a rough measure of β, we can take half the difference between the two extreme angles at which the intensity is zero, which amounts to assuming that the diffraction line is triangular in shape. We now write path difference equations for these two angles, related to the entire thickness of the crystal rather to the distance between adjacent planes.

$$2D_g \sin\theta_1 = (m+1)\lambda \qquad (3.15)$$

$$2D_g \sin\theta_2 = (m-1)\lambda \qquad (3.16)$$

By subtraction we find:

$$D_g (\sin\theta_1 - \sin\theta_2) = \lambda \qquad (3.17)$$

$$D_g 2\cos\left(\frac{\theta_1 + \theta_2}{2}\right)\sin\left(\frac{\theta_1 - \theta_2}{2}\right) = \lambda \qquad (3.18)$$

But θ_1 and θ_2 are both very nearly equal to θ, so that $\theta_1 + \theta_2 \approx 2\theta$ and $\sin\left(\frac{\theta_1 - \theta_2}{2}\right) \approx \left(\frac{\theta_1 - \theta_2}{2}\right)$ so that equation (3.18) can be written as:

$$2D_g \cos\theta\left(\frac{\theta_1 - \theta_2}{2}\right) = \lambda \qquad (3.19)$$

From equation (3.14) and equation (3.19) we get:

$$\beta.D_g \cos\theta = \lambda$$

$$D_g = \frac{\lambda}{\beta\cos\theta} \qquad (3.20)$$

A more exact empirical treatment yields:

$$D_g = \frac{0.9\lambda}{\beta\cos\theta}, \qquad (3.21)$$

which is known as the Scherrer's formula. It is used to estimate the particle size of very small crystals from the measured width of their diffraction curves.

3.6 Random Anisotropy Model (RAM)

The soft magnetic properties of Finemet type of nanocrystalline materials are based on Random Anisotropy Model (RAM) proposed by Herzer [3.24]. Soft magnetic properties of nanocrystalline alloys are strongly dependent on the grain size and grain boundary structure. In order to interpret the behavior of the magnetic properties for atomic scale grains, the RAM was originally proposed by Alben *et al.* [3.25] for amorphous ferromagnets. The basic idea is sketched in Fig 3.4 and starts from an assembly of ferromagnetically coupled grains of size D_g with magneto-crystalline anisotropies K_1 oriented at random.
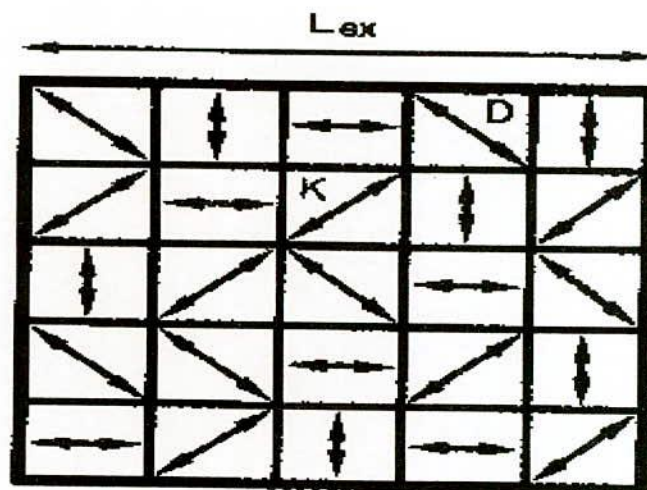
Fig.3.4: Schematic representation of the random anisotropy model. The arrows indicate the randomly fluctuating magnetocrystalline anisotropies

The concept of a magnetic exchange length (L_{ex}) and its relationship to the domain wall width (δ_w) and nano domain size is important in the consideration of magnetic anisotropy in nanocrystalline soft magnetic materials [3.26]. These can be defined by appealing to a Helmholz free energy function as described by Coey [3.27]. These length scales are:

$$\delta_W = \pi \sqrt{\frac{A}{K_1}} \qquad \text{and} \qquad L_{ex} = \sqrt{\frac{A}{4\pi M_s^2}} \qquad (3.22)$$

Herzer considers a characteristic volume whose linear dimension is the magnetic exchange length, $L_{ex} \sim \left(\frac{A}{K_1}\right)^{\frac{1}{2}}$, where K_1 is the magnetocrystalline anisotropy. Given the discussion above, the unstated constant of proportionality should be $\left(\frac{k}{\pi}\right)$ which for materials with very small K_1 can in fact be quite large. Ignoring this constant of proportionality, the Herzer's argument considers N grains, with random easy axes, within a volume of L_{ex}^3 to be exchange coupled. Since the easy axes are randomly oriented, a random walk over all N grains will yield an effective anisotropy which is reduced by a factor of $\left(\frac{1}{N}\right)^{\frac{1}{2}}$ from the value K_1 for any one grain, thus $K_{eff} \approx \frac{K_1}{\sqrt{N}}$. Now the number of grains in this exchange coupled volume is just $N \approx \left(\frac{L_{ex}}{D_g}\right)^3$, where D_g is the average diameter of individual grains. The ferromagnetic correlation volume $V = L_{ex}^3$ is determined by the exchange length L_{ex}. Relevant to the magnetization process, results from averaging over the $N = V_{cr} \left(\frac{L_{ex}}{D_g}\right)^3$ grains, volume fraction V_{cr}, with magneto crystalline anisotropy oriented at random.

Treating the anisotropy self-consistently then;

$$K_{eff} = V_{cr} \frac{K_1}{\sqrt{N}} = V_{cr}^{\frac{1}{2}} K_1 \left(\frac{D_g}{L_{ex}}\right)^{\frac{3}{2}} \qquad (3.22)$$

The ferromagnetic exchange length, $L_o = \sqrt{\frac{A}{K_1}}$

The exchange length L_{ex}, has to be normalized by substituting $4\pi M_s^2 = K_{eff}$ in equation (3.22) i.e. L_{ex} is self-consistently related to the average anisotropy by

$$L_{ex} = \left(\frac{A}{K_{eff}}\right)^{\frac{1}{2}} \qquad (3.23)$$

The combination of equation (3.22) and equation (3.23) then

41

$$K_{eff} = \sqrt{V_{cr}}\ K_1 \left[\frac{D_g}{\sqrt{\frac{A}{K_{eff}}}} \right]^{1/2}$$

$$= \sqrt{V_{cr}}\ K_1 \left[\frac{D_g \sqrt{K_{eff}}}{\sqrt{A}} \right]^{3/2}$$

$$= \sqrt{V_{cr}}\ K_1 \left[\frac{D_g \sqrt{K_{eff}}}{L_o \sqrt{K_1}} \right]^{3/2}$$

$$K_{eff}^{\ 4} = V_{cr}^{\ 2} K_1^{\ 4} \frac{D_g^{\ 6} \left(\sqrt{K_{eff}}\right)^6}{L_o^{\ 6} \left(\sqrt{K_1}\right)^6}$$

$$= V_{cr}^{\ 2} K_1^{\ 4} \frac{D_g^{\ 6}}{L_o^{\ 6}} \frac{K_{eff}^{\ 3}}{K_1^{\ 3}}$$

$$K_{eff} = V_{cr}^{\ 2} K_1 \left(\frac{D_g}{L_o} \right)^6$$

$$K_{eff} = V_{cr}^{\ 2} K_1 \frac{D_g^{\ 6}}{\left(\sqrt{\frac{A}{K_1}} \right)^6}$$

$$= V_{cr}^{\ 2} K_1 \frac{D_g^{\ 6}}{A^3} K_1^{\ 3}$$

$$= V_{cr}^{\ 2} D_g^{\ 6} \frac{K_1^{\ 4}}{A^3}$$

$$K_{eff} = \frac{V_{cr}^{\ 2} D_g^{\ 6} K_1^{\ 4}}{A^3} \tag{3.24}$$

Since the coercivity can be taken as proportional to the effective anisotropy, this analysis leads to Herzer's prediction that the effective anisotropy and therefore the coercivity should grow as the 6th power of the grain size:

$$H_c \sim D_g^{\ 6} \tag{3.25}$$

For such a reduction in the coercivity to be realized, Herzer noted that the nanocrystalline grains must be exchange coupled. This to be contrasted with uncoupled

particles that have an exchange length, comparable to the particle diameter are susceptible to super paramagnetic response.

The most significant feature predicted by the RAM is the strong variation K_{eff} with the 6th power of the grain size. Thus for $D_g \approx \dfrac{L_o}{3}$, i.e. grain sizes in the order of 10-15 nm, the magneto crystalline anisotropy is reduced by three order of magnitude towards a few J/m^3, i. e., small enough to enable superior soft magnetic behavior .

The K_{eff} , essentially determines the magnetic softness' since H_c and inverse of initial permeability (μ_i) are proportional to K_{eff}. Therefore it is expected that these quantities have similar dependence on grain size and have been confirmed experimentally [3.28]. Herzer explained the grain size dependence of the H_c based on RAM considering the nanocrystalline materials as single-phase magnetic system. Hernando et al. [3.29] extended this model for two-phase materials and were able to explain the thermal dependence of the coercivity [3.30-3.31]. Hernando has generalized RAM [3.28], taking into account the two phase character of nanocrystalline materials, and it explained the previously maintained hardening as well as other features which could not be understood without the generalization. Since the dimensions of the crystallites dictate the unique properties by controlling the annealing temperature of the specimens, the magnetic softness or hardness in respect of permeability is determined by the grain size, grain distribution and the volume fraction, which are developed on the amorphous matrix in the nanostructure system.

3.7   Theories of Permeability

The initial permeability (μ_i) is defined as the derivative of induction **B** with respect to the initial field **H** in the demagnetization state.

$$\mu_i = \frac{dB}{dH} \mid H \to 0, B \to 0 \tag{3.26}$$

In electromagnetism, permeability is the degree of magnetization of materials that responds linearly to an applied magnetic field. Permeability is defined as the

43

proportionality constant between the magnetic field induction **B** and applied field intensity **H**;

$$B = \mu H \qquad (3.27)$$

This definition needs modification when magnetic material is subjected to an ac magnetic field as given below

$$H = H_0 e^{i\omega t} \qquad (3.28)$$

In such a field the magnetic flux density (**B**) experience a delay with respect to **H**. The delay is caused due to the presence of various losses and is thus expressed as,

$$B = B_0 e^{i(\omega t - \delta)} \qquad (3.29)$$

where δ is the phase angle and marks the delay of B with respect to H, the permeability is then given by

$$\mu_i = \frac{B}{H}$$

$$= \frac{B_0 e^{i(\omega t - \delta)}}{H_0 e^{i\omega t}}$$

$$= \frac{B_0 e^{-i\delta}}{H_0}$$

$$= \frac{B_0}{H_0}\cos\delta - i\frac{B_0}{H_0}\sin\delta$$

$$\mu_i = \mu' - i\mu'' \quad , \qquad (3.30)$$

$$\text{where } \mu' = \frac{B_0}{H_0}\cos\delta \text{ and } \mu'' = \frac{B_0}{H_0}\sin\delta \qquad (3.31)$$

The real part μ' of complex permeability μ_i as expressed in equation (3.30) represents the component of B which is in phase with H, so it corresponds to the normal permeability. If there are no losses, we should have $\mu_i = \mu'$.

The imaginary part μ'' corresponds to that part of B, which is delayed by phase angle ranging up to 90° from H. The presence of such a component requires a supply of energy to maintain the alternating magnetization, regardless of the origin of delay.

It is useful to introduce the loss factor or loss tangent $(\tan\delta)$. The ratio of μ'' to μ', from equation (3.31), gives

$$\frac{\mu''}{\mu'} = \frac{\dfrac{B_0}{H_0}\sin\delta}{\dfrac{B_0}{H_0}\cos\delta} = \tan\delta \qquad (3.32)$$

This $\tan\delta$ is called the Loss factor or Loss tangent. The Q-factor or quality factor is defined as the reciprocal of this loss factor, i.e.

$$Q = \frac{1}{\tan\delta} \qquad (3.33)$$

and the relative quality factor $= \dfrac{\mu_i}{\tan\delta}$. The behavior of μ' and μ'' versus frequency is called the permeability spectrum. The initial permeability of a ferromagnetic substance is the combined effect of the wall permeability and rotational permeability mechanism.

3.7.1 Measurement of Initial Permeability

The real part of initial permeability is calculated by using the formula

$$\mu' = \frac{L}{L_0} \qquad (3.34)$$

Where L is the self-inductance of the sample core and

$$L_0 = \frac{\mu_0 N^2 S}{\pi d} \qquad (3.35)$$

Where L_0 is the inductance of the winding coil without sample core and N is the number of the coil (here N=10), S is the area of cross-section as given below

$$S = \frac{m}{\pi\rho d} \qquad (3.36)$$

Where m = weight of the ribbon, d and ρ are the mean diameter and density of the sample as follows

$$d = \frac{d_1 + d_2}{2} \quad \text{and} \quad \rho = \frac{8M}{Na^3} \tag{3.37}$$

For our present experiment the amorphous ribbon was wound into toroid shape. The initial permeability of this toroid shaped sample was measured by obtaining the L value provided by an inductance analyzer used for permeability measurement as value of L_0 is derived by the calculation given above.

3.7.2 Relative Permeability

At microwave frequency, and also in low anisotropic amorphous materials, dB and dH may be in different directions, the permeability thus as tensor character. In the case of amorphous materials containing a large number of randomly oriented magnetic atoms the permeability will be scalar. As we have

$$B = \mu_o (H + M) \tag{3.38}$$

and Susceptibility

$$\chi = \frac{dM}{dH} = \frac{d}{dH}\left[\frac{B}{\mu_o} - H\right] \tag{3.39}$$

$$\chi = \frac{1}{\mu_o}\left(\frac{dB}{dH}\right) - 1 = \frac{\mu}{\mu_o} - 1 \tag{3.40}$$

Relative permeability, sometimes denoted by μ_r, is the ratio of the permeability of a specific medium to the permeability of free space μ_o.

$$\mu_r = \frac{\mu}{\mu_o} \tag{3.41}$$

In terms of relative permeability, the magnetic susceptibility is

$$\chi_m = \mu_r - 1 \tag{3.42}$$

3.7.3 High Frequency Behavior and Losses

The frequency dependence of the absolute value of complex permeability and its imaginary part μ'' are expressed in terms of the relative loss factor $\dfrac{\mu''}{|\mu|^2}$. The later is directly related to the cycle losses at constant induction amplitude B by

$$\frac{p}{f} = \frac{\pi B^2 \mu''}{\mu_o |\mu|^2} \qquad\qquad (3.43)$$
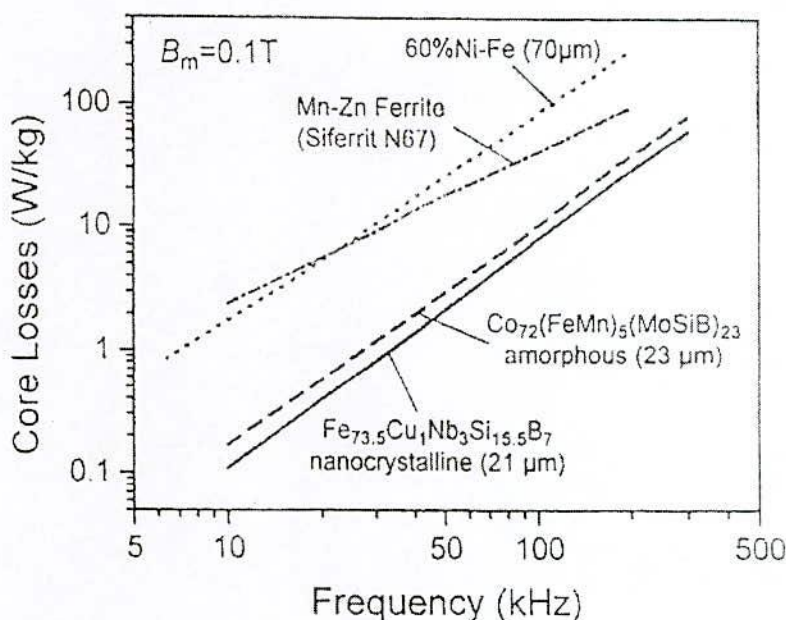
Fig. 3.5 Low core losses of Fe-based nanocrystalline alloy at high frequency

The favorable high frequency behavior is essentially related to (i) the thin ribbon gauge of $d \approx 20\mu m$ inherent to the production technique and (ii) to a relatively high electrical resistivity of typically $\rho \approx 115\mu\Omega - cm$ related to the high Si-content in the bcc grains [3.32] and the intergranular amorphous phase. Both parameters are comparable to amorphous metals and yield low eddy current losses p_e, which in thin sheets at a frequency f and a induction level B are given per volume by [3.33]

$$p_e = \left(\frac{3\sinh x - \sin x}{x\cosh x - \cos x} \right) \frac{(\pi d f B)^2}{6\rho}$$

$$|p_e|_{x\angle\angle 1} = \frac{(\pi d f B)^2}{6\rho} \tag{3.44}$$

$$\text{with } x = 2\sqrt{\frac{f}{f_w}}, \quad \text{where } f_w = \frac{4\rho}{\pi\mu_o\mu_i d^2}, \tag{3.45}$$

is the limiting frequency above which the exciting magnetic field no longer fully penetrates the specimen and, accordingly, the permeability decreases as a function of the frequency.

3.8   Magnetic Dipole Moments and Magnetization

The vast majority of soft magnetic materials have one or more of the ferromagnetic transition metal elements Fe, Co or Ni or the rare earth metal Gd as a majority component. The magnetic dipole moments of elemental and alloy magnets are most completely understood through the Band Theory of Solids [3.34]. The band theory of solids considers the broadening of localized atomic state with discrete eigenvalues into a continuum of states for more itinerant electrons over a range of energies. The theory allows for calculation of energy dispersion (i.e. energy as a function of wave vector) and orbital angular momentum specific and spin resolved densities of states. The calculation of spin resolved energy bands and densities of states allows for the description of atom resolved magnetic dipole moments and therefore, spontaneous magnetization of elemental and alloy magnetic properties are:

(i)   The prediction of non-integral or half integral atomic dipole moments and resulting ground state magnetizations in metals and alloys.

(ii)   The prediction that band width and exchange splitting (energy differences between spin up and spin down bands) are intimately dependent on magnetic coordination number and atomic value.

Table-3.1 summarizes absolute zero and room temperature (where applicable) magnetizations and atomic dipole moments for some important transition metal and rare earth elemental magnets. Also shown are Curie temperature i.e. ferromagnetic ordering

temperatures which are not ground state properties that are directly calculable from band theory.

Table-3.1 Spontaneous and room temperature magnetizations, magnetic dipole moments and Curie temperatures for elemental ferromagnets

Element	μ_m @ 0K (μ_B)	M_S @ 0K	M_S @ RT	T_c (K)
Fe	2.22	1740	1707	1043
Co	1.72	1446	1400	1388
Ni	0.606	510	485	627
Gd	7.63	2060	......	292
Dy	10.2	2920	.....	88

The number of spin up, n_+ and spin down n electrons in each band can again be calculated by integrating these densities of state:

$$n_+ = \int_0^{E_F^+} g_+(E)dE \quad \text{and} \quad n_- = \int_0^{E_F^-} g_-(E)dE \tag{3.46}$$

Here the Fermi energies, E_F, are the same and the zero's of energy are different for the two spin bands and the atom resolved (i.e. Fe and Co) magnetic magnetic dipole moments can be calculated

$$\mu_m = (n_+ - n_-)\mu_B \tag{3.47}$$

Knowledge of atomic values or alloy density, then allows for the direct calculation of the alloy magnetization. Fe-Co alloys exhibit the largest magnetic inductions of any material, and also have Curie temperatures which are desirable for high temperature applications. Fe rich alloys typically have smaller inductions and lower Curie temperatures than Fe-Co alloys. Co alloys can also be soft but only if the f.c.c. phase of Co is present. Co rich alloys typically have smaller inductions asnd larger T_C's.

3.8.1 Ferromagnetic ordering (Curie) Temperatures

Ferromagnetism is a collective phenomenon since individual atomic moments interact so as to promote alignment with one another. This collective interaction gives

rise to the temperature dependence of the magnetization. Two models have explained the interaction between atomic moments. Mean Field Theory considers the existence of a non-local internal magnetic field, called the Weiss field, which acts to align magnetic dipole moments even in the absence of an applied field H_a. Heisenberg Exchange Theory considers a local (usually nearest neighbor) interaction between atomic moments (spins) which acts to align adjacent moments even in the absence of a field.

The basic assumption of the mean field theory is that this internal field is non-local and is directly proportional to the sample magnetization.

$$H_{INT} = \lambda_W M , \tag{3.48}$$

where the constant of proportionality, λ_W, is called the Weiss molecular field constant.

To consider ferromagnetic response in applied field, H_a, as well as the randomizing effects of temperature, we consider the superposition of the applied and internal magnetic fields. By analogy with the problem of paramagnetic moments, the average atomic dipole moment can be expressed in terms of the Brillouin function

$$< \mu_m > \ = \mu_m^{atom} B_J \left(\alpha' \right) , \tag{3.49}$$

where $\alpha' = -\left(\dfrac{\mu_0 \mu_m^{atom}}{K_B T} \right)(H + \lambda_W M)$ for a collection of classical dipole moments. The saturation magnetization

$$M_S = N_m < \mu_m^{atom} > \tag{3.50}$$

$$\frac{M}{N_m \mu_m^{atom}} = \frac{M}{M_s} = B_J \left[H + \lambda_w M \right] \tag{3.51}$$

Under appropriate conditions, this leads to solutions for which there is a non-zero magnetization (spontaneous magnetization) even in the absence of an applied field.

For $T > T_c$, the ferromagnetic Curie temperature the only solution to equation (4.43) is $M = 0$, i.e., no spontaneous magnetization and thus paramagnetic response. For $T < T_c$, we obtain solutions with a non-zero, spontaneous magnetization, the defining feature of a ferromagnet.

Ferromagnetic exchange interactions set the scale for Curie temperatures in ferromagnetic alloys. Interatomic exchange couplings can be calculated from first principles by considering the energy change associated with rotation of individual spins in the host material. These exchange interactions can be used within a mean field theory to estimate the Curie temperature. An empirical description of the variations of the exchange energy with interatomic spacing called the Bethe-Slater curve is instructive in describing the effect of alloying on ferromagnetic Curie temperatures. The interplay between electron-electron Coulomb interactions and the constraints of the Pauli Exclusion Principle determine the sign of the exchange interaction.

In transition metal solids a measure of the overlap between nearest neighbor d-orbital is given by the ratio of the atomic to the 3d ionic (or nearest neighbor) radius. In mean field theory the Curie temperature can be related to the exchange energy as follows:

$$T_C = \frac{2S(S+1)}{3K_B} \sum_{ij} T_{ij} \ ,$$
(3.52)

where S is the total spin angular momentum, K_B is the Boatman's constant and T_{ij} is the exchange interaction between atoms at the position r_i and r_j .

In first case, a unique constant exchange interaction between the magnetic atoms is assumed and the amorphous nature of the alloy is taken into account by calculating a random distribution of the local anisotropy field [3.33]. In the second approach is treating this problem of distribution of exchange integrals assumed in order to reflect the structural fluctuations in the amorphous alloy [3.35]. Both approaches predict that M vs. T curve will flat below that for the crystalline counter part.

3.8.2 Hysteresis

Magnetic hysteresis is an important phenomenon and refers to the irreversibility of the magnetization and demagnetization process, when a material shows a degree of irreversibility it is known as hysteretic. When a demagnetized ferromagnetic material is placed in as applied magnetic field grows at the expanse of the other domain wall. Such growth occurs by motion of the domain walls. Initially domain wall motion is reversible, and if the applied field is removes the magnetization will return to the initial demagnetized state. In this region the magnetization curve is reversible and therefore

does not show hysteresis. The crystal will contain imperfections which the domain boundaries encounter during their movement. These imperfections have an associated magnetostatic energy when a domain wall intersects the crystal imperfection this magnetostatic energy can be eliminated as closure domains from this pins the domain wall to the imperfection as it if a local energy minima.

A great deal of information can be learned about the magnetic properties of a material by studying its hysteresis loop. A hysteresis loop shows the relationship between the induced magnetic flux density (**B**) and the magnetizing force (**H**). It is often referred to as the B-H loop. An example hysteresis loop is shown in Fig.-2.6.
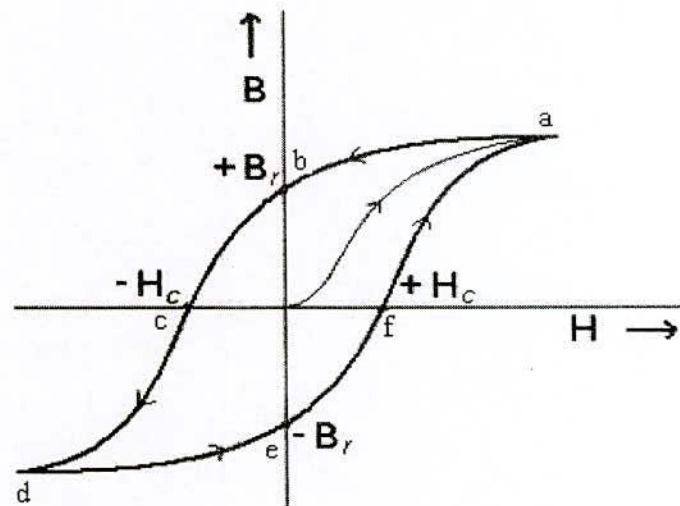
Fig. 3.6   Magnetic hysteresis loop

The loop is generated by measuring the magnetic flux of a ferromagnetic material while the magnetizing force is changed. A ferromagnetic material that has never been previously magnetized or has been thoroughly demagnetized will follow the dashed line as **H** is increased. As the line demonstrates, the greater the amount of current applied (+**H**), the stronger the magnetic field in the component (+**B**). At point "a" almost all of the magnetic domains are aligned and an additional increase in the magnetizing force will produce very little increase in magnetic flux. The material has reached the point of magnetic saturation. When **H** is reduced to zero, the curve will move from point "a" to point "b". At this point, it can be seen that some magnetic flux remains in the material even though the magnetizing force is zero. This is referred to as the point of retentivity on

52

the graph and indicates the remanence (B_r) or level of residual magnetism in the material. (Some of the magnetic domains remain aligned but some have lost their alignment). As the magnetizing force is reversed, the curve moves to point "c", where the flux has been reduced to zero. This is called the point of coercivity on the curve (The reversed magnetizing force has flipped enough of the domains so that the net flux within the material is zero).

The force required to remove the residual magnetism from the material is called the coercive force (H_c) or coercivity of the material. As the magnetizing force is increased in the negative direction, the material will again become magnetically saturated but in the opposite direction (point "d"). Reducing **H** to zero brings the curve to point "e." It will have a level of residual magnetism equal to that achieved in the other direction. Increasing **H** back in the positive direction will return **B** to zero. Notice that the curve did not return to the origin of the graph because some force is required to remove the residual magnetism. The curve will take a different path from point "f" back to the saturation point where it with complete the loop.

From the hysteresis loop, a number of primary magnetic properties of a material can be determined.

(i) **Retentivity:** A measure of the residual flux density corresponding to the saturation induction of a magnetic material. In other words, it is a material's ability to retain a certain amount of residual magnetic field when the magnetizing force is removed after achieving saturation. The value of **B** at point "b" on the hysteresis curve.

(ii) **Residual Magnetism** or **Residual Flux:** the magnetic flux density that remains in a material when the magnetizing force is zero. Residual magnetism and retentivity are the same when the material has been magnetized to the saturation point. However, the level of residual magnetism may be lower than the retentivity value when the magnetizing force did not reach the saturation level.

(iii) **Coercive Force:** The amount of reverse magnetic field which must be applied to a magnetic material to make the magnetic flux return to zero. The value of **H** at point "c" on the hysteresis curve.

Chapter -IV

Experimental Details

Experimental Details

4.1 Thermal Analysis Techniques

Thermal analysis comprises of a group of techniques in which a physical property of a substance is measured as a function of temperature, while the substance is subjected to a controlled temperature programme. The differential Thermal Analysis (DTA) ia an important technique for studying the structural change occurring both in solid and liquid materials under heat treatment. These changes may be due to dehydration, transition from one crystalline variety to another, destruction of crystalline lattice, oxidation, decomposition etc. The principle of DTA consists of measuring the heat changes associated with the physical or chemical changes that occur when a standard substance is gradually heated. This technique can also be used to identify magnetic ordering of nanocrystalline amorphous ribbons. The related technique of differential scanning calorimetry relies on difference in energy required to maintain the sample and reference at an identical temperature.

This technique has been used in determining the first crystallization temperature $\left(T_{x_1} \right)$ and secod crystallization temperature $\left(T_{x_2} \right)$ of our nanocrystalline soft magnetic material. The first crystalline temperature is defined as the temperature at which the alloy passes from the solid to liquid state. For our purpose it is sufficient to describe T_{x_1} as the temperature at which atomic mobility is great enough to allow diffusive rearrangement to occur in a matter of minutes. The crystallization temperature T_{x_2} is defined as the temperature at which crystallization occurs with long range ordering. Metallic nanocrystalline glass ribbons usually are ductile in the as quenched condition, but may often embrittled by exposure to elevated temperature.

DTA technique have been used to determine T_{x_1} and T_{x_2} of our nanocrystalline ribbon of composition $(Fe_{0.95}Co_{0.05})_{73.5}Cu_1Nb_3Si_{13.5}B_9$. Based on Kissinger plots, crystallization activation energy of T_{x_1} and T_{x_2} phases have been evaluated.

4.1.1 The Principle of Differential Thermal Analysis

The DTA technique was first suggest by Le Chatelier [4.1] in 1887 and was applied to the study of clays and ceramics. DTA involves heating or cooling a test sample and inert reference under identical conditions, while recording any temperature difference between the sample and reference. DTA is the process of accurately measuring the difference in temperature between a thermocouple embedded in a sample and a thermocouple in a standard inert material such as aluminum oxide, while both are being heated at a uniform rate. These differences of temperature arise due to phase transition or chemical reactions in the sample involving the evolution of heat or absorption of heat due to exothermic reaction or endothermic reaction measured. The exothermic and endothermic reactions are generally shown in data in the DTA trace as positive and negative deviations respectively from a baseline. This differential temperature is then plotted against time, or against temperature. When a sample and reference substance are heated or cooled at a constant rate under identical environment, their temperature differences are measured as a function of time or temperature as shown by the curve in Fig.4.1 (a).
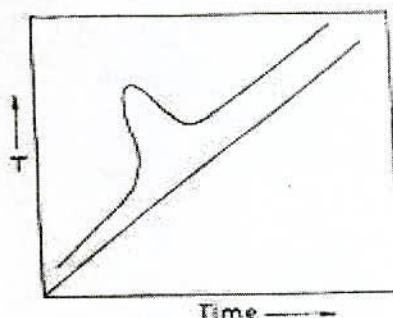
Fig. 4.1(a) Heating curve of sample and reference substance

The temperature of the reference substance, which is thermally inactive, rises uniformly when heated, while the temperature of the sample under study changes anomalously when there is physical or a chemical change of the active specimen at a particular temperature. When there is an exothermic reaction there is a peak in the

temperature versus time curve, heat supplied from outside is consumed by the reaction. And when the reaction is over, the sample temperature gradually catch up the temperature of the inactive specimen. The temperature difference ΔT is defined, amplified and recorded by a peak as shown in Fig. 4.1 (b).
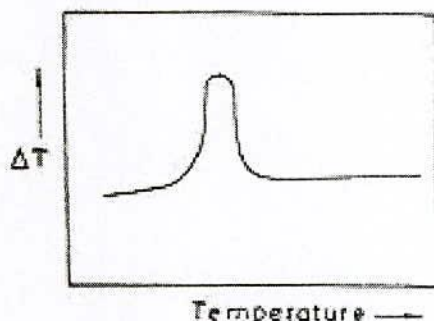
Fig.4.1 (b) DTA Curve

For any endothermic reaction or change the active specimen absorbs heat which is reflected in the corresponding the trough in temperature versus time curve. Changes in the sample, which leads to the absorption or evolution of heat, can be detected relative to the inert reference. Differential temperatures can also arise between two inert samples when their response to the applied heat treatment is not identical. DTA can therefore be used to study thermal properties and phase changes which do not lead to a change in enthalpy.

Changes in the sample, either exothermic or endothermic, can be detected relative to the inert reference. Thus, a DTA curve provides data on the transformations that have occurred, such as glass transitions, crystallization, melting and sublimation. The baseline of the DTA curve showed then exhibit discontinuities at the transition temperatures and the slope of the curve at any point will depend on the microstructural constitution at that temperature. The area under a DTA peak can be related to the enthalpy change and is not affected by the heat capacity of the sample. DTA may be defined formally as a technique for recording the difference in temperature between a substance and a reference material against either time or

56

temperature as the two specimens are subjected to identical temperature regimes in an environment either heated or cooled at a controlled rate.

4.1.2 Apparatus

The key features of a DTA kit are as shown in Fig. 4.2 sample holder comprising thermocouples, sample containers and a ceramic or metallic block, a furnace, temperature programmer, recording system. The essential requirements of the furnace are that it should provide a stable and sufficiently large hot-zone and must be able to respond rapidly to commands from the temperature programmer. A temperature programmer is essential in order to obtain constant heating rates. The recording system must have a low inertia to faithfully reproduce variations in the experimental set-up.
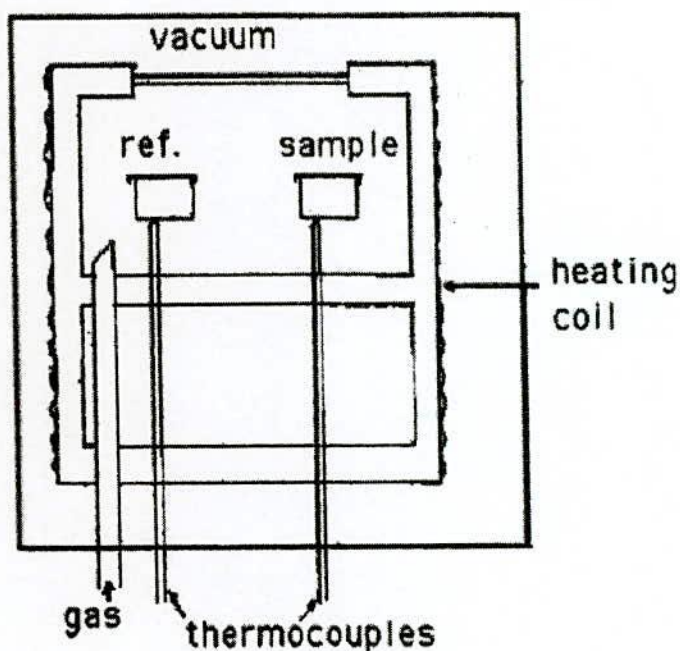
Fig.4.2 Schematic illustration of a DTA cell

The sample holder assembly consists of a thermocouple each for the sample and reference, surrounded by a block to ensure an even heat distribution. The sample is contained in a small crucible designed with an indentation on the base to ensure a

57

snug fit over the thermocouple bead. The crucible may be made of materials such as pyrex, silica, nickel or platinum, depending on the temperature and nature of the tests involved. The thermocouples should not be placed in direct contact with the sample to avoid contamination and degradation, although sensitivity may be compromised. Metallic blocks are less prone to base-line drift when compared with ceramics which contain porosity. On the other hand, their high thermal conductivity leads to smaller DTA peaks.

The sample assembly is isolated against electrical interference from the furnace wiring with an earthed sheath, often made of platinum-coated ceramic material. The sheath can also be used to contain the sample region within a controlled atmosphere or a vacuum.

During experiments a temperature problems are encountered in transferring heat uniformly away from the specimen. These may be mitigated by using thermocouples in the form of flat discs to ensure optimum thermal contact with the now flat-bottomed sample container, made of aluminum or platinum foil. To ensure reproducibility, it is then necessary to ensure that the thermocouple and container are consistently located with respect to each other.

4.1.3 Experimental Factors

Care is necessary in selecting the experimental parameters. For example, the effects of specimen environment, composition, size and surface to volume ratio all affect powder decomposition reactions, whereas these particular variables may not affect solid state phase changes. Experiments are frequently performed on powders so the resulting data may not be representative of bulk samples, where transformations may be controlled by the build up of strain energy. The packing state of any powder sample becomes important in decomposition reactions and can lead to large variations between apparently identical samples.

In some circumstances, the rate of heat evolution may be high enough to saturate the response capability of the measuring system; it is better than to dilute the test sample with inert material. For the measurement of phase transformation

temperatures, it is advisable to ensure that the peak temperature does not vary with sample size. The shape of a DTA peak does depend on sample weight and the heating rate used. The influence of heating rate on the peak shape and disposition can be used to advantage in the study of decomposition reactions, but for kinetic analysis it is important to minimize thermal gradients by reducing specimen size or heating rate.

4.1.4 Interpretation and Presentation of DTA

There are difficult with the measurement of transition temperatures using DTA curves. The onset of the DTA peak in principle gives the start-temperature, but there may be temperature lags depending on the location of the thermocouple with respect to the reference and test samples or the DTA block. It is wise to calibrate the apparatus with materials of precisely known melting points. The peak area (A), which is related to enthalpy changes in the test sample, is that enclosed between the peak and the interpolated baseline. When the differential thermocouples are in thermal, but not in physical contact with the test and reference materials, it can be shown that A is given by,

$$A = \frac{mq}{gk} \quad , \tag{4.1}$$

where m is the sample mass, q is the enthalpy change per unit mass, g is a measured shape factor and k is the thermal conductivity of sample.

With porous, compacted or heaped samples, the gas filling the pores can alter the thermal conductivity of the atmosphere surrounding the DTA container and lead to large errors in the peak area. The situation is made worse when gases are evolved from the sample, making the thermal conductivity of the DTA-cell environment different from that used in calibration experiments. The DTA apparatus is calibrated for enthalpy by measuring peak areas on standard samples over specified temperature ranges. The calibration should be based upon at least two different samples, conducting both heating and cooling experiments.

In the present work, SEIKO TG/DTA 6300 has been used for thermal analysis. The TG/DTA is a simultaneous measurement instrument combining TG, which utilizes a horizontal differential type balance beam, with the highly flexible DTA

feature. This instrument is used for reaction velocity and acceleration degradation tests, as well as analysis of the water and ash content in samples, and evaluation of decomposition, oxidation and heat resistance of samples.

The features are:

(i)   As a forerunner in the balance beam mechanism, this instrument utilizes a horizontal differential type balance beam. The lightweight structure of the balance beam mechanism provides the following strong points: stability in regards to temperature fluctuations, buoyancy reduction and highly sensitive balance, as well as the ability of the differential balance to deal with disturbances such as oscillation.

(ii)   Through the utilization of an automatic cooling unit, the instrument is now automatically cooled to a set temperature after measurements, which raises the effectiveness of measurements.

(iii) As with the DSC, the auto sampler is easily attached to the TG/DTA.

Temperature range is ambient to 1773 K; balance method is horizontal differential type; TG measurement range is ± 200 mg; DTA measurement range is ± 1000 μV; program rate is 0.01 to 100 K/min; gas flow rate is 0 to 1000 ml/min; cooling rate is less than 15 minutes from 1273 to 323 K.

4.2   Annealing

Annealing in metallurgy and materials science, is heat treatment wherein a material is altered, causing changes in its properties such as strength and hardness. It is a process that produces conditions by heating to above the critical temperature, maintaining a suitable temperature, and then cooling. Annealing is used to induce ductility, soften material, relieve internal stresses, refine the structure by making it homogeneous, and improve cold working properties.

In the cases of copper, steel, silver and brass, this process is performed by substantially heating the material (generally until glowing) for a while and allowing it to cool. Unlike ferrous metals, which must be cooled slowly to anneal, copper, silver and brass can be cooled slowly in air or quickly by quenching in water. In this fashion

the metal is softened and prepared for future work such as shaping, stamping, or forming.

Annealing occurs by the diffusion of atoms within a solid material, so that the material progresses towards its equilibrium state. Heat is needed to increasing the rate of diffusion by providing the energy needed to break bonds. The movement of atoms has the effect of redistributing and destroying the dislocations in metals and (to a lesser extent) in ceramics. This alternation in dislocations allows metals to deform more easily, so increases their ductility.

4.2.1 Stages

There are three stages in the annealing process, with the first being the recovery phase, which results in softening of the metal through removal of crystal defects (the primary type of which is the linear defect called a dislocation) and the internal stresses which they cause. Recovery phase covers all annealing phenomena that occur before the appearance of new strain-free grains. The second phase is recrystallization, where new strain-free grains nucleate and grow to replace those deformed by internal stresses. If annealing is allowed to continue once recrystallization has been completed, grain growth will occur, in which the microstructure starts to coarsen and may cause the metal to have less than satisfactory mechanical properties.

4.2.2 Setup and Equipment

Typically, large ovens are used for the annealing process. The inside of the oven is large enough to place the work piece in a position to receive maximum exposure to the circulating heated air. For high volume process annealing, gas fired conveyor furnaces are often used. For large work piece or high quantity parts, Car-bottom furnaces will be used in order to move the parts in and out with ease. Once the annealing process has been successfully completed, the work pieces are sometimes left in the oven in order for the parts to have a controlled cooling process. While some work pieces are left in the oven to cool in a controlled fashion, other materials and alloys are removed from the oven. After being removed from the oven, the work pieces are often quickly cooled off in a process known as quench hardening. Some

typical methods of quench hardening materials involve the use of media such as air, water, oil or salt. Quench hardening is generally applicable tp some ferrous alloys, but not copper alloys.

4.3 Thermal Treatment of the Amorphous Ribbon

With a view to study nanocrystallization behavior by XRD and magnetic properties upon evaluation of nanocrystalline phase on amorphous matrix thermal treatment, i.e. annealing is required to perform. For XRD, as prepared amorphous ribbon were cut into small pieces of about 2cm lengths and for magnetic measurement such as permeability torodial core were wound for annealing treatment. A laboratory built vacuum system made by quartz tube capable of evaluating up to 10^{-5} torr was used for their purpose. The samples were put into the quartz tube and evaluated (10^{-5} torr) before it had been put inside the tabular furnace heated to a present temperature and kept for the time required to complete the annealing. In this way all the isothermal annealing as a function of time were performed.

4.4 Powder/ Polycrystalline Diffraction

About 90% of all solid materials can be described as crystalline. When X-ray interact with a crystalline substance (phase) one get a diffraction pattern. The X-ray diffraction pattern of a pure substance is, therefore, like a fingerprint of the substance. The powder diffraction method is thus ideally suited for characterization and identification of polycrystalline phases. Today about 50000 inorganic and 25000 organic single component, crystalline phase, diffraction patterns have been collected and stored on magnetic or optical media as standers. The main use of powder diffraction is to identify components in a sample by a search/ match procedure. Furthermore, the areas under the peak are related to the amount of each phase present in the sample.
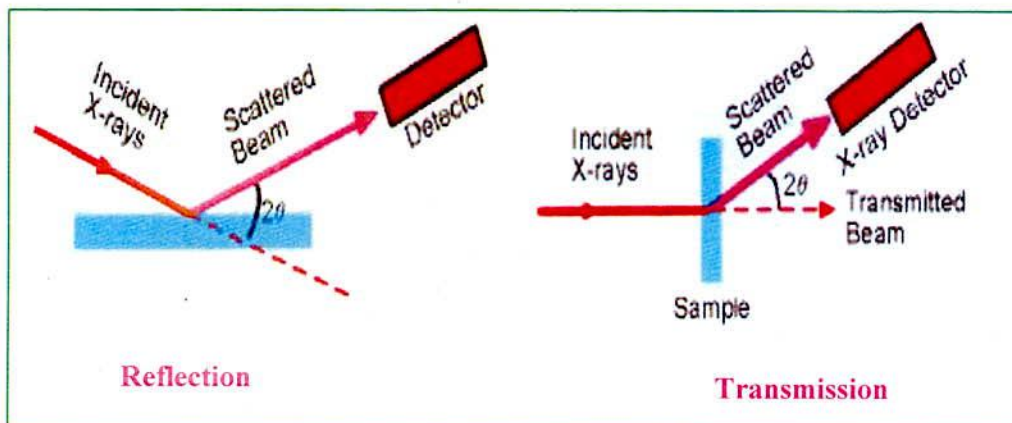
Fig. 4.4 Reflection and Transmission geometry of powder diffraction

4.4.3 Experimental Technique for X-ray diffractometer

X-ray diffraction (XRD) is a versatile non-destructive analytical technique for identification and quantitative determination of various crystalline phases of powdered or solid samples of any compound. For each set of composition, ribbons are cut into several pieces; each of length 20 mm. Heat treatment was performed on the amorphous ribbons using a naber muffle furnace, where each piece of ribbon was wrapped by aluminum foil separately. After heat treatment, samples were removed from the aluminum foil carefully and kept separately for XRD experiment.

For XRD experiment each sample was set on a glass slides and fixed the sample by putting adhesive tape at the two ends of the sample. After the pattern is obtained the value of 2θ is calculated for each diffraction line; set of 2θ values is the raw data for the determination of the lattice parameters of the unit cell. Fig. 4.5: Shows the block diagram of Phillips PW 3040 X'Pert PRO X-ray diffractometer. A PHILIPS PW 3040 X'Pert PRO X-ray diffractometer was used for the lattice parameter determination in the Materials Science Division, Atomic Energy Centre, Dhaka. Fig. 4.6 shows the inside view of the X'Pert PRO XRD system. The X'Pert Pro diffraction system utilizes a modular system approach to provide performance for application ranging from routine characterization to in-depth research investigation.

65
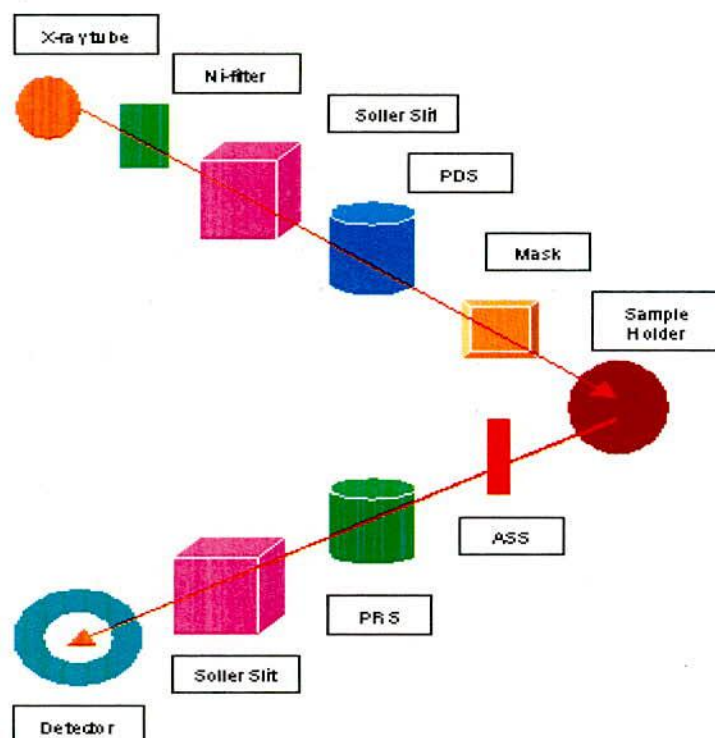
Fig. 4.5 Block diagram of the PHILIPS PW 3040 X'Pert PRO XRD system

The powder diffraction technique was used with a primary beam power of 40 kV and 30 mA for Cu radiation. A nickel filter was used to reduce Cu-K$_\alpha$ radiation and finally Cu-K$_\alpha$ radiation was only used as the primary beam. A (θ- 2θ) scan was taken from 30° to 90° to get possible fundamental peaks of the sample with the sampling pitch of 0.02° and time for each step data collection was 1.0 sec. Both the programmable divergence and receiving slits were used to control the irradiated beam area and output intensity from the sample, respectively.

An anti scatter slit was used just after the sample holder to reduce air scattering. Two solar slits were used just after the tube and in front of the detector to get parallel beam only. All the data of the samples were stored in the computer memory and later analyzed those using computer software "X PERT HIGHSCORE".

The Specifications of Philips X'Pert Pro Multipurpose X-ray Diffractometer systems are as follow:

- **X-ray Sources:** 3 kW Copper tube and 2 kW Cobalt tube
- **Optics:** Focussing and parallel PreFix optics, programmable slits, tunable diffracted beam monochromator.
- **Detectors:** Xe proportional counter and solid state X'cellerator
- **Sample stages:** Single sample holder, 15-sample changer, sample spinning capability
- **Variable temperature capability:** Anton-Paar 77 to 725 K and 300 to 1475 K cameras
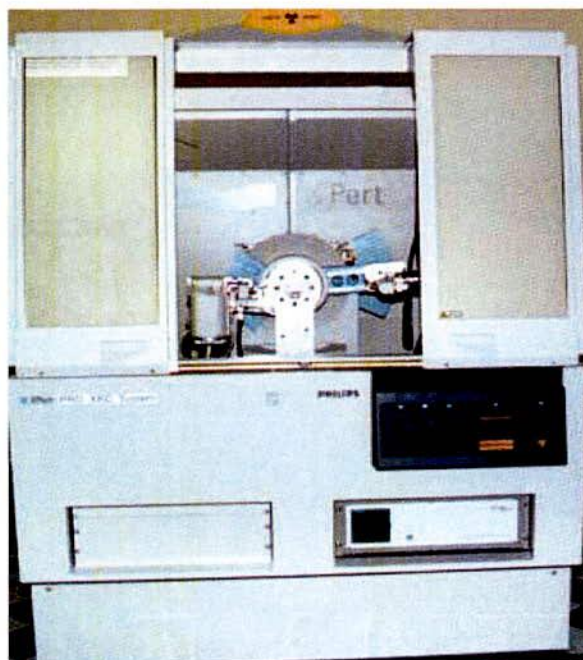
Fig.4.6 A Philips PW 3040 X'Pert PRO X-ray diffractometer

- **Software and databases:** ICDD PDF-2 database (2002). Hi-Score search-match software, X'Pert Plus crystallographic analysis software with Rietveld capability, ProFit line profile analysis software.

- **Instrument statistics:** The system uses Cu-K$_\alpha$ radiation that has a wavelength of 1.54Å. Analysis are commonly run using a 40 kV 45mA X-ray tube voltage, a 0.04° solar slits, 1° divergence and antiscatter slits, and ½° (for powder) or ¼° (for clays) receiving slit.

4.4.4 Analysis of XRD data

The XRD data consisting of θ_{hkl} and d_{hkl} values corresponding to the different planes from which the following structural information of the nanocrystalline ribbon sample was evaluated.

(i)   Identification of phases

(ii)   Lattice parameter determination

(iii)   Average grain size determination

(iv)   Si- content determination in nanograins

(i)   Identification of phases

The most common use of powder (polycrystalline) diffraction is chemical analysis. This can include phase identification (search/match), investigation of high/low temperature phase, solid solutions and determination of unit cell parameter of new materials.

X-ray diffractometer has become a very popular and useful instrument for routine X-ray analysis of ribbon samples. In fact the diffractometer technique is often preferred to Debye-Scherrer technique owing to its several inherent merits. The most striking difference between the two methods is in the use of different intensity detection and measuring devices. XRD pattern of as-cast indicates just amorphous pattern of said composition. The XRD patterns are identified as bcc α-Fe(Si) solid solution, which are developed on the amorphous ribbon after heat treatment. The peak pattern is observed for all the samples at different heat treatment temperatures indicating the bcc α-Fe(Si) phase, which is developed on amorphous ribbons after heat treatment. Present experiment revels that 450°C is not sufficient temperature to

68

start forming of crystalline nanograins of bcc Fe(Si) on the amorphous ribbon of the studied alloy composition.

(ii)   Lattice Parameter Determination

Lattice parameter of crystalline bcc Fe-Si nanograins has been determined for all the two different amorphous compositions at different heat treatment temperatures. Normally, lattice parameter of an alloy composition is determined by the Debye-Scherrer method after extrapolation of the curve. In this method, at least five fundamental reflections are required to determine lattice parameter. In the present case, only one reflection (110) is prominent in all XRD patterns and we would like to understand how the value of lattice parameter changes with annealing temperature. We have, therefore, determined the lattice parameter using only that particular reflection using equation $2d\sin\theta = \lambda$ and $a_0 = d\sqrt{2}$, where $\lambda = 1.54178\,\text{Å}$ for $Cu - K_\alpha$ radiation and a_0 is the determined lattice parameter within an error estimated to be $\pm 0.0001\,\text{Å}$.

(iii)   Grain Size Determination

The main aim (vital point) of the present study is to determine the nanocrystalline grain size for all the heat treated samples of the alloy composition by using Scherrer method. The XRD pattern of (110) reflection for different steps of heat treatment temperature of the alloy composition is used to calculate grain size. Grain size is determined using the following formula,

$$D_g = \frac{0.9\lambda}{\beta\cos\theta},\tag{4.3}$$

where $\lambda = 1.54178\,\text{Å}$ for $Cu - K_\alpha$ radiation and β = FWHM (full width at half maximum) of the peak in radian. Considering β in degree we get the following relation

$$D_g = \frac{79.5}{\beta \cos\theta} \qquad\qquad (4.4)$$

All the values of grain size for every steps of heat treatment temperature of the alloy composition were determined. The FWHM of the peak is large at the early heat treatment temperature and with the increase of heat treatment temperature the value of FWHM becomes smaller which means that the grain size is increasing gradually.

(iv)　Si-content in Nanograins

Crystalline nanograins were formed on the amorphous matrix of the ribbon in the process of heat treatment having the composition of Fe-Si. It is, therefore important to determine the concentration of Fe and Si in the nanograin. As because the alloy consists of Fe and Si and we have experimentally determined the lattice parameter of the alloy nanograin for the two compositions at different temperatures. It is easy to calculate the Si content in the nanograins from the data of Pearsons who was established the relationship between the lattice parameter as dependent on Si content in Fe-Si alloys covering a wide range of composition [4.2]. From the relationship, we have constructed a simple equation to calculate Si content from lattice parameter. The equation is

$$X = \frac{(a_0 - 2.8812)}{0.0022}, \qquad\qquad (4.5)$$

where X is at.% Si in the nanograins, a_0 is the determined lattice parameter of nanograins. Si-contents for the nanograins develop during the isothermal annealing at various temperatures have been calculated.

4.5　Impedance Analyzer

The Hewlett Packard 4192A LF Impedance Analyzer can measure eleven impedance parameters absolute value of impedance (|Z|), absolute value of admittance (|Y|), phase angle (θ), resistance (R), reactance (X), conductance (G), susceptance (B), inductance (L), capacitance (C), dissipation factor (D) and quality factor (Q).

Measurement range of $|Z|/R/X$ is 0.1 mΩ; to 1.2999 MΩ; $|Y|/G/B$ is 1ns to 12.999s; θ is -180.00° to +180.00°; L is 0.01 mH to 1.000 kH; C is 0.1 pF to 100.0 mF; D is 0.0001 to 19.999; Q is 0.1 to 1999.9. All have a basic accuracy of 0.1% and resolution of $4\frac{1}{2}$ digits. Number of display digits dependence on measuring frequency and OSC level setting. We made use of the excellent experimental facilities available at the Materials Science Division, Atomic Energy Centre, Dhaka.

The 4192A can provide measuring frequency, OSC level, and dc bias voltage equivalent to actual operating conditions. The sweep capabilities of the built-in frequency synthesizer and dc bias source permits quick and accurate measurements. The built- in frequency synthesizer can be set to measuring frequency within the range from 5 Hz to 13 MHz with 1 mHz maximum resolution. OSC level is variable from 5 mV to 1.1 Vrms with 1 mV resolution. The internal dc bias voltage source provides ± 35 V in 10 mV increments. Measuring frequency or dc bias voltage can be automatically or manually swept in either direction. OSC level can be manually swept in either direction in 1 mV increments (5 mV for levels above 100 mV). Actual test voltage across or test signal current through the device under test is also measured. Thus the 4192A can evaluate components and circuits under a wide variety of measurements conditions.

Moreover, the 4192A's high measurement performance and capable functionality delivers a powerful tool to circuit design and development as well as materials research and development (both electronic and non electronic materials) environments:

*Accurate measurement over wide impedance range and wide frequency range.

* Powerful impedance analysis function.

* Ese of use and versatile PC connectively.

The following are application examples;

- Impedance measurement of two terminal components such as capacitors, inductors, ferrite beads, resistors, transformers, crystal/ceramic resonators, multi-chip modules or array/network components.

Semiconductor components

- C – r characteristic analysis of varac for diodes.
- Parasitic analysis of a diode, transistor or IC package terminal/leads.
- Amplifier input/output impedance measurement.
- Impedance evaluation of printed circuit boards, relays, switches, cables, batteries etc.

Dielectric materials

- Permittivity and loss tangent evaluation of plastics, ceramics, printed circuit boards and other dielectric material

Magnetic materials

- Permeability and loss tangent evaluation of ferrite, amorphous and other magnetic materials.

Semiconductor material

- Permittivity, conductivity and C – V characteristics of semiconductor materials.
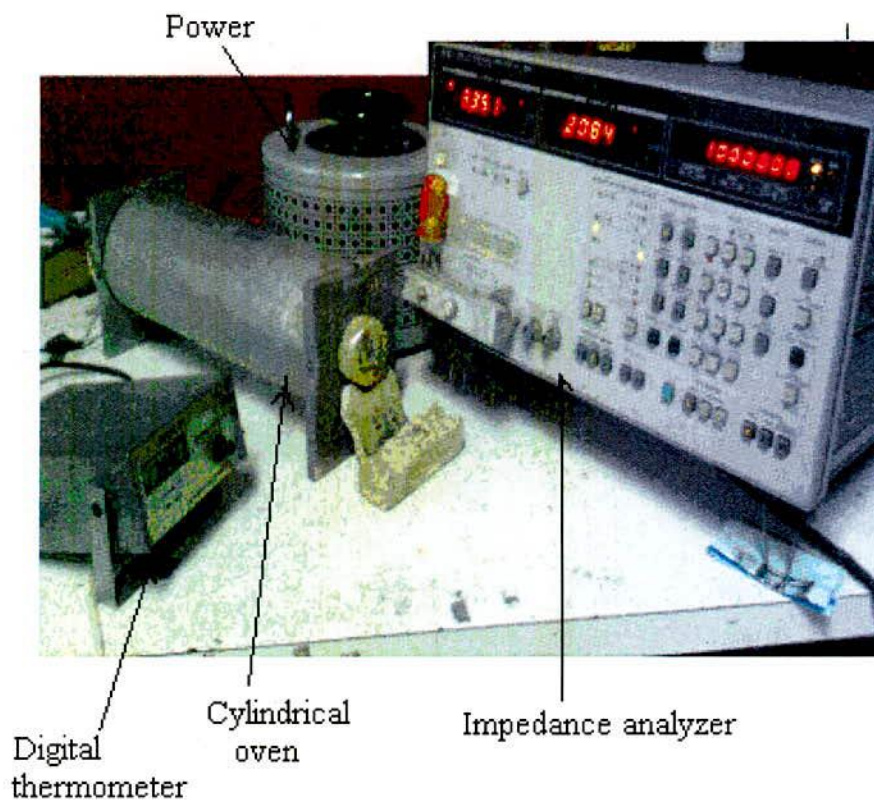
Fig. 4.7   Impedance Analyzer Model-Hewlett-Packard 4192A

72

4.5.1 Preparation of the Samples for Complex Permeability Measurement

The amorphous ribbon were wound into toroidal having outer and inner diameters 13 to 15 mm and with the ratio of outer and inner diameters always kept less than 1.2 in order to improve the homogeneity of the applied field, as also to reduce the possibility of an inhomogeneous inductance response. Toroids were wound with 5 turns around to apply AC magnetic fields over a wide range of amplitudes. While measuring the permeability of the amorphous ribbon cores at high frequency, the high electric resistance of these materials generally precludes the trouble some skin effect found in ribbons. However, the cross-section of the amorphous ribbon core to be measured may have to be kept small in order to avoid dimensional resonance phenomena. To avoid an increase in resistance owing to skin effect, braided copper wire is used at frequencies higher than 100 kHz.

At higher frequencies the capacitance arising from winding gives inaccurate values of R and L_s. It is, there fore, necessary to keep the capacitance of the winding as low as possible. Frequency response characteristics were then investigated on these ring shaped specimens as a function of frequency.

4.5.2 Components of Complex Permeability Measurements

The real (μ') and imaginary (μ'') part of the complex permeability of the as-cast and annealed ribbons were measured as a function of frequency using the Hewlett Packward 4192A LF Impedance Analyzer, Atomic Energy Centre, Dhaka. From the frequency dependence of complex permeability, evolution of permeability and magnetic loss component at different stages of nanocrystallization as affected by thermal treatment at different temperatures was determined using toroids prepared from the ribbons wound with insulating Cu wire.

The HP 4192 A impedance analyzer directly measure the value of inductance, L˙and loss factor,

$$D = \tan \delta \qquad (4.6)$$

From inductance the value of real part of complex permeability, μ' can be obtained by using the relation

$$\mu' = \frac{L}{L_0} \tag{4.7}$$

Here, L is the inductance of the toroid and L_0 is the inductance of the coil of same geometric shape in vacuum. L_0 is determined by using the relation

$$L_0 = \frac{\mu_0 N^2 S}{\pi d} \tag{4.8}$$

Where $S = \dfrac{m}{\pi \rho d}$, μ_0 is the permeability of the vacuum, m is the mass of the sample, N is the number of turns, S is the cross-sectional area of the toroid, d is the average diameter and ρ is the density of the material. The imaginary part of complex initial permeability can be determined by using the relation,

$$\tan \delta = \frac{\mu''}{\mu'} \tag{4.9}$$

and the relative loss factor is calculated with the relation $\dfrac{\tan \delta}{\mu'}$ or $\mu'Q$

4.6   Curie Temperature Measurements

Curie temperature, T_c, is the most important parameter of magnetic materials. The magnetic properties and magnetic structures are effectively changed within the Curie temperature. Curie temperature provides substantial information on magnetic states of substances in respect of the strength of exchange interaction. So the determination of Curie temperature accurately is of great importance. Curie temperature can be determined from the temperature dependence of permeability, temperature dependence of magnetization curve and Arrott plot. Sometimes an operational procedure needs to be adopted for the determination of T_c. A standard procedure for determination T_c in ferromagnetic materials is based on symmetry principle. Arrott [4.3], Belov [4.4], and Kouvel [4.5] have pioneered the use of classical form of expression for magnetization and field near a ferromagnetic phase transition.

Temperature dependence of the initial permeability of the as-cast and annealed ribbons have been measured using a laboratory built furnace and Wayne Kerr 3255 B inductance meter with continuous heating rate of $\approx$ 5 K / min with very low applied ac field of $\approx 10^{-3}$ Oe. From this measurement, T_c of the as-cast and annealed samples have been determined. In addition to the measurement of T_c, temperature dependence of initial permeability at different stages of crystallization has been studied for $(Fe_{0.95}Co_{0.05})_{73.5}Cu_1Nb_3Si_{13.5}B_9$ soft nanocrystalline magnetic materials.

4.6.1 Inductance Analyzer

The 3255B Precision Magnetics Analyzer provides 2-terminal measurement of inductors and transformers over the frequency range 20 Hz to 500 kHz. DC resistance measurements are performed at a drive level of 100 mV. The drive level for AC measurements can be varied from 1 mV to 10 V rms. Automatic level control (ALC) can maintain the drive level at the component. During AC measurements the 3255B can supply a DC bias current which is variable between 1 mA and 1 A and when used with external 3265B DC bias units, up to 125 A DC bias current is available.

The analyzer's measurement, display and control facilities include:

- Spot frequency measurements;
- Multi-frequency measurements at a number of user-defined frequencies;
- Display of actual measurement values;
- Output of measurement results to an Epson-compatible printer;
- Strong of components into bias according to their measured value and/or minor term (option)

All the above functions can be selected via manual front panel control or remote control via the GPIB interface for fully-automated high-speed testing. Self calibration is performed to set calibration constants for signal processing elements in the measurement hardware and signal generation system, and to compensate for components, which drifted with time. To maintain full specified accuracy it should be run at least every three months. To measure the inductance of a component the analyzer should be powered up with the test leads or fixture connected to the font panel BNC connectors. The analyzer should be operated in Measurement Mode. The

component to be measured is connected to the test leads or fixture. The measurement may be performed as single short mode for single measurement or repetitive mode for continuous measurement.

4.7   Magnetization Measurement Techniques

In the present study magnetization has been performed using a Vibrating Sample Magnetometer (VSM).

4.7.1   Vibrating Sample Magnetometer (VSM)

A vibrating sample magnetometer (VSM) operates on Faraday's Law of Induction, which tells us that a changing magnetic field will produce an electric field. This electric field can be measured and can tell us information about the changing magnetic field. A VSM is used to measure the magnetic behavior of magnetic materials. Vibrating Sample Magnetometer is a versatile and sensitive method of measuring magnetic properties developed by S. Foner [4.6-4.7] and is based on the flux change in a coil when the sample is vibrated near it. The Vibrating Sample Magnetometer (VSM) is designed to continuously measure the magnetic properties of materials as a function of temperature and field. In this type of magnetometer, the sample is vibrated up and down in a region surrounded by several pickup coils. The magnetic sample is thus acting as a time-changing magnetic flux, varying inside a particular region of fixed area. From Maxwell's law it is known that a time varying magnetic flux is accompanied by an electric field and the field induces a voltage in pickup coils. This alternating voltage signal is processed by a control unit system, in order to increase the signal to noise ratio. The result is a measure of the magnetization of the sample.

4.7.2 Principle of VSM

If a sample is placed in a uniform magnetic field, created between the poles of a electromagnet, a dipole moment will be induced. If the sample vibrates with sinusoidal motion a sinusoidal electrical signal can be induced in suitable placed pick-up coils. The signal has the same frequency of vibration and its amplitude will be

76

proportional to the magnetic moment, amplitude, and relative position with respect to the pick-up coils system. Fig 4.8 shows the block diagram of vibrating sample magnetometer. The sample is fixed to a sample holder located at the end of a sample rod mounted in a electromechanical transducer. The transducer is driven by a power amplifier which itself is driven by an oscillator at a frequency of 90 Hz. So, the sample vibrates along the Z axis perpendicular to the magnetizing field. The latter induced a signal in the pick-up coil system that is fed to a differential amplifier. The output of the differential amplifier is subsequently fed into a tuned amplifier and an internal lock-in amplifier that receives a reference signal supplied by the oscillator.

The output of this lock-in amplifier, or the output of the magnetometer itself, is a DC signal proportional to the magnetic moment of the sample being studied. The electromechanical transducer can move along X, Y and Z directions in order to find the saddle point. Calibration of the vibrating sample magnetometer is done by measuring the signal of a pure Ni standard of known saturation magnetic moment placed in the saddle point. The basic instrument includes the electromechanical system and the electronic system (including a personal computer). Laboratory electromagnets or superconducting coils of various maximum field strengths may be used.
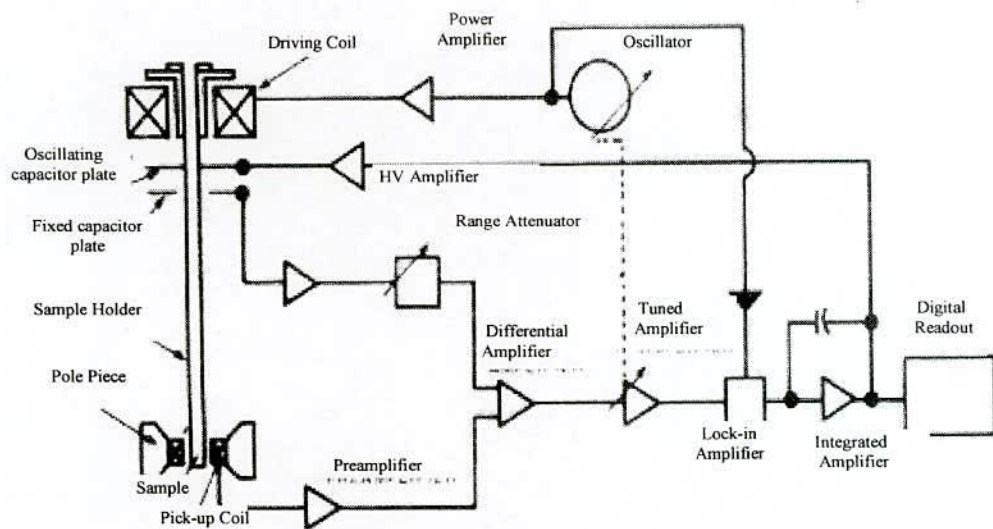
Fig. 4.8 Block diagram of vibrating sample magnetometer

77
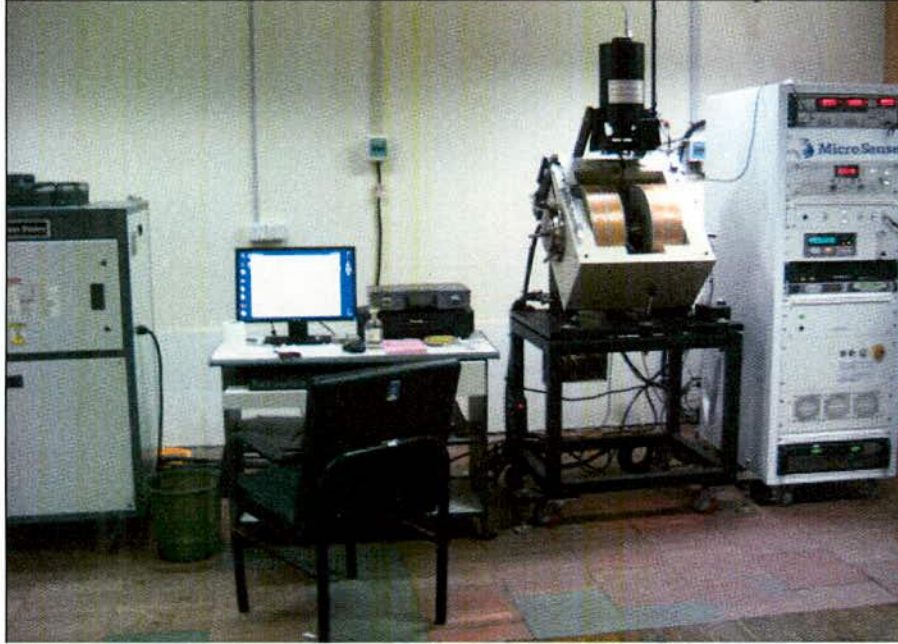
Fig. 4.9 Vibrating sample magnetometer

Chapter - V

Result and Discussions

Chapter-V Result and Discussions

5.1 Crystallization Behavior of $(Fe_{0.95}Co_{0.05})_{73.5}Cu_1Nb_3Si_{13.5}B_9$ Alloy

The understanding of the crystallization kinetics of magnetic amorphous / nanocrystalline alloys has various scientific and technical interest because of the enhancement as well as deterioration of magnetic properties extremely depends on the degree of crystallization. Calorimetric studies of amorphous alloys provide substantial fundamental information concerning the kinetics of crystallization and structural relaxation effects. The kinetics of the onset of crystallization has been studied calorimetrically by Clements and Cantor [5.1] and both calorimetrically and magnetically by Loborsky [5.2] in a variety of amorphous magnetic alloys. Crystallization kinetics is often determined from Differential Scanning Calorimetry (DSC), Differential Thermal Analysis (DTA) and in magnetic materials from the Thermomagnetic Analysis (TMA) [5.3-5.5]. Crystallization kinetics have also been studied by a variety of techniques including high resolution transmission electron microscope (HRTEM), in-situ XRD (X-ray Diffraction), Extended X-ray Absorption Fine Structure (EXAFS) measurements and resistance measurements.

If the amorphous alloy is to be used as a precursor for the production of nanocrystalline FINEMET of composition Fe-CU-Nb-B-Si then the primary and secondary crystallization temperatures are of importance. Because the structure of the beneficial ferromagnetic nanocrystalline phase is composed of Fe(Si), which is the product of primary crystallization. The secondary crystallization product is the Fe-B phase. The phase is detrimental for the soft magnetic properties because of its high anisotropy energy. For the present research on $(Fe_{0.95}Co_{0.05})_{73.5}Cu_1Nb_3Si_{13.5}B_9$ alloy, DTA has been performed to identify the crystallization temperatures as well as activation energy required for crystallization and the XRD experiment was undergone to identify the evolution of phases with heat treatment.

5.1.1 DTA Results of $(Fe_{0.95}Co_{0.05})_{73.5}Cu_1Nb_3Si_{13.5}B_9$ Alloy

Crystallization is non-reversible, exothermic process [5.6-5.7]. Calorimetric studies of amorphous alloy provide substantial and fundamental information concerning the kinetics of crystallization. DTA is a direct and effective way to analyze the kinetics of nanocrystalline materials in respect of phase transition.

The change of composition affects the growth kinetics in a complicated way, which can only be determined experimentally. The composition of the alloy affects both the primary and secondary crystallization phases, because the time needed for the constituent atom to have long range order depends on their bond energies [5.8-5.9]. Good soft magnetic properties of the materials require not only small grain size but at the same time the absence of boron compound. The separation between the primary crystallization of bcc Fe(Si) and the secondary product of Fe-B compounds not only is determined by the Cu and Nb additions but also on boron content. With the increase of boron content the separation between the two products decreases [5.10]. We kept at a moderate level of boron content in the nominal composition in order to obtain an optimum nanoscaled structure.

Regarding the study of FINEMET as an amorphous alloy, the identification of primary and secondary crystallization temperature carries much significance. Because the nanocrystalline phase comprising of FeCo(Si), is the product of primary crystallization. Again identification of the secondary crystalline product is FeCoB is also important because evolution of this phase is detrimental to soft magnetic properties. The separation between these two phases is required to be verified because the ultra soft magnetic behavior expected from the FeCoSi phase can be suitably achieved when boride phases do not overlap with this phase.

The crystallization process is affected by heating rate as well as by composition. To keep the stability of the nanocrystalline alloy to achieve the expected soft magnetic behavior, both the nucleation and growth rate of nanocrystallites must be controlled. To study the effect of composition on the stability of the amorphous and nanocrystalline alloy, heating

rate must be kept constant at any single DTA treatment. DTA is a direct and effective technique for analyzing the kinetics of crystallization of amorphous materials.

5.1.2 Study of DTA Traces of $(Fe_{0.95}Co_{0.05})_{73.5}Cu_1Nb_3Si_{13.5}B_9$ Alloy

DTA traces of as-cast amorphous $(Fe_{0.95}Co_{0.05})_{73.5}Cu_1Nb_3Si_{13.5}B_9$ alloy taken in nitrogen atmosphere with heating at the rates of 10 - 50 ^{0}C/minute at the step of 10 ^{0}C with continuous heating from room temperature to 900 ^{0}C, are presented in Fig. 5.1(a) to Fig.-5.1(e) respectively. In each of the figures, two exothermic peaks are distinctly observed corresponding to two different crystallization events initiated at temperature T_{x_1} (primary crystallization) and T_{x_2} (secondary crystallization) respectively.

The primary crystallization temperature T_{x_1} corresponds to evolution of nanocrystalline FeCo(Si) phase, which provides the expected soft magnetic properties. The secondary crystallization temperature T_{x_2} corresponds to the boride phases i.e. FeB and/ or FeCoB phase which cause magnetic hardening of the nanocrystalline alloy. Phase identification cannot be done from a DTA scan. XRD has been used for the identification of phases and would be discussed later on. Thus, the identification of these two temperature, is necessary to understand the appropriate temperature range for heat treatment in order to achieve the nanocrystalline phase and thereby, suitable range of temperature for application of alloy.

Both the samples display exothermic peak, i.e. release of heat during the crystallization of FeCO(Si) and FeB phases since the transition from amorphous solid to crystalline solid is on exothermic process. The temperature gap between T_{x_1} and T_{x_2} are 144 ^{0}C, 148 ^{0}C, 116 ^{0}C, 142 ^{0}C and 146 ^{0}C for the heating rates 10 ^{0}C, 20 ^{0}C, 30 ^{0}C, 40 ^{0}C, and 50 ^{0}C per minutes respectively. From different investigations [5.11] it was reported that this temperature gap evolutions for inclusion of copper in FINEMET type alloys. Since only the product of primary crystallization i.e. the nanocrystalline FeCo(Si) phase is responsible for the desired ultra soft magnetic behavior and on the contrary.
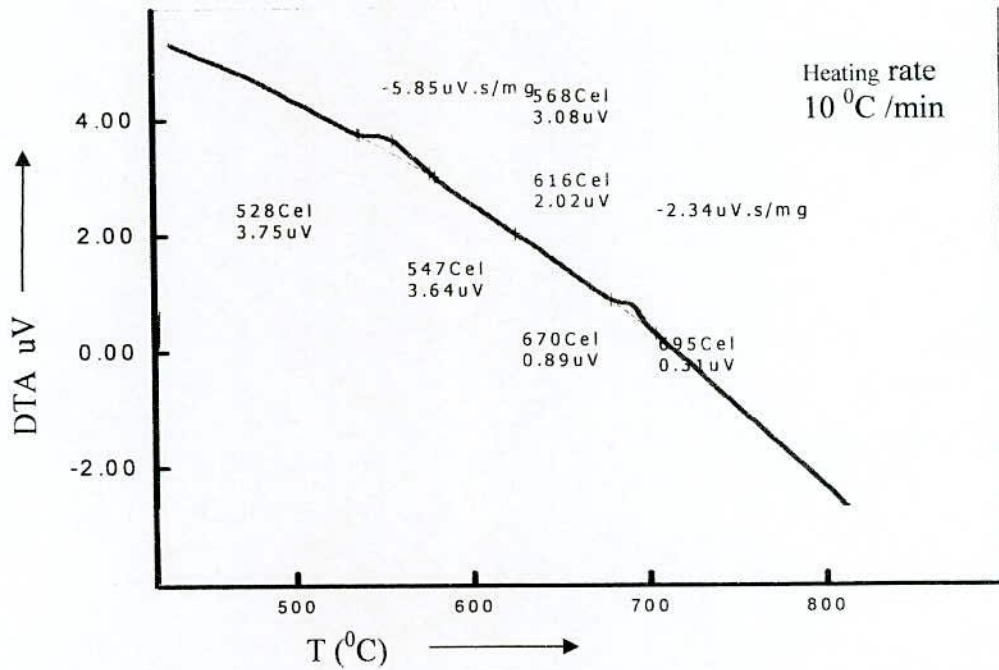
Fig. 5.1(a): DTA trace of as-cast nanocrystalline amorphous ribbon $(Fe_{0.95}Co_{0.05})_{73.5}Cu_1Nb_3Si_{13.5}B_9$ at the heating rate $10\ ^0C/min$.
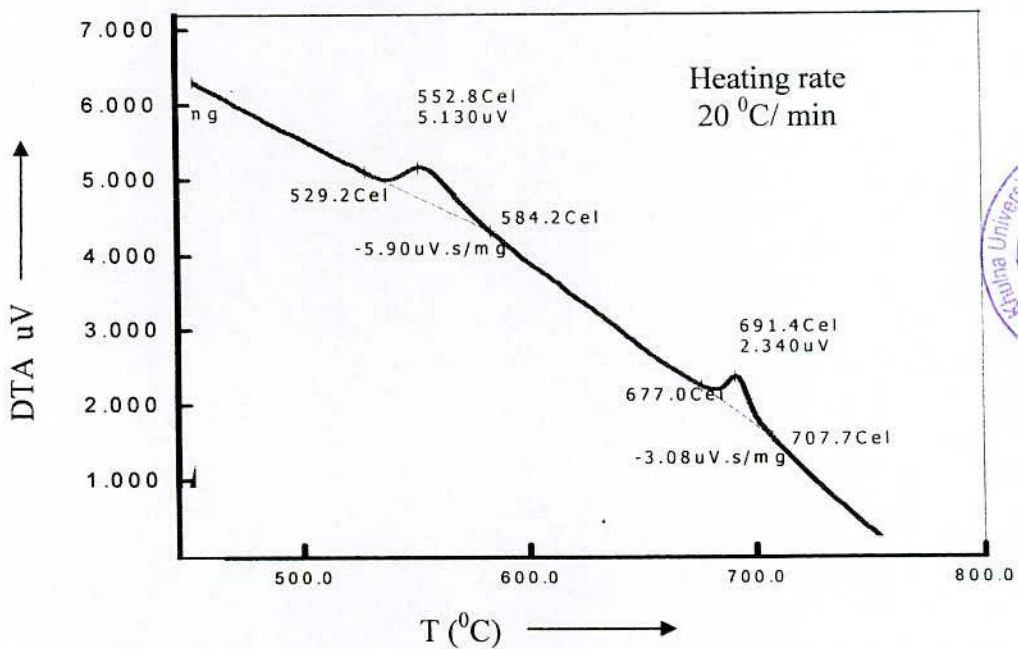
Fig. 5.1(b): DTA trace of as-cast nanocrystalline . amorphous ribbon $(Fe_{0.95}Co_{0.05})_{73.5}Cu_1Nb_3Si_{13.5}B_9$ at the heating rate $20\ ^0C/min$.

82
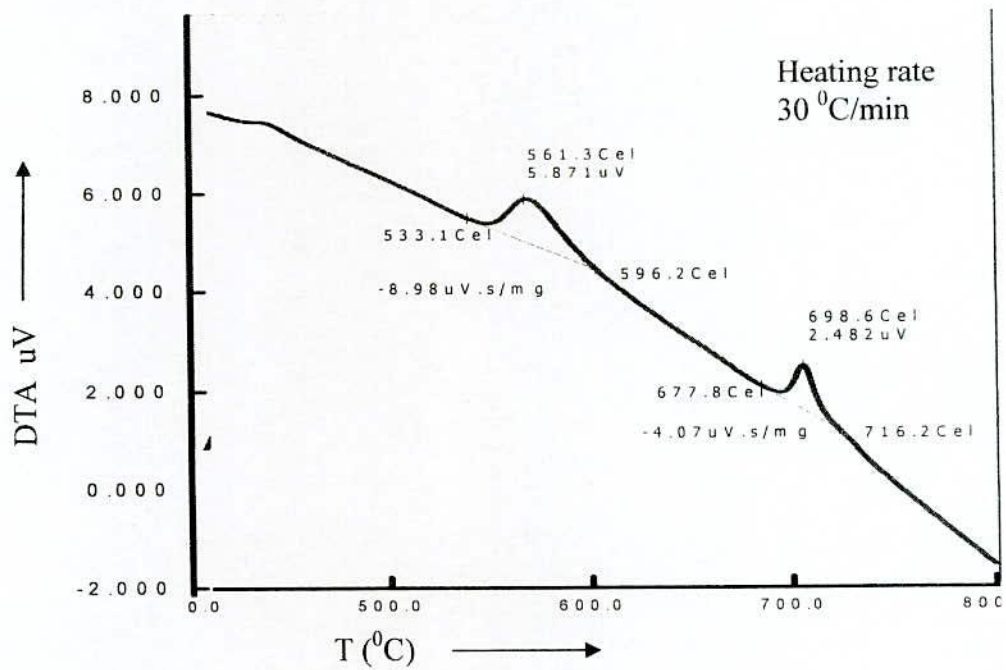
Fig. 5.1(c): DTA trace of as-cast nanocrystalline amorphous ribbon $(Fe_{0.95}Co_{0.05})_{73.5}Cu_1Nb_3Si_{13.5}B_9$ at the heating rate 30 ^{0}C/min.
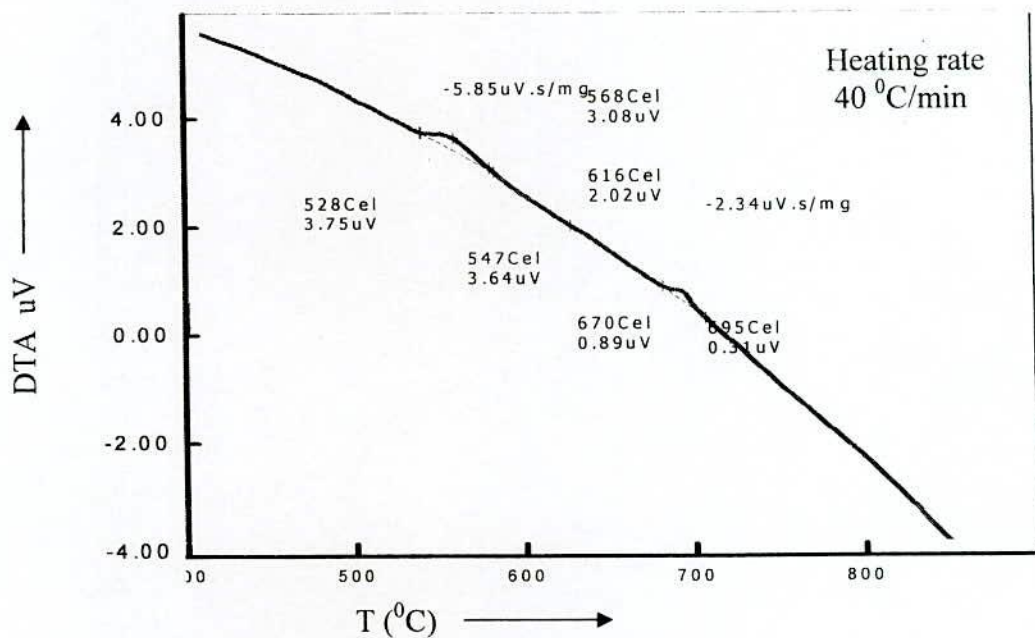
Fig. 5.1(d): DTA trace of as-cast nanocrystalline amorphous ribbon $(Fe_{0.95}Co_{0.05})_{73.5}Cu_1Nb_3Si_{13.5}B_9$ at the heating rate 40 ^{0}C/min.

83
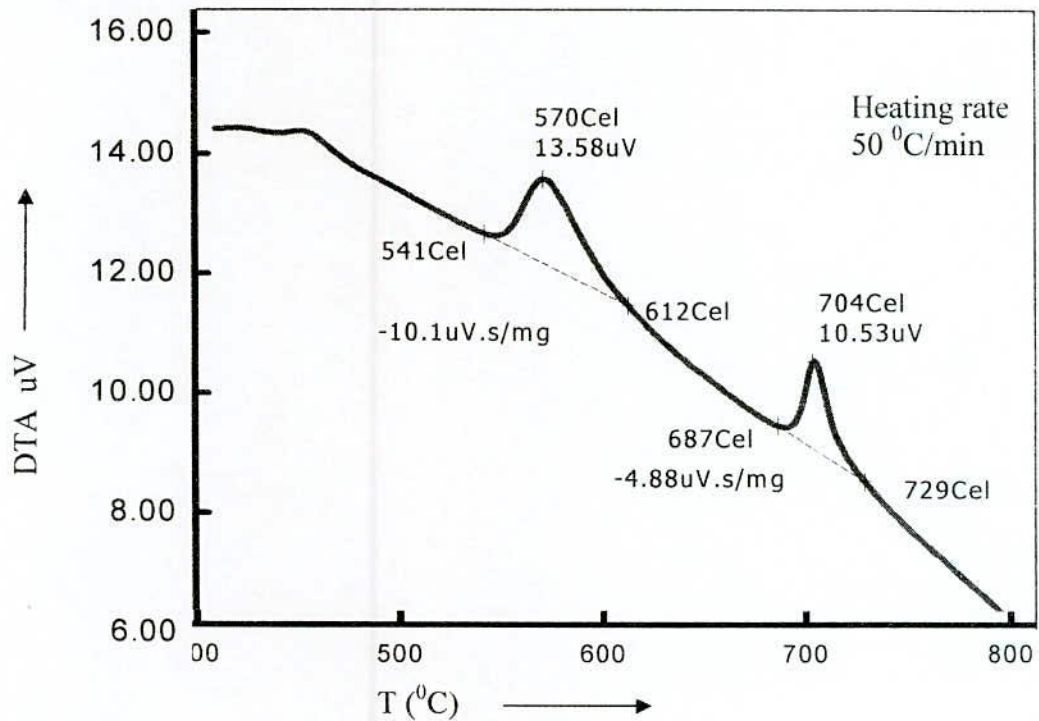
Fig. 5.1(e):   DTA trace of as-cast nanocrystalline amorphous ribbon $(Fe_{0.95}Co_{0.05})_{73.5}Cu_1Nb_3Si_{13.5}B_9$ at the heating rate 50 ^{0}C/min.

The secondary crystalline FeB and /or FeCoB phase causes magnetic hardening, so keeping a suitable temperature gap between T_{x_1} and T_{x_2} is important. This is to note that for obtaining good soft magnetic properties T_{x_1} and T_{x_2} corresponding to primary and secondary crystallized phases should be well separated from each other at a annealing temperature $T_{x_1} < T < T_{x_2}$. So that only primary crystallization product α-FeCo(Si) is crystallized. The reason is that the secondary crystallization product FeB and/ or FeCoB is extremely detrimental for the soft magnetic properties.

The transition from amorphous to crystalline state is an exotherimic process. It means both the peaks arise due to release of heat energy at particular temperatures. At that temperature, atoms arte arranged in a crystalline periodic order, i.e. in a long range

84

atomic order by consuming heat energy supplied through the process. The first crystallization peak temperature T_{P_1} corresponds to structural relaxation i.e. release of stress initially formed by rapid solidification process. The second crystallization peak temperature T_{P_2} corresponds to recrystallization i.e. reordering of atoms to form another crystalline phase.

From Fig.-5.2 represents a combination of all DTA traces of amorphous $(Fe_{0.95}Co_{0.05})_{73.5}Cu_1Nb_3Si_{13.5}B_9$ ribbon. It is observed that the crystallization of each phase has occurred over a wide range of temperatures and that the peak temperatures shift to higher values with the increase of heating rate. That means, it requires more heat energy for the formation of crystalline phases with increasing heating rates.

From each of the DTA traces, it is obvious that the area under the first crystallization peak is larger than the area covered by the second crystallization peak. In Table-5.1 crystallization peak temperatures of two phases (T_{P_1} and T_{P_2}) and crystallization onset temperatures of two phases (T_{x_1} and T_{x_2}) are given for different heating rates. It has been observed that crystallization temperature range of first phase occurred within 19 ^{0}C to 29 ^{0}C but this range for the crystallization of second phase is 12 ^{0}C to 17 ^{0}C.

So it is notable that the crystallization temperature range for the first peak is always larger than the second peak. It is also observed that the peak temperature shift to higher values and the crystallization temperature range increases with the increase of heating rates. Only the crystallization of the broide phases is yet to occur, the heat consumption is observed more during the primary crystallization. Since the crystallization of FeCo(Si) is completed before the onset of secondary crystallization, the less amount of heat is consumed during rest of the crystallization process, i.e. during the secondary crystallization.
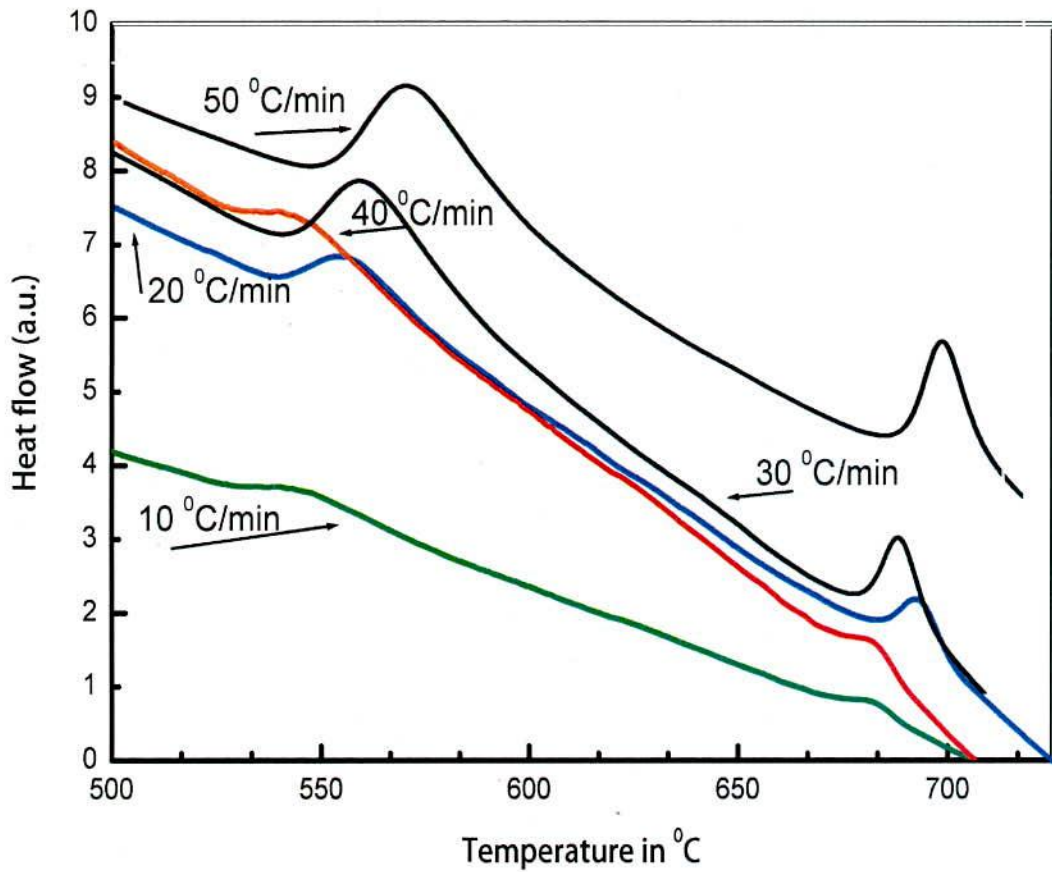
Fig.-5.2   Effects of heating rate on DTA traces of naocrystalline amorphous ribbon $(Fe_{0.95}Co_{0.05})_{73.5}Cu_1Nb_3Si_{13.5}B_9$ at the heating rate of 10 to 50 ^{0}C/min.

From Fig.-5.2 it is seen that two crystallization phenomena have taken within a large temperature gap of around 114 ^{0}C to 138 ^{0}C, evaluated from the difference between two successive peak temperatures. This temperature gap exists because the clustering of copper atoms initiates the formation of primary crystallization product i.e. FeCo(Si) at temperature lower than the alloy without cobalt.

Table-5.1: Effect of heating rate on 1st. and 2nd. Crystallization states of the nanocrystalline amorphous ribbon with composition $(Fe_{0.95}Co_{0.05})_{73.5}Cu_1Nb_3Si_{13.5}B_9$ alloy.

Heating rate °C / min.	1st starting T_{x_1} °C	1st Peak T_{P_1} °C	Temperature range of 1st state in °C	2nd starting T_{x_2} °C	2nd Peak T_{P_2} °C	Temperature range of 2nd state in °C	$T_{x_2} - T_{x_1}$	$T_{P_2} - T_{P_1}$
10	528	547	19	670	684	14	142	137
20	529	553	24	677	691	14	148	138
30	533	561	28	677	698	21	144	137
40	528	568	40	670	682	12	142	114
50	541	570	29	687	704	17	146	134

The opposite scenario has been observed when the substitution of Co for Fe in the FINEMET $(Fe_{0.95}Co_{0.05})_{73.5}Cu_1Nb_3Si_{13.5}B_9$ alloys is made [5.12]. The crystasllization peak temperature (T_{P_1}) and the activation energy for the primary crystallization E_1 decreases gradually with Co content. This result indicates that the role of Co is to facilitate the formation of crystalline α-FeCo(Si) phase. This is to note that the onset of crystallization temperature has been taken as the temperature at which the exothermic peak starts rising. The understanding of the crystallization onset, crystallization peak temperature and the end of crystallization temperature is essential for the determination of appropriate annealing temperature for nanocrystallization. Temperature and time of annealing is crucial for controlling the size and volume fraction of nanocrystals, which ultimately controls the magnetic properties of the FINEMET type of amorphous soft magnetic alloys.

Finally if the DTA of samples would be repeated after crystallization, no peak corresponding to crysatallization would be observed. This quite expected because the specimen were subjected to irreversible transformation.

5.1.3 The Activation Energies for Formation of Nanocrystalline Phase

The activation energy of crystasllization of T_{x_1} and T_{x_2} phases have been calculated using Kissinger equation [5.13]

$$\beta = T_P^2 e^{-E/kT_P}$$

$$\ln\left(\frac{\beta}{T_P^2}\right) = -\frac{E}{kT_P}$$

$$E = -kT_P \ln\left(\frac{\beta}{T_P^2}\right) \tag{5.1}$$

Where β is the heating rate, T_P is the crystallization peak temperature, E is the activation energy and k is the Boltzmann constant.

The activation energy of the first crystallization phase α-FeCo(Si) and the second crystalline phase (FeB and /or FeCoB) have been calculated using Kissinger's plots shown in Fig.-5.3(a) and Fig.-5.3(b) respectively and the values are given by in Table-5.2. It is found that first thermal crystallization activation energy (E_1) af α-FeCo(Si) phase 2.40 eV and that of second FeB and /or FeCoB phase (E_2) is 4.31 eV.

Table-5.2: Comparison of the activation energies and peak temperature of original FINEMET [5.14] and $(Fe_{0.95}Co_{0.05})_{73.5}Cu_1Nb_3Si_{13.5}B_9$ alloy

Heating rate °C	$(Fe_{0.95}Co_{0.05})_{73.5}Cu_1Nb_3Si_{13.5}B_9$					$Fe_{73.5}Cu_1Nb_3Si_{13.5}B_9$				
	T_{P_1} °C	T_{P_2} °C	$(T_{P_2}-T_{P_1})$ °C	E_1 eV	E_2 eV	T_{P_1} °C	T_{P_2} °C	$(T_{P_2}-T_{P_1})$ °C	E_1 eV	E_2 eV
10	547	684	137			550	686	136		
20	553	691	138			554	700	146		
30	561	698	137	2.40	4.31	561	708	147	3.21	3.81
40	568	682	114			567	715	148		
50	570	704	134							
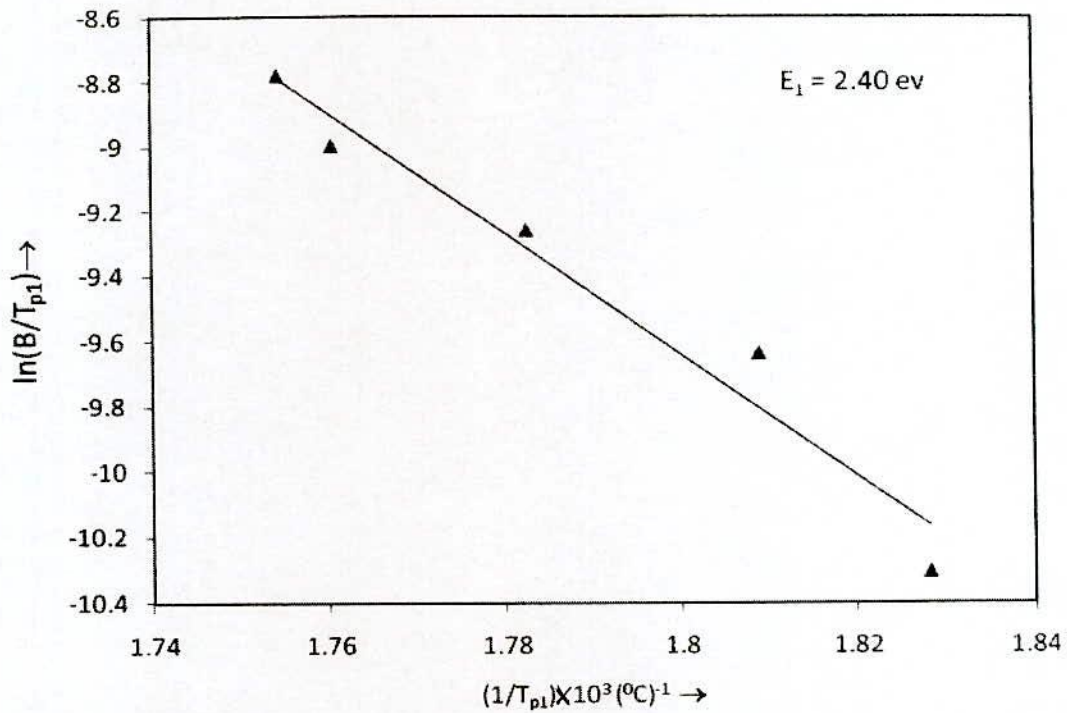
Fig.-5.3(a)   Kissinger's plot to determine the activation energy of FeCo(Si) phase.
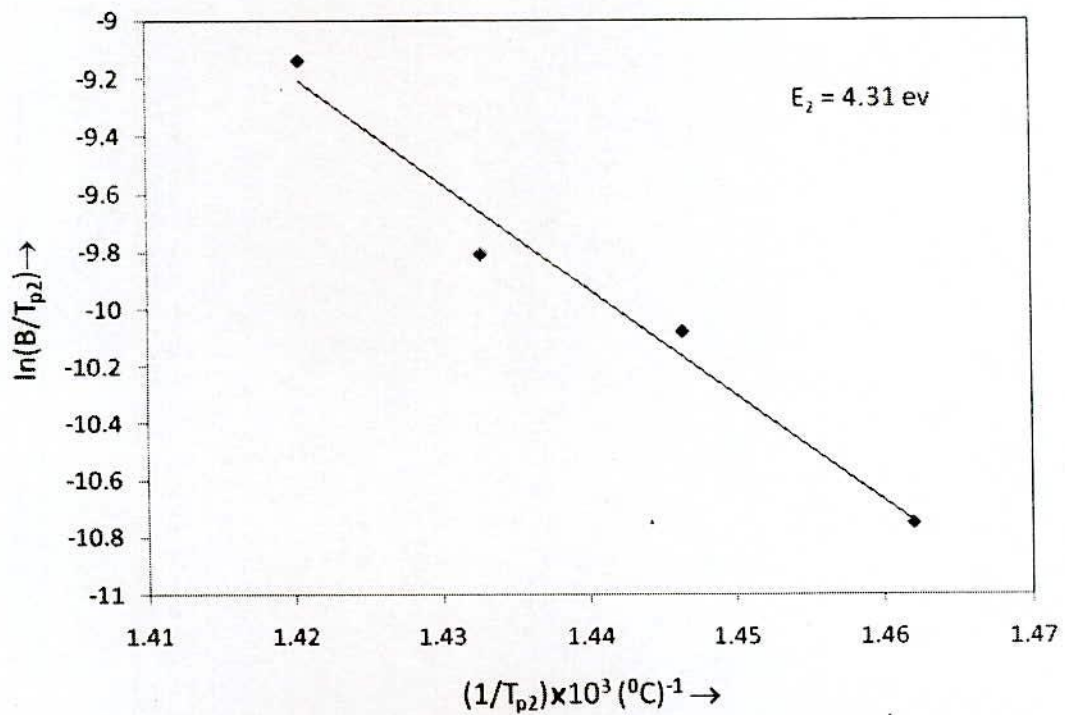
Fig.-5.3(b)   Kissinger's plot to determine the activation energy of boride phase.

As depicted above, the apparent energy E_c in fact is composed of two parts: nucleation and growth with respect to activation energy E_n and E_g respectively. The early stage of crystallization is expected to be dominated by the nucleation process for a crystalline phase. At this stage, formation of Cu clusters leads to a low activation energy for preferential nucleation. However, with the increase of crystalline volume fraction, the Cu-rich regions gradually run out. At the same time, the Nb and B atoms, which are not suitable in the bcc phase are excluded from the crystallized regions and the surrounding regions rich in Nb and B, in turns block the further growth of grains. The higher the Nb and B contents the stronger is the growth blocking process [5.14]. Consequently, the crystallization activation energy for nucleation and growth increases. The formation of Cui-rich regions reduces the activation energy for nucleation E_n of α-FeCo(Si), so that the phase may nucleate and precipitate preferentially in the Cu-rich regions [5.15].

5.1.4 A Comparison Between DTA Results of $(Fe_{0.95}Co_{0.05})_{73.5}Cu_1Nb_3Si_{13.5}B_9$ Alloy and other FINEMET

The comparative values of DTA results for present alloy and that for original FINEMET sample are given in Table-5.2. The results show that the peak temperature corresponds to crystallization with addition of Co [5.16]. This indicates that the crystallization process began at lower temperature which occurs due to existence of cobalt that reduces the glass forming ability [5.17]. So, due to replacement of Co, the evolution of expected nanocrystalline phases FeCo(Si) can be found at a lower temperature. From Table-5.2 it is also found that the temperature gap between successive crystallization is less for the present sample than the alloy without cobalt except heating rates /min. This result indicates that the role of Co is facilities the formation of nanocrystalline α-FeCo(Si) phase.

5.2 Microstructural Analysis of Amorphous and Nanocrystalline $(Fe_{0.95}Co_{0.05})_{73.5}Cu_1Nb_3Si_{13.5}B_9$ Alloy by XRD Analysis

In the present work, in order to study the crystallization onset temperature, X-ray diffraction spectra have been recorded for the nominal composition $(Fe_{0.95}Co_{0.05})_{73.5}Cu_1Nb_3Si_{13.5}B_9$ annealed at 550 ^{0}C to 750 ^{0}C for 30 minutes. The appropriately annealed samples were subjected to XRD by using a Philips X'Pert PRO X-ray diffractometer to examine the micro structural evaluation as a function of annealing temperature. From the experiment, we obtained results of the three kinds of structural parameters including lattice parameter, grain size and silicon content of nanocrystalline FeCo(Si) grains from which we shall further attempts to find out the intrinsic and extrinsic magnetic properties with evaluation of micro structures at different annealing temperatures. There must have some effect of structural parameters on soft magnetic properties of the alloy which we shall try to explain afterwards.

X-ray pattern of $T_a = 550$ ^{0}C, clearly confers the presence of crystalline phase identified as a result a α-FeCo(Si) solid solution developed in the amorphous matrix lattice parameters for all the annealed samples have been determined from (110), (200) and (211) diffraction peak using formula $a_0 = d\sqrt{2}$, while grain size have been calculated using equation (4.4). Silicon content of Fe(Si) nanograins was calculated from the established quantitative relationship between lattice parameter and Si-content in Fe-Si alloys by Bozroth [5.18]. All the results of θ, d-values, fullwidth at half maxima (FWHM) of the intensity peak corresponding to (110) planes, grain size D_g and Si content from XRD analysis are listed in Table-5.3.

5.2.1 Identification of Phases by XRD Analysis

The XRD patterns for the $(Fe_{0.95}Co_{0.05})_{73.5}Cu_1Nb_3Si_{13.5}B_9$ annealed at temperature 550 ^{0}C, 600 ^{0}C, 625 ^{0}C, 650 ^{0}C, 675 ^{0}C, 700 ^{0}C, 725 ^{0}C, and 750 ^{0}C each for 30 minutes are presented in Fig.-5.4.
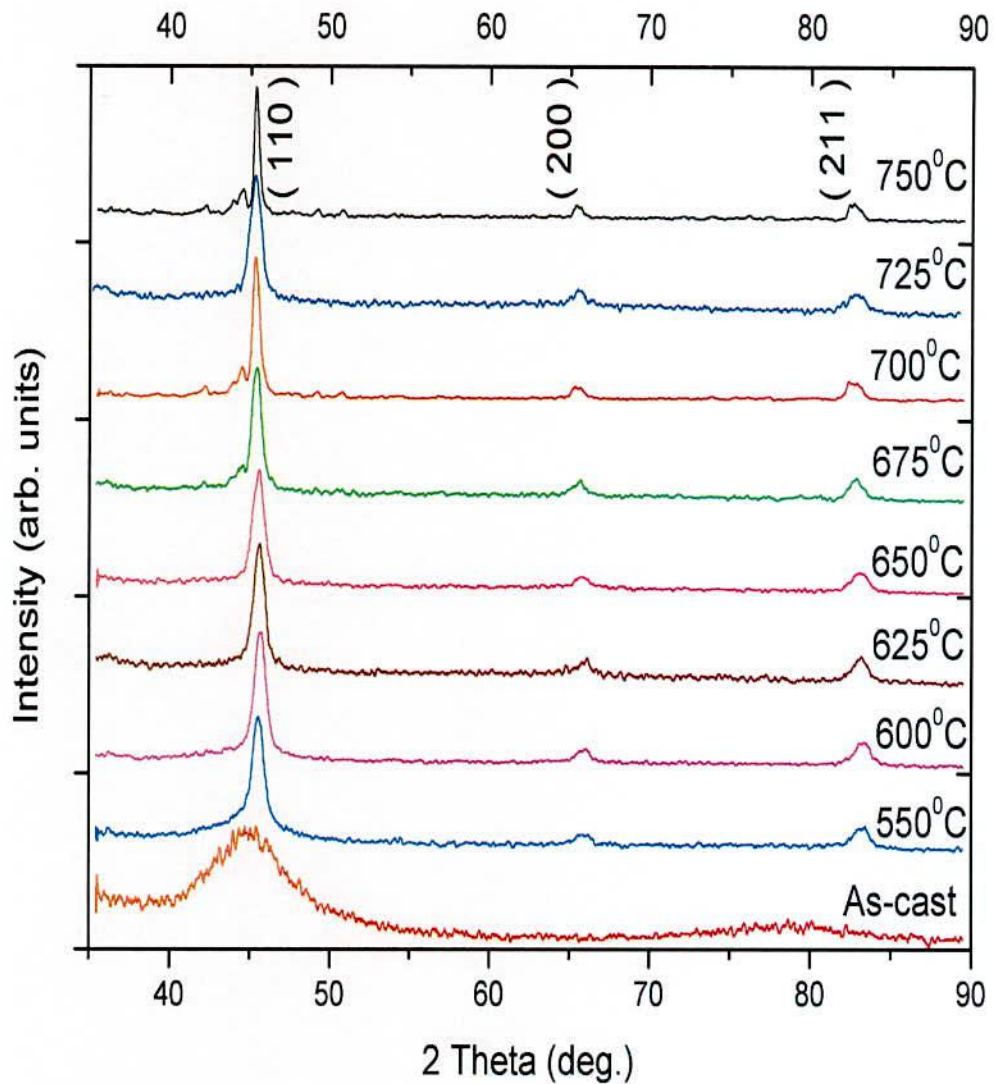
Fig.-5.4 XRD patterns of $(Fe_{0.95}Co_{0.05})_{73.5}Cu_1Nb_3Si_{13.5}B_9$ alloy for as cast and annealed at different annealing temperatures for 30 minutes.

It is evident from Fig.-5.4 when the sample annealed below 550 ^{0}C i.e. at 550 ^{0}C, it exhibit only one broad peak around $\theta = 45^0$ at the position of d_{110} reflection which is generally known as diffuse hallow. This diffuse hallow indicates the amorphous nature of the sample. It means at the annealing temperature below 550 ^{0}C, no crystalline peak has

been detected. So, the onset of crystallization temperature determined from this result is 550 ^{0}C.

The value of FWHM of the peak at the annealing temperature, 550 ^{0}C is 0.93, which for 600 ^{0}C is 0.83. For the higher annealing temperatures, FWHM value is getting smaller. It shows that crystallization occurs to a good extent at the annealing temperature 600 ^{0}C. The crystallization onset temperature from DTA experiments for different heating rates, were found in the range of 530 ^{0}C to 541 ^{0}C, which shows a good consistency with the XRD results.

Due to annealing at 550 ^{0}C, the first crystallization peak was found at an angle 45.19^0. But from the XRD data, no evidence of Si content was found to be partitioned in the crystalline part at that temperature. It reveals that α-FeCo is the first crystalline phase to segregate out in the system during crystallization process, which is also found by Mössbauer spectra in several investigations [5.18].

Investigation by Mössbauer study [5.19] have been identification that addition of Co causes alternation of disordered DO$_3$ type structure of FeSi grains, occurred in classical nanocrystallite FINEMET, into FeCo(Si) solid solution of low silicon concentration. For a annealing at higher temperature i.e. 600 ^{0}C, 625 ^{0}C, 650 ^{0}C, 675 ^{0}C, 700 ^{0}C, 725 ^{0}C, and 750 ^{0}C, the FeCo(Si) phases were found at the lower values of 2θ at.% 45.39^0, 45.29^0, 49.25^0, 45.07^0, 44.99^0, 45.29^0 and 45.07^0 respectively with 100% peak intensity on (110) line. The other two fundamental peaks corresponding to α-FeCo(Si) on (200) and (211) diffraction line for annealing temperatures at and above 550 ^{0}C is obtained in this Fig.-5.4. But due to their low intensity, they are not clearly visible before 550 ^{0}C annealing. Two fundamental peaks (200) and (211) at 2θ = 65.81^0 and · 83.69^0 around corresponds to bcc FeCo(Si) phase. But due to their low intensity, there are not clearly visible before 600 ^{0}C annealing. The balance of composition is maintained by the distribution of amorphous phase in the system.

From DTA result it is expected that FeCoB phase would form beyond 675 ^{0}C. But the formation of crystalline phase other than FeCo(Si) in the XRD pattern has not been

detected for T_a up to 750 ^{0}C for the sample as expected from the DTA analysis of $(Fe_{0.95}Co_{0.05})_{73.5}Cu_1Nb_3Si_{13}$. Absence of FEB phase in XRD spectra is possibly due to very small volume fraction of boride phase [Fe_3B, Fe_2B, $Fe_{23}B_6$ and / or $(FeCo)_{23}B_6$] [5.20 -5.21].

The XRD patterns illustrated in Fig.-5.4 reveal that the difference in the Bragg's peak as well as the intensity of the fundamental reflections become gradually stronger as the temperature of the heat treatment increases. This increase in the sharpness of the intensity peaks with the annealing temperature indicates that crystalline volume fraction has been increases and also, annealing temperature indicates that crystalline volume fraction has been increased and also, grains become coarser with increased spectra of the thermally treted samples of Co substituted FINEMET's evidence of α-FeCo and $(FeCo)_3(BSi)$ crystalline phases might be found along with iron oxides (α-Fe_2O_3 and λ-Fe_2O_3) of less than 1% of the total composition [5.11]. Reason of oxide formation lies in fact of performing annealing in air atmosphere. In spite of addition of refractory elements it should be suggested that the heat treatment should be done in an inert (non-reactive) atmosphere to avoid oxidation and other reactions.

The systematic but negligible shift of peak towards the larger angles with increasing temperature indicates that lattice parameter of the phase gradually decreases due to the increasing of silicon content of the α-FeCo phase. Both the decrease in lattice parameter and increase in intensity of the fundamental peak with increasing annealing temperature suggest that Si atom diffuse most intensively into the bcc FeCO with increase of annealing temperature. The diffusion of Si in bcc α-FeCo is finally found as the nanocrystalline bcc FeCo(Si) lattice which is identified by XRD and therefore we see the increase in intensity due to increase of the crystalline part in the alloy.

The lattice parameter, the silicon contents in bcc nanograins and the grain size of bcc grain can easily be calculated from the fundamental peak of (110) reflection. All the results are shown in Table-5.3.

Table -5.3 Experimental XRD data of $(Fe_{0.95}Co_{0.05})_{73.5}Cu_1Nb_3Si_{13.5}B_9$ alloy for as cast and annealed at different annealing temperature for 30 minutes

$T_a(^0C)$	θ^0	$d(\text{Å})$	$a_0(\text{Å})$	$FWHM(\theta^0)$	$Si(at\%)$	$D_g(nm)$
550	22.6188	2.0044	2.8347	0.93	21.14	9
600	22.6343	2.0031	2.8328	0.83	22.00	10
625	22.6438	2.0023	2.8317	0.81	22.50	10
650	22.6355	2.0030	2.8327	0.75	22.05	11
675	22.6021	2.0058	2.8367	0.69	20.23	13
700	22.5701	2.0085	2.8404	0.45	18.55	19
725	22.5145	2.0132	2.8471	0.41	15.50	22
750	22.4791	2.0162	2.8514	0.33	13.55	26

5.2.2 Lattice Parameter Measurement

We have, therefore, determined the lattice parameter using only that particular reflection using equation:

$$2\,dSin\,\theta = \lambda \quad \text{and} \quad a_0 = d\sqrt{2} \tag{5.2}$$

Where, $\lambda = 1.54178$ Å is the wavelength of Cu-K_α radiation and a_0 is determined lattice parameter of the grain, d is the inter-planar spacing and θ is the diffraction angle.

For every steps lattice parameter was determined with an error estimated to be ±0.0001 Å using eq^n(5.2) and all values are listed in Table-5.3 and the pattern of changes in lattice parameter with respect to annealing temperature is presented in Fig.-5.5. In Fig.-5.5 all the variation of lattice parameter as a function of annealing temperature T_a for 30 minutes annealing time is presented for the sample under study at annealing temperature ranging 550 ^0C to 750 ^0C.

Fig.-5.5 shows that, with the increase in annealing temperature, the lattice parameter was not changed notably up to the annealing temperature 750 ^0C. The lattice parameter of pure Fe is 2.8664 Å. The reason of decrease in lattice parameter can be explained from the fact of relative atomic sizes of the main two constituents of the bcc

phase, i.e. Fe and Si. But the lattice parameter at various annealing temperatures for the present alloy are significantly less than that of pure Fe. Si having a smaller atomic size compared to Fe, diffuses in the α-FeCo lattice during annealing at different temperatures which results in a contraction of α-FeCo lattice.
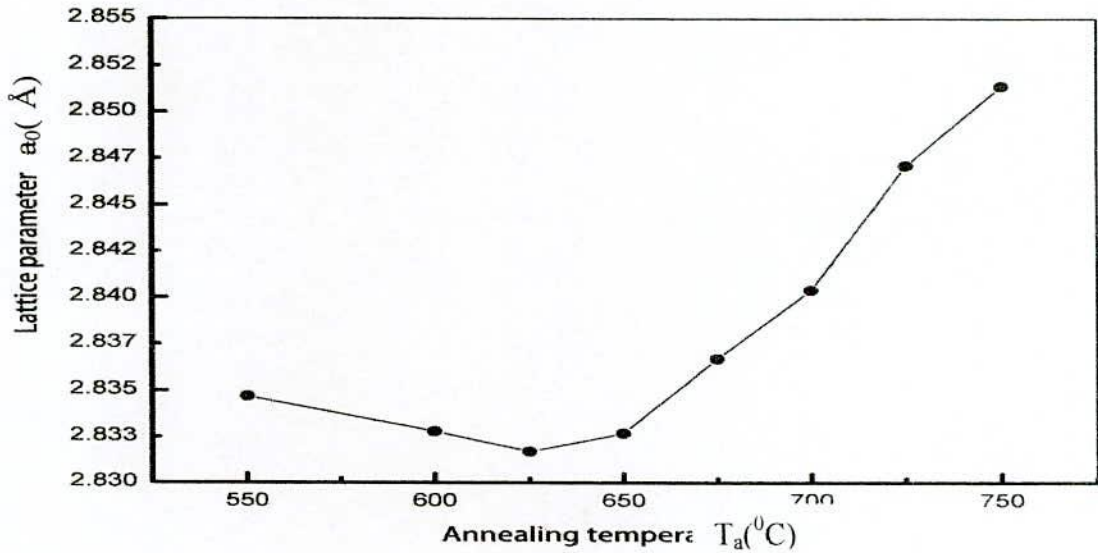
Fig.-5.5 Variation of lattice parameter with annealing temperature

Thus, the newly formed substitution solid solution of α-FeCo(Si) during the crystallization process has a smaller size comparing to the α-FeCo lattice. So, the more diffusion of Si, there should be more contraction of the α-FeCo lattice and thereby, the decrease of lattice parameter. Decrease of lattice parameter with annealing temperature suggests negligible peak shift due to stacking fault as in general no peak is observed experimentally.

In the present sample, there is a partial replacement of Co for Fe. Researchers found that the average TM-TM (Transition Metal) near neighbor distance decreases with the increase of Co concentration [5.22] which results in the decrease of lattice parameter comparing to the original FINEMET. As the presence of Co produce, a decrease in the lattice parameter, the actual Si content would be less in the crystalline phase. So the contribution of Si content for the change of lattice parameter would be less. This might be

the reason for which the variation in lattice parameter with annealing temperature is not so obvious for the present sample comparing to original FINEMET up to700 ^{0}C.

When the sample is annealed above 700 ^{0}C, the increase of lattice parameter with subsequent decrease of Si-content, as showed in Fig.-5.5 and Fig.-5.6 indicates that silicon diffuses out of α-FeCo(Si) grains for which the size of α-FeCo lattice is regained. Thus there happened a recrystallization of the α-FeCo(Si) grains beyond 700 ^{0}C. This results is compatible with those reported for similar composition [5.23].

The behavior of lattice parameter with annealing temperatures provides interesting information about compositions of nanocrystalline phase formed by primary crystallization. All the obtained values of lattice parameter in this work are always significantly smaller than that of pure α-Fe. Hence it could be speculated that the metalloid elements of alloy has been dissolved in the bcc FeCo phase. But the metalloid element boron is practically insoluble in α-Fe (<<0.01 at.%) and the solubility of Cu and Nb are very low (< 0.2 at.% Cu; < 0.1 at.% Nb; only above 500 ^{0}C) [2.24]. Hence the nanocrystalline phase in this experiment for sample $(Fe_{0.95}Co_{0.05})_{73.5}Cu_1Nb_3Si_{13.5}B_9$ consists essentially of Fe, Co and Si only.

5.2.3 Silicon Content in Nanograins

Lattice parameter measurements give the hint about a non negligible solute content establishing the fact that the bcc ferromagnetic phase consists of iron, cobalt and silicon essentially.

The silicon contents of the alloy $(Fe_{0.95}Co_{0.05})_{73.5}Cu_1Nb_3Si_{13.5}B_9$ at different annealing temperatures 550 ^{0}C to 750 ^{0}C for 30 minutes annealing time are found to be in the range of 13.79% to 22.50%. All these results are presented in Table-5.3 and the pattern of change in silicon content with respect to annealing temperature is presented in Fig.-5.6.
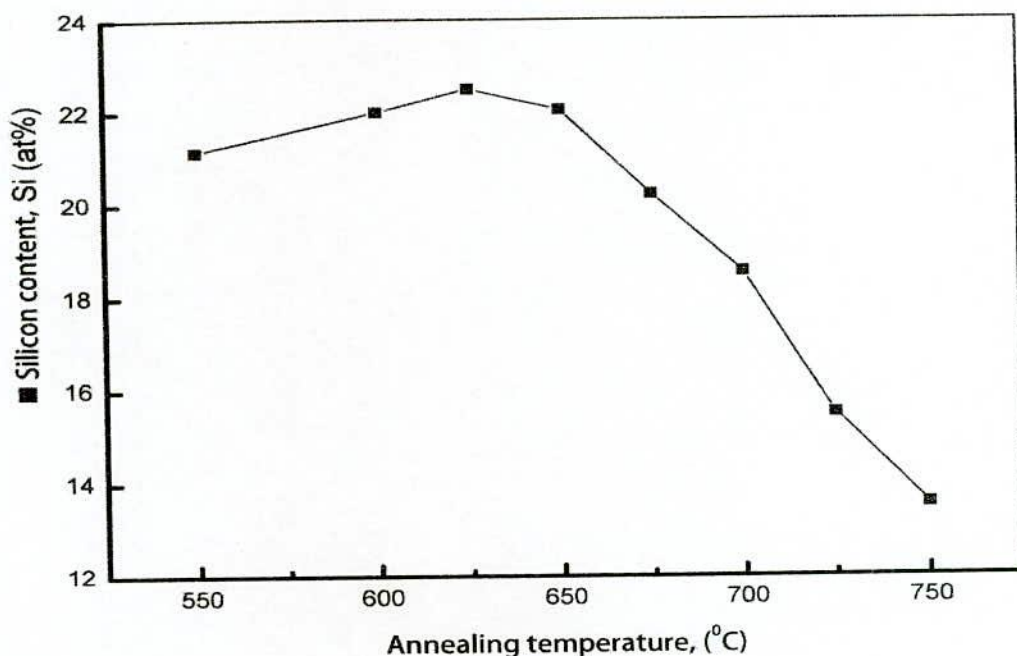
Fig.-5.6 Variation of Si% with annealing temperature

Fig.-5.6 shows the percentage of Si in α-FeCo(Si) phases with the gradual increase of annealing temperature attaining a maximum value of 22.50 at.% at 625 ^{0}C. It is notable that Si contents in the nanocrystallites at different annealing temperatures are higher than Si content of the amorphous precursor which 13.5 at.%. This increase of Si content in the crystalline phase with increasing annealing temperature can be explained by the fact that the element Si form the amorphous phase diffuses into α-FeCo space lattice during crystallization process to form α-FeCo(Si) nanograins. This means that the crystallization of this alloy is a diffuse controlled process with temperature as controlling parameter. So, higher annealing temperature results in more diffuse of Si enriching the α-FeCo(Si) nanograins. The fact of increase in intensity of diffraction peaks and besides in the Si-content in nanograins with increase of annealing temperature that the diffusion of Si results in the increase of nanocrystalline volume fraction in the amorphous precursor.

The percentage of partitioned Si in the nanocrystalline α-FeCo(Si) phase is maximum at 625 ^{0}C. After 625 ^{0}C, decrease in Si content is observed which can be

explained by the fact that at higher temperatures silicon diffuses out of nanograins due to recrystallization corresponding to formation of boride phases which is consistent with the Result of other FINEMET's [5.23].

Fig.-5.7(a) Variation of lattice parameter and Si at.% with annealing temperature

Fig.5.7(b) Variation of Si at.% with lattice parameter

Fig.-5.7(b) presents the inverse relationship between lattice parameter and silicon content. This kinds of relation between lattice parameter and Si content was observed in the reports [5.23], which are verified in present work effectively. Fig.-5.7(a) shows the initial stage of crystall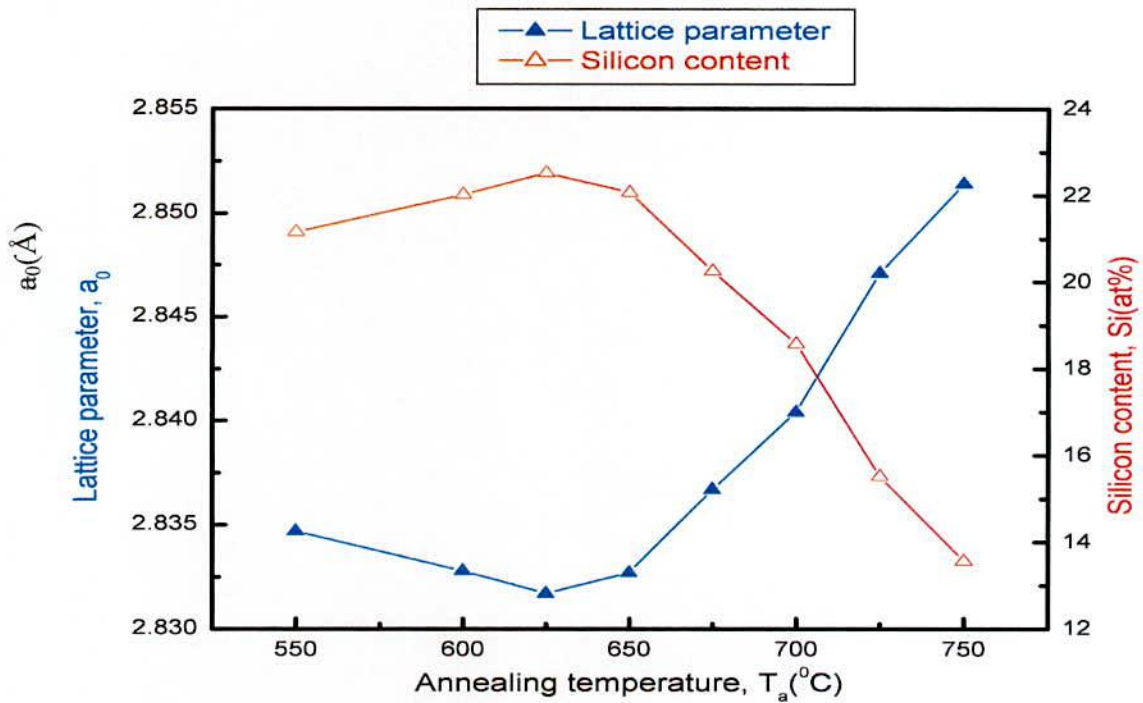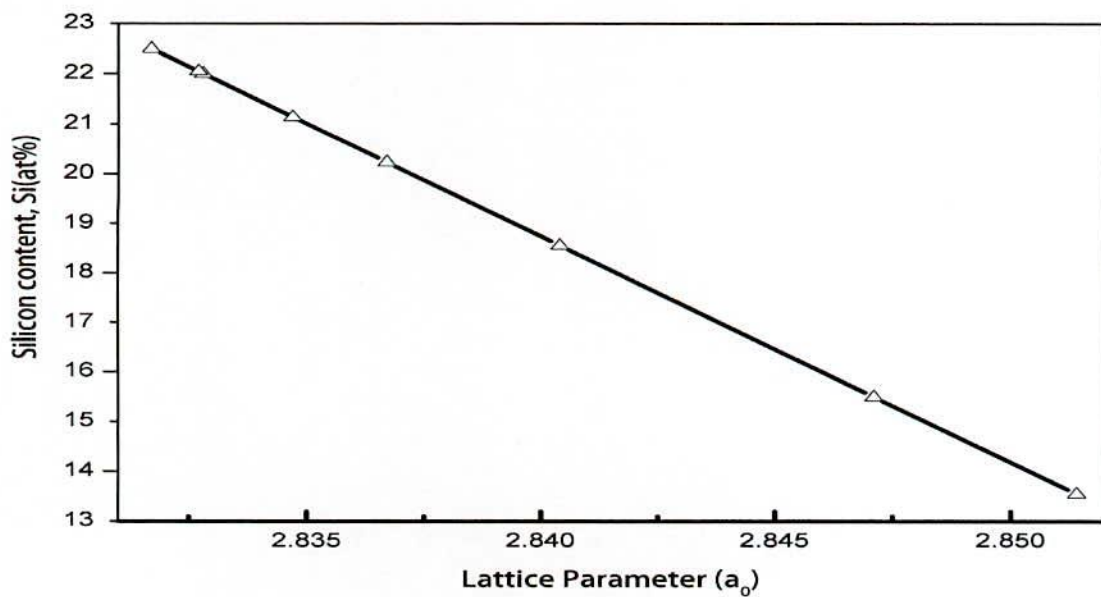ization lattice parameter first decreases with increase of silicon content, because silicon diffuses in the bcc FeCo phase, to form the soft nanocrystalline α-FeCo(Si) phases. Such decrease of lattice parameter with increase of silicon content prevails up to750 ^{0}C, beyond which the lattice parameter with increase of silicon content. This is the sequence of recrystallization when silicon diffuses out initiating formation of boride phases.

5.2.4 Grain Size Determination

In 1963 Kneller and Luborsky [5.25] studied on nanograins. The found that the magnetic properties of isolated grains change drastically as their size is reduced to the nanometer range. When these nanometric grains are consolidated to form a nanostructured material, the magnetic properties are largely determined by the grain size and the exchange interaction between the adjacent grains. Herzer [5.26] successfully established the theoretical explanation on the grain size dependence of superior soft magnetic properties based on his Random Anisotropy Model (RAM) after the pioneer experimental invention of FINEMET alloy by Yoshizawa et. al. [5.11]. One member of the FINEMET family is the sample $(Fe_{0.95}Co_{0.05})_{73.5}Cu_1Nb_3Si_{13.5}B_9$, which is under investigation of the present work. This is important part of the present study was to determine the nanocrystalline size.

.   Grain size of all annealed samples of the alloy composition was determined using Scherrer method [5.27]. Grain size was determined from XRD pattern of (110) reflections for different annealing temperature at constant annealing time 30 minutes from which grain size was determined using the formula:

$$D_g = \frac{0.9\lambda}{\beta Cos\,\theta}$$

(5.3)

Where $\lambda = 1.54178$ Å is the wavelength of Cu-K_α radiation, θ is the diffraction angle and β is the full width at half maximum (FWHM) of diffraction peak in radian for different steps of annealing temperature.

Instrumental broadening of the system was determined from θ - 2θ scan of standard Si. At the position of (110) reflection, the value of instrumental broadening was found to be 0.07^0. This value of instrumental broadening was subtracted FWHM value of each peak. Asymmetrical broadening of the peak due to stacking fault of bcc crystal was corrected negligible in the present case. All determined grain size was values for every steps of heat treatment are listed in Table-5.3. In Fig.-5.4 it is clear that at lower annealing temperature 550 ^{0}C, the FWHM of the peak is large and with the increase of annealing temperature, the value of FWHM are getting smaller. The peaks are, therefore becoming sharper with the shifting of peak position towards higher 2θ value. The peak shifts indicate the change of the values of silicon content of nanograins and therefore, the change of the values of lattice parameter of nanograins.

From Fig.-5.8 and Table-5.3 that grain size increases with annealing temperature from a value of $D_g = 9$nm for $T_a = 550$ ^{0}C to $D_g = 26$nm for the sample annealed at $T_a = 750$ ^{0}C while Si-content decrease with annealing temperature. The increasing of annealing temperature initiates partitioning of Si in the bcc FeCo phase and thus grain growth due to formation of nanocrystalline bcc FeCo(Si) grains. In the range of annealing temperature 550 ^{0}C to 675 ^{0}C, the grain size remains in the range of 9 to 12 nm corresponding to soft magnetic bcc FeCo(Si) phases. Above 675 ^{0}C, grain grow rapidly and attain value of 19nm at 700 ^{0}C indicating formation of FeB and or FeCoB phases. Formation of boride phase is detrimental to soft magnetic properties. These factsa reveals that heat treatment temperature should be limited within 550 ^{0}C to 650 ^{0}C to obtain optimum soft magnetic behavior, which will be clear that constant grain size.

The formation of the nanometric microstructure corresponding to the grain growth with the increase of annealing temperature is ascribed to combined effects of Cu and Nb and their low solubility in iron. Cu which is insoluble in α-FeCo, segregates prior to at the very beginning of nanocrystallization forming Cu-rich clusters and the nucleation of

101

FeCo(Si) grains is thought to be multiplied by clustering of Cu which stands as the reason for the grain growth at the initial stage of crystallization. On the other hand the rejection of Nb at the crystal interface causes hindrance to grain growth for which the change in grain size is not so obvious constant up to 650 ^{0}C. The increase of nucleation density caused by Cu as well as inhibition of grain growth by Nb results in homogeneous distribution of nano grains in the surrounding amorphous matrix. Our results corresponds well with the reported results of Rubinstein et. al. [5.28].
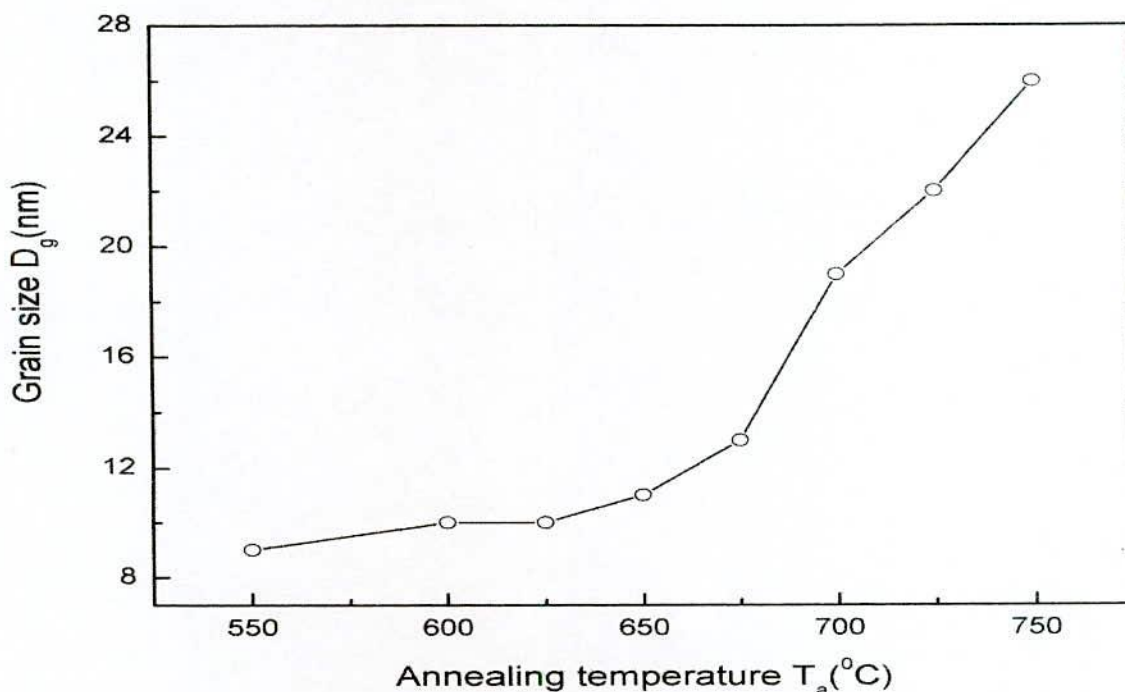
Fig.-5.8 Variation of grain size with annealing temperature

As mentioned earlier in the simple Scherrer formula, the width of given reflection is used for grain size determination which under estimates the grain size as the strains evidently present in the nanostructures are not taken into account. However, the short coming regarding evaluation of structural parameters does not affect much in correct estimation of the parameters and still XRD is a widely used experiment for investigation of microstructure of crystals. It was observed that grain size 9nm for the sample annealed at 550 ^{0}C for 30 minutes to a limiting values of 10 – 13nm between annealing temperature 600 ^{0}C to 675 ^{0}C.

5.3   Dynamic Magnetic Properties of $(Fe_{0.95}Co_{0.05})_{73.5}Cu_1Nb_3Si_{13.5}B_9$ Alloy

Dynamic magnetic properties of as-quenched nanocrystalline samples with composition $(Fe_{0.95}Co_{0.05})_{73.5}Cu_1Nb_3Si_{13.5}B_9$ has been measured as a function of frequency in the range 1kHz to 13MHz. Permeability measurements were performed on toroidal samples at frequency of 1kHz to 13MHz and an applied ac driving field $\approx$ 0.4A/m to ensure the measurements of initial permeability. Frequency spectrum of real and imaginary parts of initial permeability, loss factor and relative quality factor are analyzed. The measurements have been done for as cast sample and samples annealed at different temperatures with constant annealing time 30 minutes. In order to avoid experimental error due to fluctuation in ribbon thickness and thermal treatment, just one piece of each ribbon has been measured at room temperature after subsequent annealing temperatures at constant annealing temperature (30 minutes) magnetic properties of amorphous nanocrystalline magnetic materials are strongly dependent on its annealing temperature [5.2]. In the present work, initial permeability of the toroidal shaped samples annealed at different temperatures are measured to understand their soft magnetic properties and correlation with the micro structural features which are obtained from XRD analysis.

5.3.1 Frequency Dependence of Initial Permeability of $(Fe_{0.95}Co_{0.05})_{73.5}Cu_1Nb_3Si_{13.5}B_9$ Alloy with Different Annealing Temperatures

In order to correlate the micro structural features on the soft magnetic properties of the alloy under study, magnetic initial permeability of toroidal shaped samples annealed at different temperatures are measured with very low field. Magnetic properties of the soft magnetic materials are mainly determined by the domain wall mobility especially in the range of irreversible magnetization. One the main purpose of this experimental was to determine empirically the optimum annealing temperature for the

constant annealing time of 30 minutes, corresponding to maximum permeability constancy of permeability and maximum frequency range over which the sample can be used as a soft magnetic material.

The measurement has been done an as-cast specimen and also on samples annealed at 525 ^{0}C to 750 ^{0}C for 30 minutes as constant annealing time. In Fig.-5.9(a, b) shows the frequency dependence of the real part of complex initial permeability for as-cast and the sample annealed at temperature 550 ^{0}C to 750 ^{0}C for a constant annealing time of 30 minutes. From the Fig.-5.9, it is observed that the low frequency value of initial permeability increases with the increase of annealing temperature and attains the maximum value at the annealing temperature of 550 ^{0}C. When the annealing temperature is higher than 525 ^{0}C, initial permeability (μ') decrease rapidly. This decrease of permeability may be attributed to the stress developed in the amorphous matrix by growing crystallites. At this temperature (550 ^{0}C) the initiation of crystallization takes place. The general characteristic of the curve is that μ' remains fairly constant up to some critical frequency characterized by the onset of resonance connected with the loss component. At critical frequencies, μ' drop rapidly. The low frequency range value of μ' generally increases with the increase of annealing temperature. In association with higher value of low frequency permeability, the frequency at which resonance occurs appears at lower frequency. These shows can be used as core materials only in a limited frequency range.

This trend of increase of low frequency permeability is observed up to the annealing temperature 550 ^{0}C. For the annealing temperature of 575 ^{0}C, the low frequency permeability decreases it drops to a very low value. The change in low frequency permeability with annealing temperature is presented in Fig.-5.9(a,b) and combined presented in Fig.-5.10. From the figures, it is observed that the low frequency value of initial permeability increase with the increase of annealing temperature attaining the maximum value at the annealing temperature of 550 ^{0}C. When the annealing temperature is higher than 550 ^{0}C, initial permeability decreases rapidly and these act the pinning centers for the domain wall mobility.
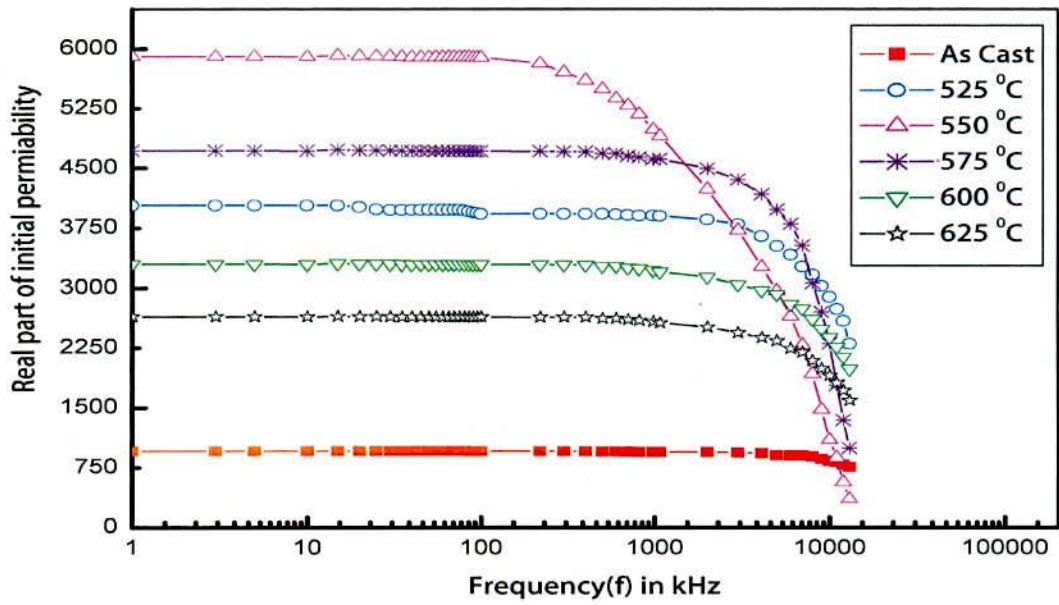
Fig.-5.9(a)
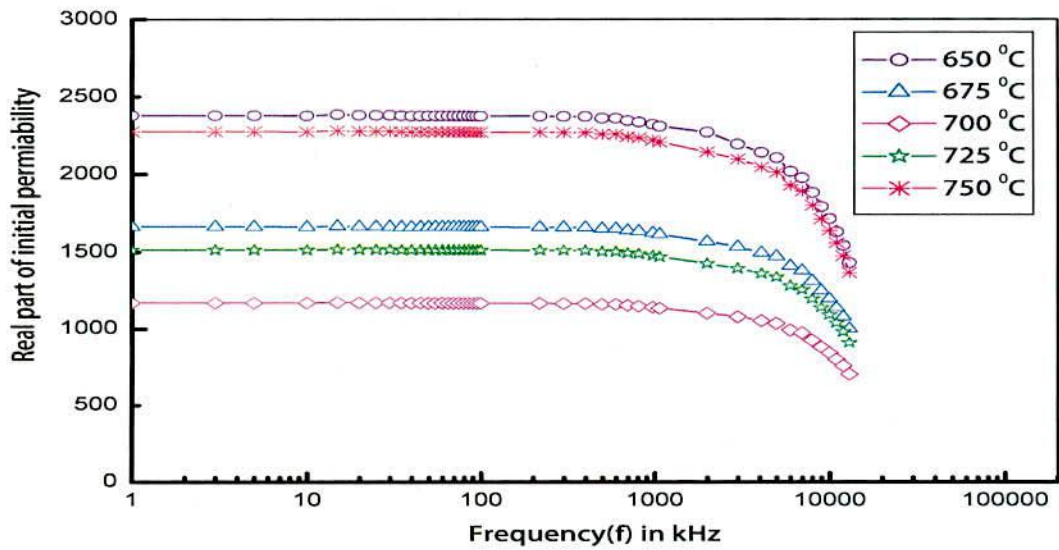
Fig.-5.9(b)

Fig.-5.9(a,b) Frequency dependent real part of complex initial permeability of $(Fe_{0.95}Co_{0.05})_{73.5}Cu_1Nb_3Si_{13.5}B_9$ alloy at as-cast and different annealing temperatures for constant annealing time 30 minutes
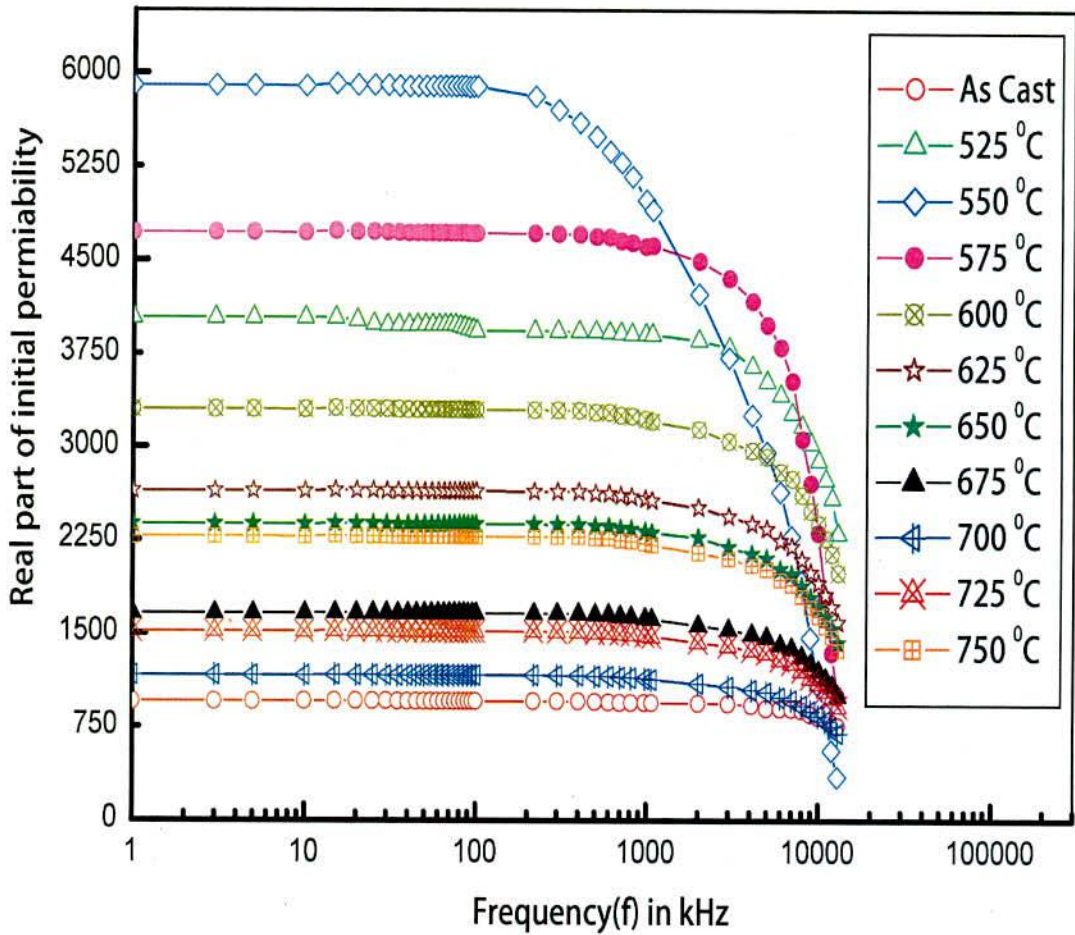
Fig.-5.10 Combined frequency dependent real part of complex initial permeability of $(Fe_{0.95}Co_{0.05})_{73.5}Cu_1Nb_3Si_{13.5}B_9$ alloy at as-cast & different annealing temperatures for constant annealing time 30 minutes

The growing crystallites are far apart from each othe representing small volume fraction that cannot be exchange coupled and the anisotropy cannot be averaged resulting in weak inter grain magnetic coupling. At this temperature, the initiation of crystallization takes places. From this Fig.-5.10, it is easy to conclude about the strong dependence of initial permeability on annealing temperature. The maximum value of at 1kHz low

frequency permeability is shown clear for the annealing temperature of 550 ^{0}C, the value of which is 5890. This temperature is very close to the crystallization onset temperature 550 ^{0}C. Sharp fall of μ' is due to stress developed by growing crystallites. These newly grown crystallites serve as pinning centers at which domain walls are pinned and creates obstructions for their mobility resulting in a decrease in μ'.

Also the growing crystallites are still small in number which cannot be exchange coupled due to large inter grain distance and have high anisotropy energy. Thus, to obtain the highst permeability the sample heat treted at 550 ^{0}C, is most suitable. In other words, the best soft magnetic property can be found at the annealing temperature of 550 ^{0}C for this alloy. For sample annealed above 550 ^{0}C, the initial permeability drops to lower value drastically. The probable reason might be evolution of boride phases and the nonmagnetic fcc phases including Cu clusters. These leads to the increase of magnetocrystalline anisotropy to a high value, which essentially reduces the local exchange correlation length weakening the intergranular magnetic coupling as a results of which magnetic hardening takes place.

From Fig.-5.10 it is seen that μ' changes little with frequency response up to average 100 kHz for 550 ^{0}C annealed samples. Above this critical frequency, μ' drops rapidly due to the increase of loss component of complex permeability. The frequency response of the samples at different annealing temperature can be general be explained in terms of the growth of crystallites and their size distribution. The increase in permeability due to annealing indicate that the high temperature annealing remove the local defects as created during preparation of sample, which facilities the domain wall movement.

5.3.2 Frequency Dependence of Imaginary part of the Complex Permeability of $(Fe_{0.95}Co_{0.05})_{73.5}Cu_1Nb_3Si_{13.5}B_9$ Alloy

The imaginary part of the complex permeability (μ'') at constant annealing time 30 minutes with different annealing temperature over the frequency range 1kHz to 13MHz are shown in Fig.-5.11(a, b). These results are quite complimentary to the results for the real part of the complex permeability of samples.

Fig.-5.11(a)

Fig.-5.11(b)

Fig.-5.11(a, b) Frequency dependence of imaginary part of complex permeability of $(Fe_{0.95}Co_{0.05})_{73.5}Cu_1Nb_3Si_{13.5}B_9$ alloy at different annealing temperatures for constant annealing time 30 minutes

108

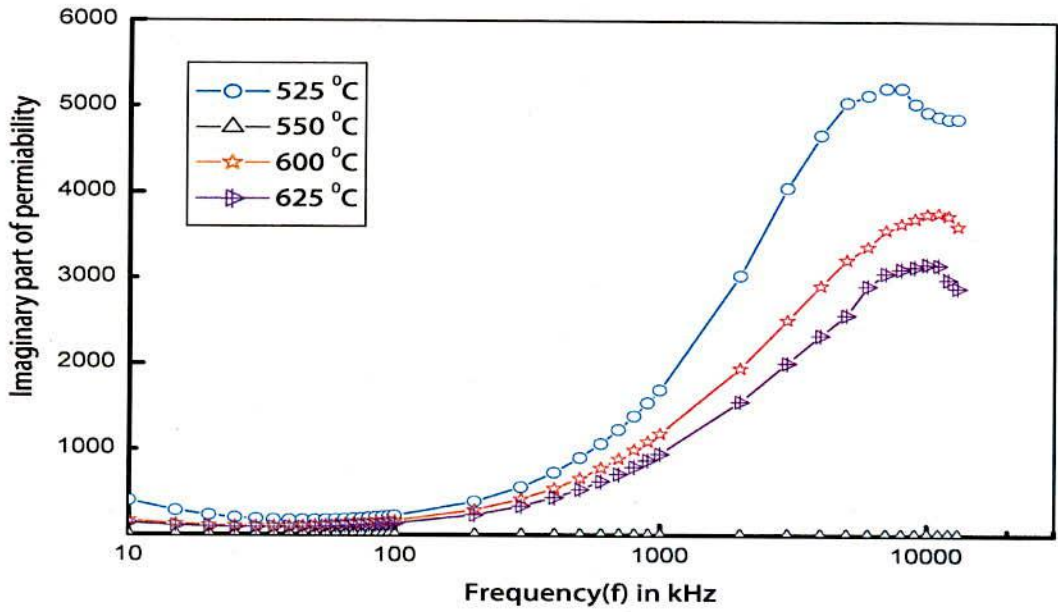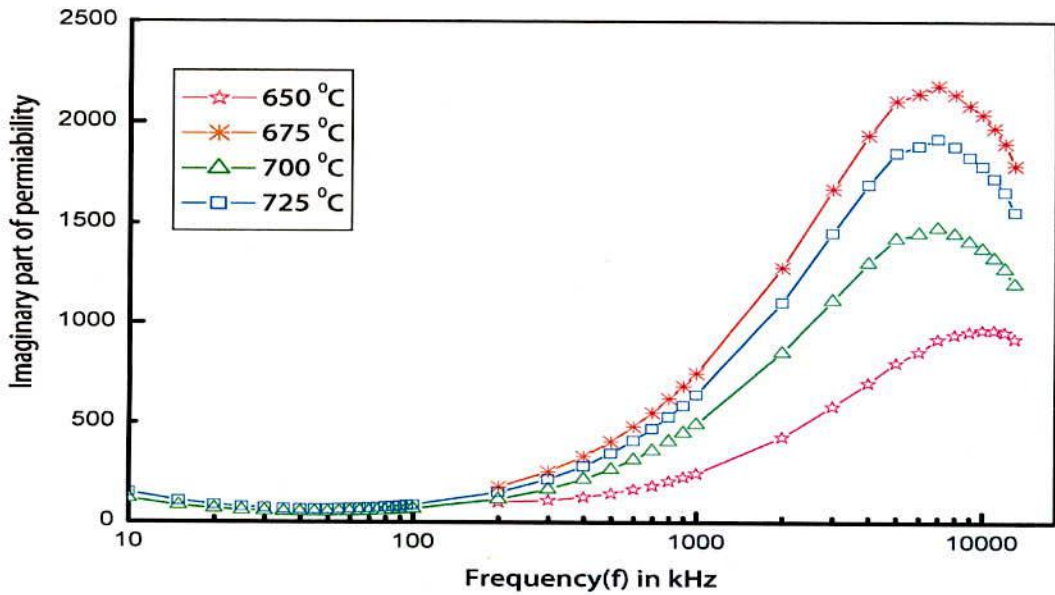These results are quite complimentary to the results for the real part of the complex permeability of samples. The complex permeability for all samples at low frequencies has relatively high value and corresponds to high loss factor and low quality factor as shown in Fig.-5.11(a, b). The origin of the loss factor can be attributed to various domain effects [5.29], which include non uniform and non-repetitive domain wall motion, domain wall bowing, localized variation of flux densities, and nucleation and annihilation of domain walls. The frequency dependence of μ'' of the samples annealed at different temperatures can be attributed to the growth and distribution of the crystallites. The μ'' increases for the annealed samples indicating higher annealing temperatures that causes further growth of crystallites and their stability.

5.3.3 Relative Quality Factor

Loss factor (tanδ) and relative quality factor ($\mu'Q$) are important parameters for the soft magnetic materials from the application point of view. Minimum loss factor and maximum relative quality factors are preconditions for achievement of good soft magnetic properties in FINEMET type alloys. The loss factor is given by the ratio of real and imaginary parts of the complex permeability i.e. $\tan\delta = \dfrac{\mu'}{\mu''}$. The loss factor arises due to eddy current loss as well as for the phase lag of the spin reorientation with respect to external field. Since the net tanδ found for this nanocrystalline material is quite complex, it is difficult to separate out the contribution from the eddy current loss and the phase lag of the spins with respect to the fields. The loss factor in general is found to be high for the entire sample at low frequency as well as for high frequency.

The frequency dependence of $\left(\dfrac{\mu'}{\tan\delta}\right)$ or $\mu'Q$ at constant annealing time 30 minutes with different annealing temperatures are shown in Fig.-5.12(a, b). It is well known that optimal annealing nanocrystalline alloys display minimum loss and very high relative quality factor, $\mu'Q$ of the order of 2×10^4 to 2×10^5. The optimal annealing temperature is determined through successive annealing of the alloys from 550 ^{0}C to 725

^{0}C. From these two figures it is observed that relative quality factor in creases with the increase of annealing temperature up to 550 ^{0}C and 550 ^{0}C the quality factor decreases and attains a minimum value at 700 ^{0}C. Further increase of temperature above 700 ^{0}C a sharp increase of $\mu^/Q$ is observed.
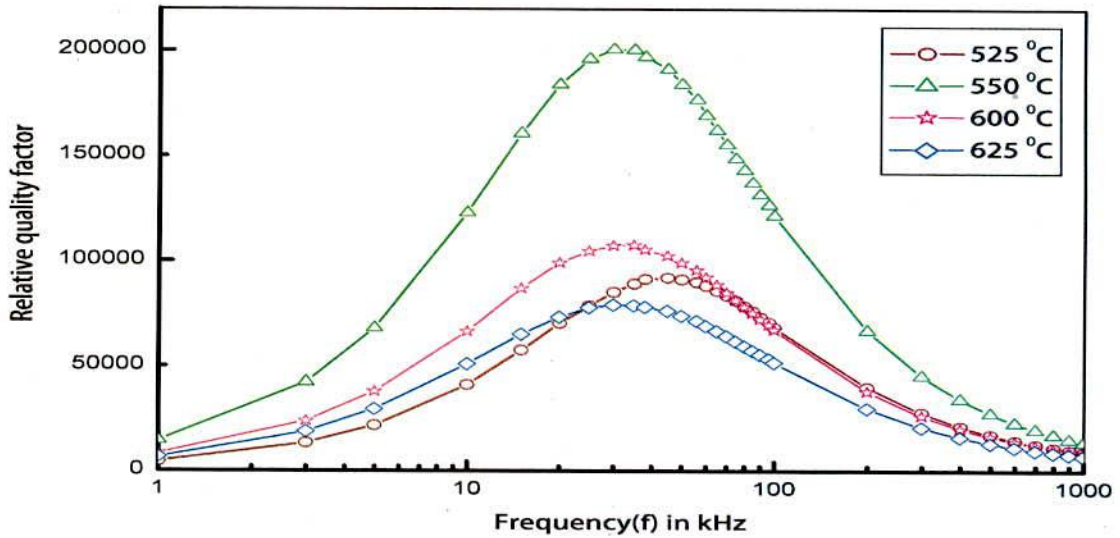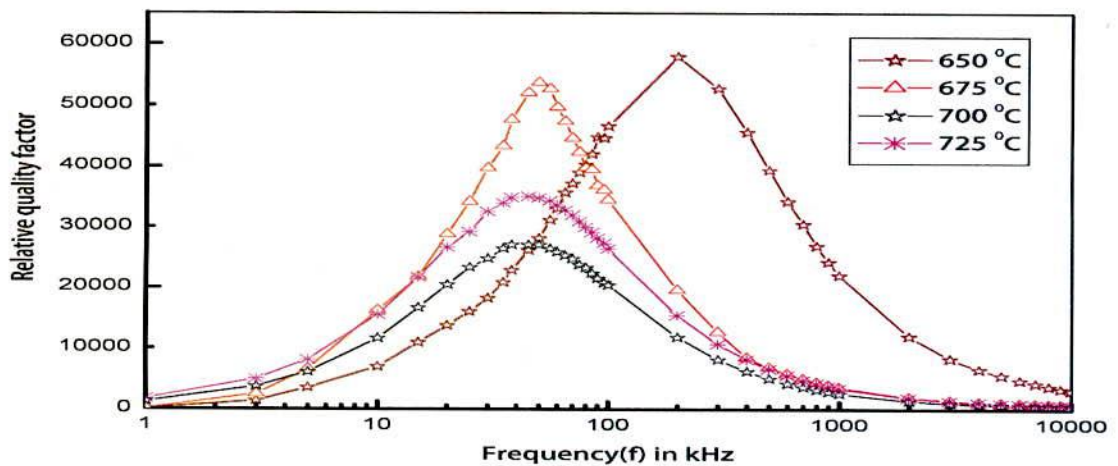
Fig.-5.12(a)

Fig.-5.12(b)

Fig.-5.12(a, b) Frequency dependence of relative quality factor of $(Fe_{0.95}Co_{0.05})_{73.5}Cu_1Nb_3Si_{13.5}B_9$ alloy at different annealing temperatures for constant annealing time 30 minutes

110

The increase of the loss factor with annealing temperature indicates that longer annealing time causes further growth of crystallites and their stability. As a result, loss is controlled mainly by interaction between grains, the size of grains and grain orientation as such the specimen thickness becomes important. The precipitation of very small percent of particles improves the high frequency losses and permeability. The phase lags between induced flux and the applied field increases but with more consistency with the increase of frequency. At low frequencies, magnetic losses are controlled by hysteresis caused by irreversible magnetization process and at high frequency, the flux penetration becomes low and loss is mainly controlled by interaction between the grains as well as eddy current.

The relative quality factor curve initially rises with respect to increasing frequency and after reaching a peak value, it decreases. The peak value for each curve represents the best soft magnetic behavior for the corresponding annealing temperature. Beyond the peak value, the quality factor is found to decrease which may be attributed to increase of loss components. This gives a choice of optimal annealing temperature for attaining best soft magnetic properties.

The highest value of quality factor is found for the sample annealed at $550\ ^0C$, which also indicates the best heat treatment temperature to obtain the highest value of quality factor. From all curves, it is noticeable that the higher values of the relative quality factor in general lie within the range of 10 kHz to 100 kHz frequencies. Thus the frequency range for application area might be chosen.

5.4   Curie Temperature Measurement of Nanocrystalline Amorphous Ribbon of $(Fe_{0.95}Co_{0.05})_{73.5}Cu_1Nb_3Si_{13.5}B_9$ Alloy.

Curie temperature (T_c) corresponds to the temperature at which a magnetically ordered material becomes magnetically disordered, i.e. becomes paramagnet. T_c also signifies the strength of the exchange interaction between the magnetic atoms. In general, determination of T_c is not that straight forward as it seems to be from the first principle and the unique volume of T_c is not that straight forward as it seems to be from the first

111

principle and the unique volume of T_c can be determined without ambiguity only when the material under study is perfectly homogeneous single phase, defect free and of high purity. The T_c of nanocrystalline amorphous of composition $(Fe_{0.95}Co_{0.05})_{73.5}Cu_1Nb_3Si_{13.5}B_9$ have been determined using μ Vs. T curves. Temperature dependence of ac initial permeability of the sample subjected to a heating rate 5 ^0C/min and the constant frequency of 100 kHz has been used for measuring T_c as shown in Fig.-5.13(a, b). The numerical values of T_c's for the samples are shown in Table-5.4.

Table-5.4 Curie temperatures of $(Fe_{0.95}Co_{0.05})_{73.5}Cu_1Nb_3Si_{13.5}B_9$ alloy for as-cast and annealed at different annealing temperature for 30 minutes

Annealing Temperature, T_a(^0C)	Curie Temperature, T_c(^0C)
As-cast	422
500	418
525	402
550	272
600	142
625	128
650	164
675	165
700	158
725	160

In Fig.-5.13(a, b) the real part of complex initial permeability μ' has been presented as a function of temperature at a fixed frequency of 100 kHz. The curve reveals strong dependence of initial permeability on annealing temperature. For samples annealed from 500 ^0C to 550 ^0C, as shown in Fig.-5.13(a), permeability passes through a maximum just before a sharp fall to near zero with the manifestation of Hopkinson effect characterizing the ferro-paramagnetic transition which is compatible with reported results [5.30]. From variation of μ' with temperature for toroidal samples annealed at 500 ^0C to 550 ^0C, Curie temperature of the residual amorphous matrix determined from the maximum value of $\frac{d\mu'}{dT}$ are 418 ^0C, 402 ^0C and 272 ^0C for the sample annealed at 500 ^0C, 525 ^0C and 550 ^0C respectively.
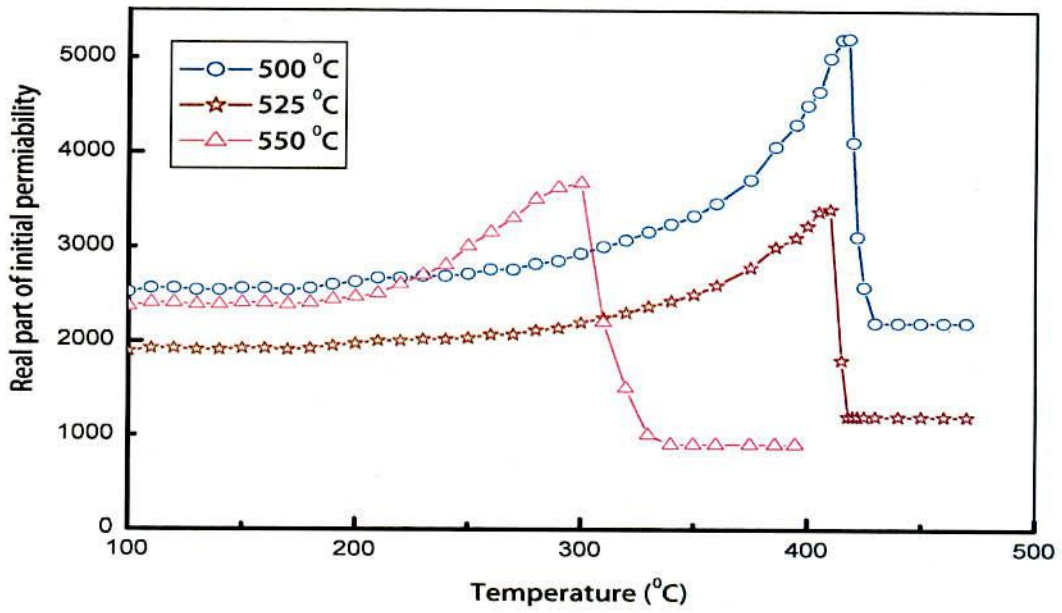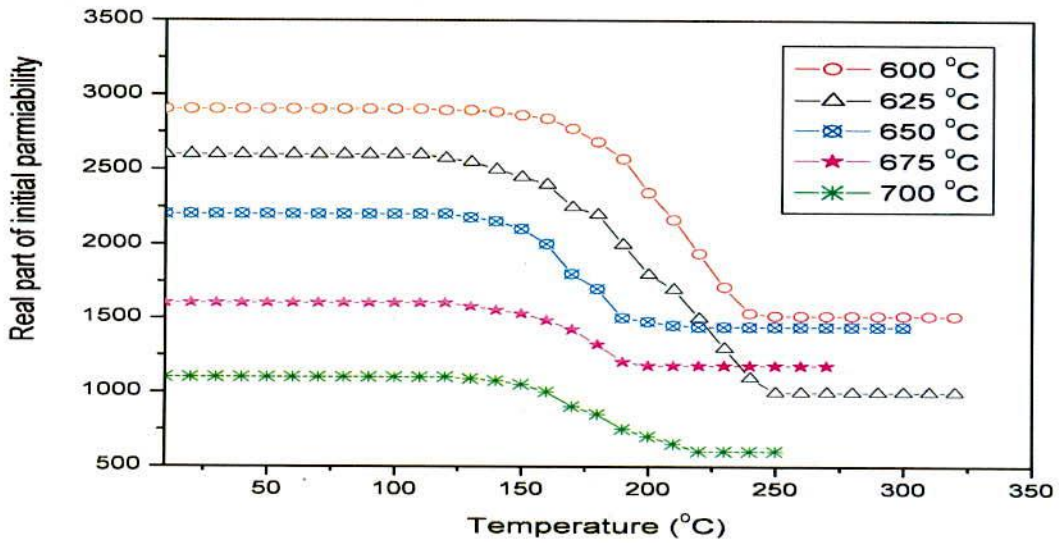
112

Fig.-5.13(a)

Fig.-5.13(b)

Fig.-5.13(a, b) Temperature dependent real part of complex initial permeability of $(Fe_{0.95}Co_{0.05})_{73.5}Cu_1Nb_3Si_{13.5}B_9$ alloy at different annealing temperature for constant annealing time 30 minutes

Practically the accurate determination of T_c of amorphous material is really difficult due to irreversible component of the structural relaxation like long range internal stress, topological and chemical short range order. The structural relaxation without destroying the amorphous state may influence T_c. Therefore, during the measurement of T_c the heating rate has been adjusted in such a way that no substantial relaxation takes place. T_c of the amorphous matrix decreases significantly when annealed at and above crystallization temperatures. The probable reason of decreasing the T_c of the amorphous phase when annealed at above the crystallization temperature is that amorphous matrix is depleted with iron and the relative amount of Nb in the amorphous matrix increases, which weakens the exchange interaction resulting in a decrease of T_c of the amorphous matrix. It is interesting to observe an enhancement of T_c again when samples are annealed at higher temperature. This increase cannot be explained in a straight forward way. Probably redistribution of atomic species, local environment of the matrix and the compositional variance of the residual amorphous matrix as well as the procedure used to determine T_c are the cause of the behavior.

The following discussion can clear some complexity regarding the phase transition temperature of the higher temperature annealed sample. The worthwhile to note that if we look into graph of μ' Vs T shown in Fig-.-5.13(b) critically we observe that decrease of μ' with temperature is quite different from that of μ' Vs T curves of Fig.-5.13(a), which is relatively smeared out. It is very difficult to find out a unique value of T_c from such diffused μ' Vs T measurements. The more diffuse character of the ferro-paramagnetic transition in the residual amorphous matrix for the samples annealed at higher temperature is attributed to the higher degree of compositional and structural disorder in the residual amorphous phase [5.31-5.32]. Varga and Rao [5.33] have interpreted this type of reduction of T_c in FINEMET alloys after annealing at higher temperature as due to compositional gradients within the remaining amorphous phase.

The feature which can be observed from Fig.-5.13(b) is that as the annealing temperature is above crystallization temperature i.e. 600 ^{0}C to 725 ^{0}C, the sharpness of fall the lower values of permeability is smeared out with the appearance of a tail in the high temperature region. This might be an indication of loss of homogeneity of the

114

sample for initiation of nucleation i.e. for proceeding of crystallization. These results in a good agreement with those previously reported for the FINEMET composition [5.34-5.35].

From the results of temperature dependent permeability for samples at 500 ^{0}C to 725 ^{0}C, the grain coupling is largely but not completely interrupted above the Curie temperature at the amorphous matrix. A system in which the magnetic coupling between particles is significant and presents super paramagnetic relaxations is termed as super ferromagnetism by S. Mфrup [5.36]. The precise coupling mechanism for this type of behavior at T > T_c^{am} may be explained in terms of exchange penetration through thin, paramagnetic inter granular layer and / or dipolar interactions.

5.4.1 The Variation of Curie Temperature with respect to Annealing Temperature

Fig.-5.15 shows the variation of Curie temperature with respect to annealing temperature. The Curie temperature of the as-cast i.e. amorphous $(Fe_{0.95}Co_{0.05})_{73.5}Cu_1Nb_3Si_{13.5}B_9$ alloy was found at 422 ^{0}C (Fig.-5.14), while for the original amorphous FINEMET of composition $Fe_{73.5}Cu_1Nb_3Si_{13.5}B_9$ it was found 354 ^{0}C [5.16]. This shows that there is an enhancement of Curie temperature due to addition of cobalt. The physical causes may be explained as follows: Curie temperature of Fe is 770 ^{0}Cand that of cobalt is 1127 ^{0}C.Replacement of Co for Fe would enhance the Curie temperature because of the much higher magnetocrystalline anisotropy of which increases thermo magnetic stability of this type alloy.

From the Table-5.4, it can be observed that the Curie temperature of the as-cast and amorphous ribbon of composition $(Fe_{0.95}Co_{0.05})_{73.5}Cu_1Nb_3Si_{13.5}B_9$ is 422 ^{0}C. Nearly same of the Curie temperature occurs when the sample is annealed in the range 500 ^{0}C – 525 ^{0}C. From X-ray diffraction, no crystalline phase was observed before the annealing temperature of 500 ^{0}C.
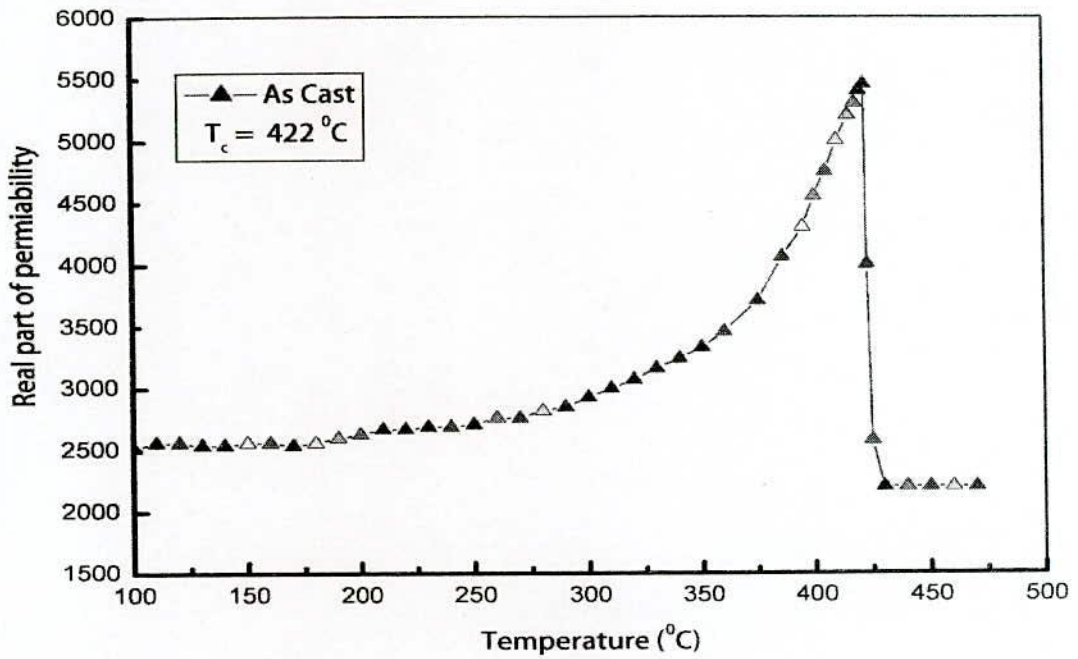
Fig.-5.14 Temperature dependent real part of complex initial permeability of $(Fe_{0.95}Co_{0.05})_{73.5}Cu_1Nb_3Si_{13.5}B_9$ alloy at as-cast
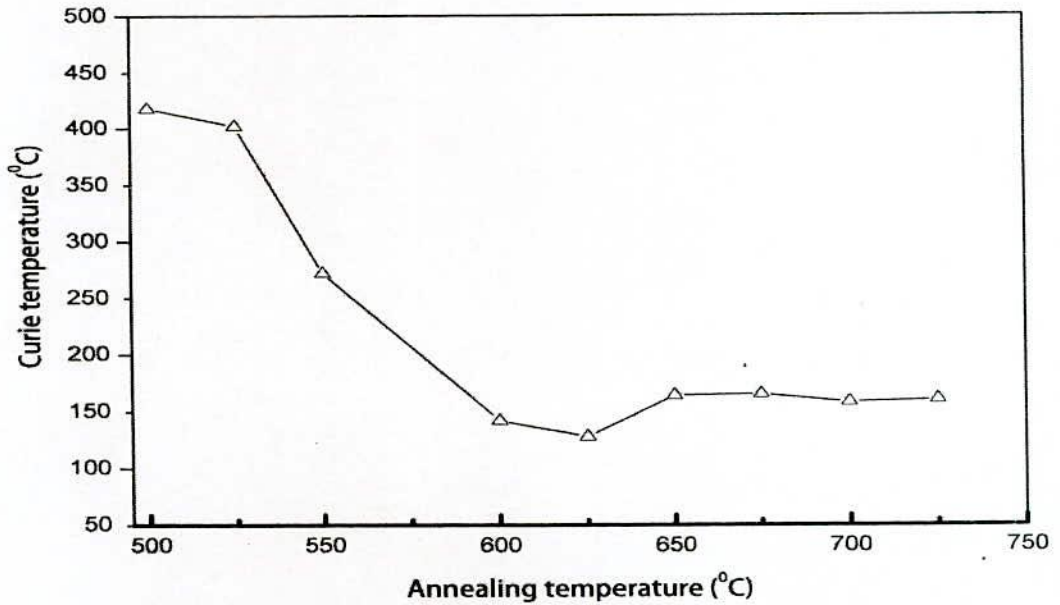

Fig.-5.15 Variation of Curie temperature with respect to annealing temperature

116

Above the crystallization temperature, Curie temperature of the amorphous matrix decreases significantly. The probable reason of decreasing the Curie temperature is that the amorphous matrix is depleted with iron and the relative amount of Nb in the amorphous matrix increases, which weakens the exchange interaction resulting in a decrease of Curie temperature of the amorphous matrix.

5.5 Specific Magnetization Measurement of Nanocrystalline Amorphous Ribbons

The magnetization of the nanocrystalline amorphous ribbons of composition $(Fe_{0.95}Co_{0.05})_{73.5}Cu_1Nb_3Si_{13.5}B_9$ alloy annealed for constant 30 minutes annealing time at varying temperature 600 ^{0}C to 750 ^{0}C have been measured as a function of magnetic field generated by an electromagnet using Vibrating Sample Magnetometer (VSM). In this type of magnetometer the sample is vibrated up and down in a region surrounded by several pick up coils. The magnetic sample is thus acting as a time changing magnetic flux, varying inside a particular region of fixed area. The magnetometer was calibrated using a high purity Ni disk considering the saturation magnetization of Ni = 54.75 emu/g at room temperature. The ribbon samples were cur into small shapes, weighed and glued to a standard sample holder.

The present work is mainly aimed at studying the magnetization process of (Fe-Co)-Cu-Nb-Si-B nanocrystalline ribbons as affected by varying annealing temperature at constant annealing temperature. This provides information about the nature of residual strain in as prepared melt-spun ribbons and their effects on domain wall pinning. This study also provides important technical information about the possibility of using this ribbon at elevated annealing temperature and the optimum operating points of this ribbon, when they are used as soft magnetic materials under varying fields. The detailed quantitative analysis of the situation is, therefore, very complex and present understanding of the problem of magnetization process as affected by these defects is not yet clear.

117

We can distinguish reversible and irreversible types of relaxation due to annealing temperature. Irreversible type of relaxation are those which are connected with thermally initiated microscope jumps of defects or ordering atomic pairs which corresponds to irreversible domain wall movements under external field [5.37-5.39]. Thus reversibility of magnetization is not possible in these cases by reversing the external field. The reversible relaxation on the other hand means micro structural atomic rearrangement with in the domain wall potential in a way that allows the reversal of the magnetic domain wall movements through reversing of the direction of the magnetic field. The present work will be confined to the later situation only.

The present results are interpreted in terms of conventional domain theory of ferromagnetism, where it is postulated that the effect of annealing temperature is to partially remove the pinning centers of the domain wall and thereby improving the magnetic softness of this ribbon.

5.5.1 Effect of Annealing Temperature on Specific Magnetization at Room Temperature

Specific magnetization (M_s) at room temperature has been measured annealed samples. The annealing has been carried out for 30 minutes at $T_a = 600\ ^0C$ to $700\ ^0C$. Fig.-5.16 and Fig.-5.17 show the field dependence of specific magnetization for nanocrystalline amorphous ribbon and thereby treated samples measured by VSM. From the curves it is clearly evidenced that the magnetization is saturate for all the samples in the annealed states within an applied field 20000 Oe. Maximum saturation magnetization is reached at $600\ ^0C$ for the sample. It can be seen that with increasing annealing temperature magnetization increase until $625\ ^0C$. Aranda et. al. [5.40] have studied the approach to saturation in nanocrystalline FINEMET materials. The magnetization prior to saturation is associated with reversible rotation and has been fitted to the law

$$M(H) = M_S \left[1 - \frac{a_1}{H} - \frac{a_2}{H^2} \right] + bH^{1/2} \tag{5.4}$$

118

Where the term $\frac{a_2}{H^2}$ was described as being a direct consequence of the random anisotropy model, and attributable to FeCo(Si) grains. The coefficient a_2 reflects the Herzer's predicted effective magnetic anisotropy of the nanocrystalline material, where as in amorphous alloy it is postulated as being caused by local stress and magnetoelastic coupling saturation magnetization 202.65emu/g observed at 600 ^{0}C. After 625 ^{0}C, M_s observed 141.45emu/g to increase up to 164emu/g observed at 675 ^{0}C.
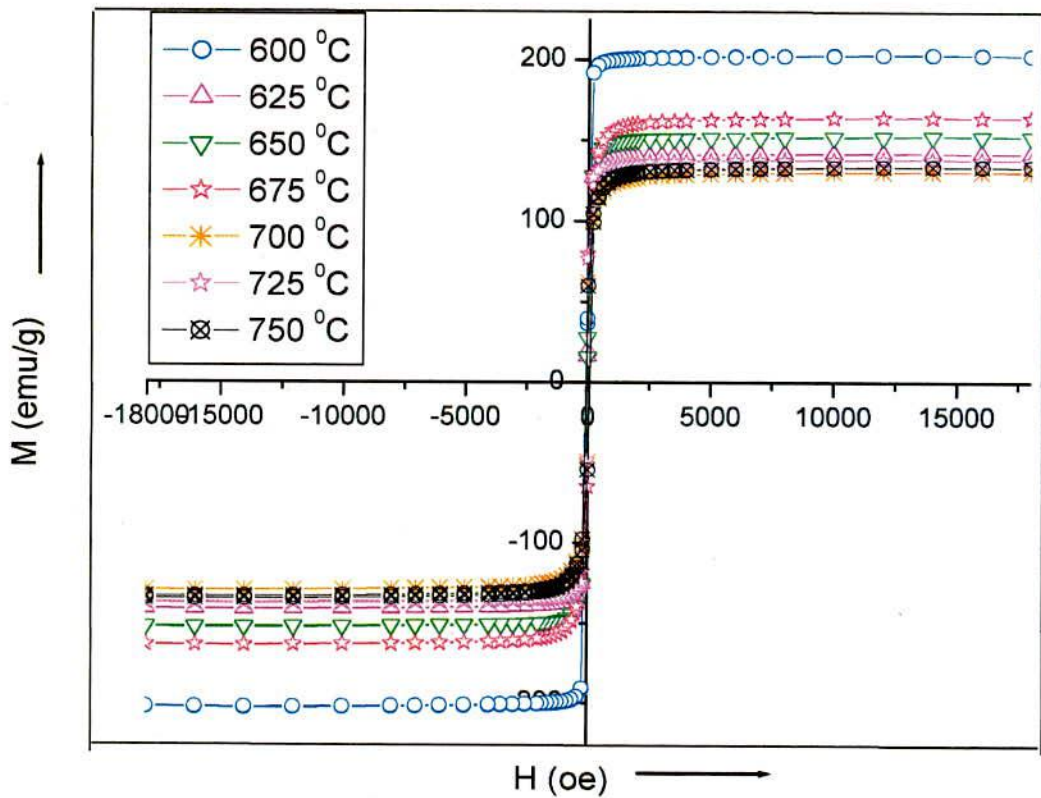
Fig.-5.16 Specific magnetization versus magnetic field of $(Fe_{0.95}Co_{0.05})_{73.5}Cu_1Nb_3Si_{13.5}B_9$ alloy at different annealing temperatures for constant annealing time 30 minutes

An increase of M_s for the annealed samples at 625 ^{0}C to 675 ^{0}C compared with amorphous state is due to the irreversible structural relaxation, changing the degree of

chemical disorder of the amorphous state [5.41] and enhanced volume fraction of FeCo(Si) nanocrystals that are exchange coupled. The saturation magnetizations are shown in Table-5.5

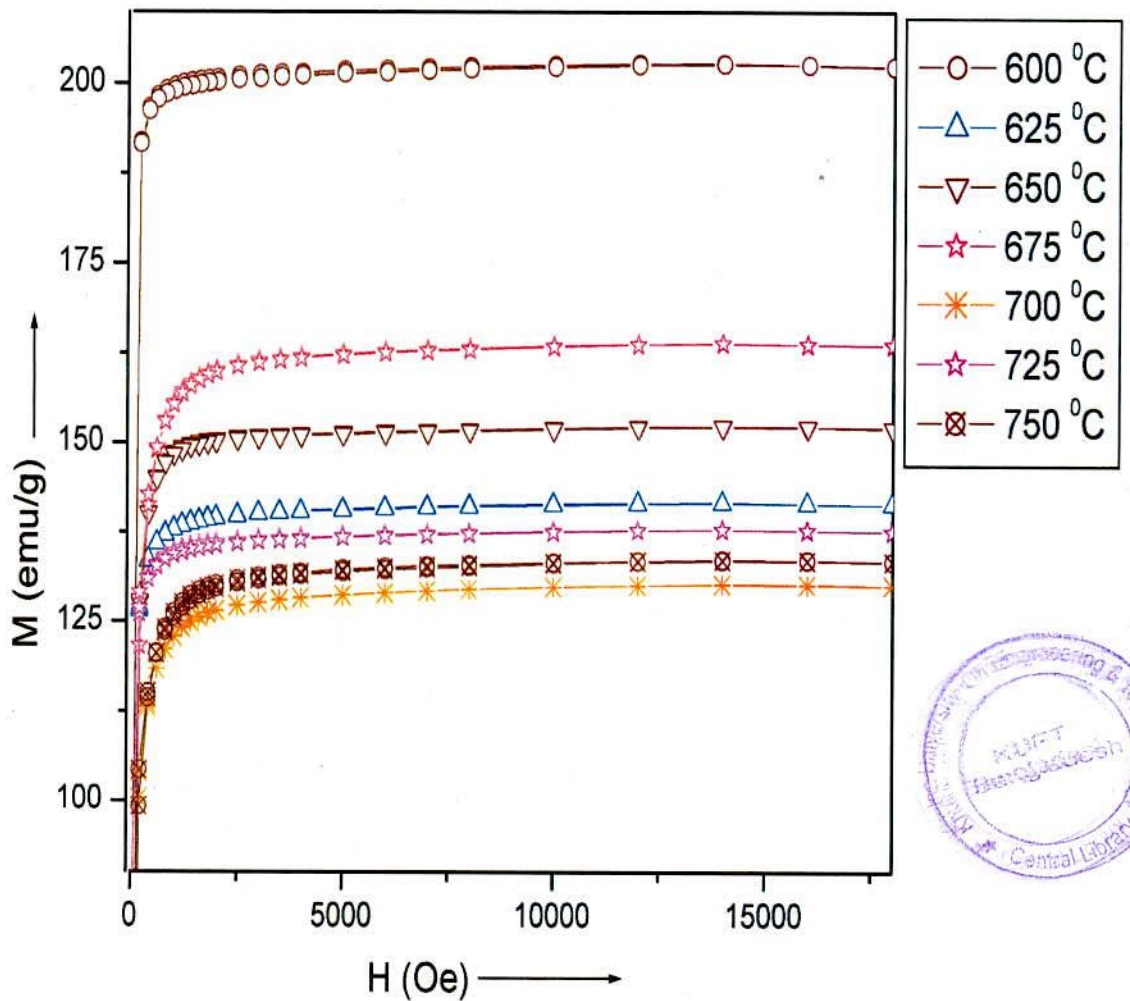Fig.-5.17 Specific magnetization versus magnetic field of $(Fe_{0.95}Co_{0.05})_{73.5}Cu_1Nb_3Si_{13.5}B_9$ alloy at different annealing temperatures for constant annealing time 30 minutes

It is to be noted that an increase in M_s due to structural relaxation has also been detected in Fe-based glasses [5.42]. A rapid decrease in M_s has been observed with increasing annealing temperature at 600 ^{0}C. The decreasing of M_s may be connected with the enrichment of the residual amorphous phase with Nb that weakens the coupling between ferromagnetic nanograins. Also the role of Si-diffusion into FeCo(Si) nanograins and these local environments also may have effect in decreasing M_s. The decrease of M_s for the sample higher annealing temperature on ordering of Fe_3Si nanograin can be not be ruled out. If a small applied field suffices to produce saturation the nanocrystalline material is said to be magnetically soft.

Table-5.5 The values of saturation magnetization of $(Fe_{0.95}Co_{0.05})_{73.5}Cu_1Nb_3Si_{13.5}B_9$ alloy at different annealing temperature with constant annealing time 30 minutes.

Annealing temperature, T_a in ^{0}C	Saturation magnetization, M_s in emu/g	Remanence , B_r in emu/g	Coercive force, H_c in Oe
600	202	...	...
625	141	79	80
650	152	...	...
675	164	...	...
700	130	76	76
725	137	61	70
750	133	59	75

Fig.-5.18(a, b, c, d) represents the B-H loops at room temperature were measured applied field. From these loops the remanence induction (B_r) and the coercive force (H_c) were determined. These results are shown in Table-5.5. It is observed that B_r and H_c both decrease with increasing annealing temperature. The different values of B_r and H_c are interpreted in a quantitative way by means of domain theory.
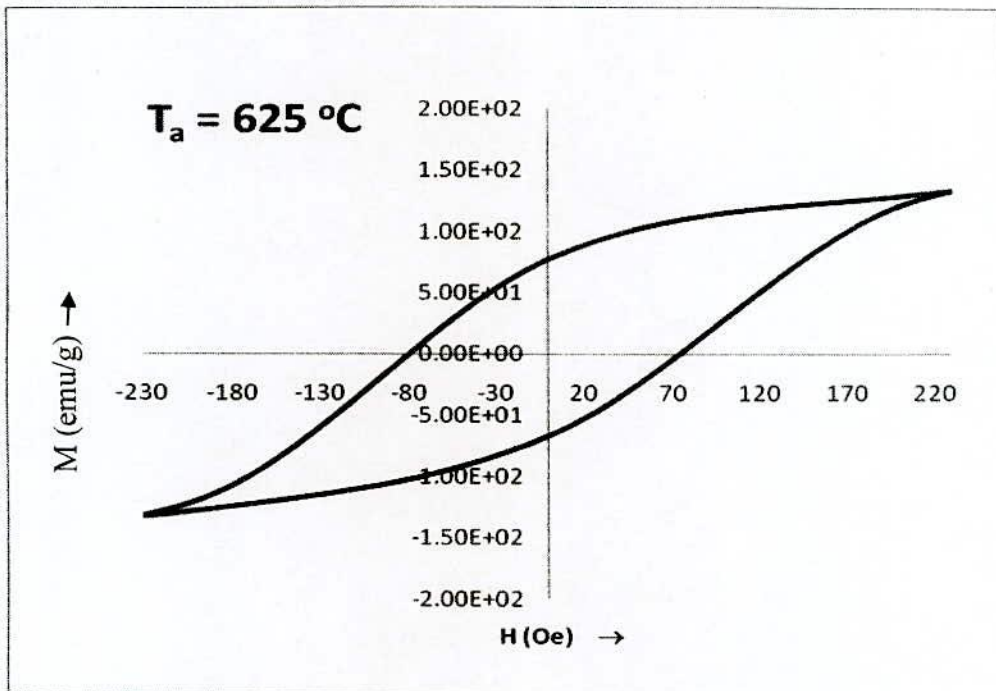
Fig.-5.18(a)

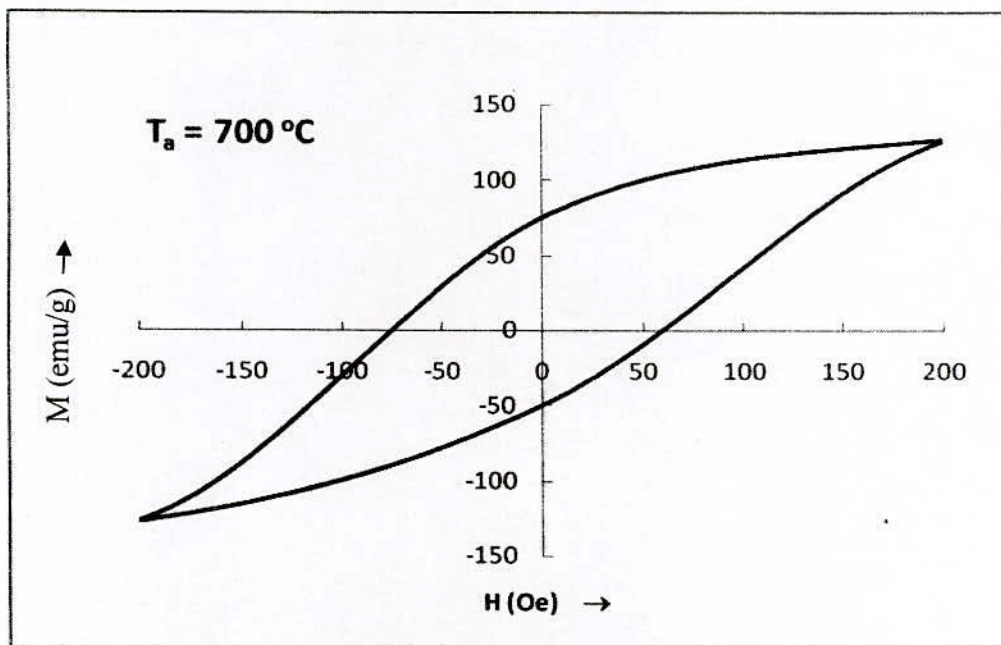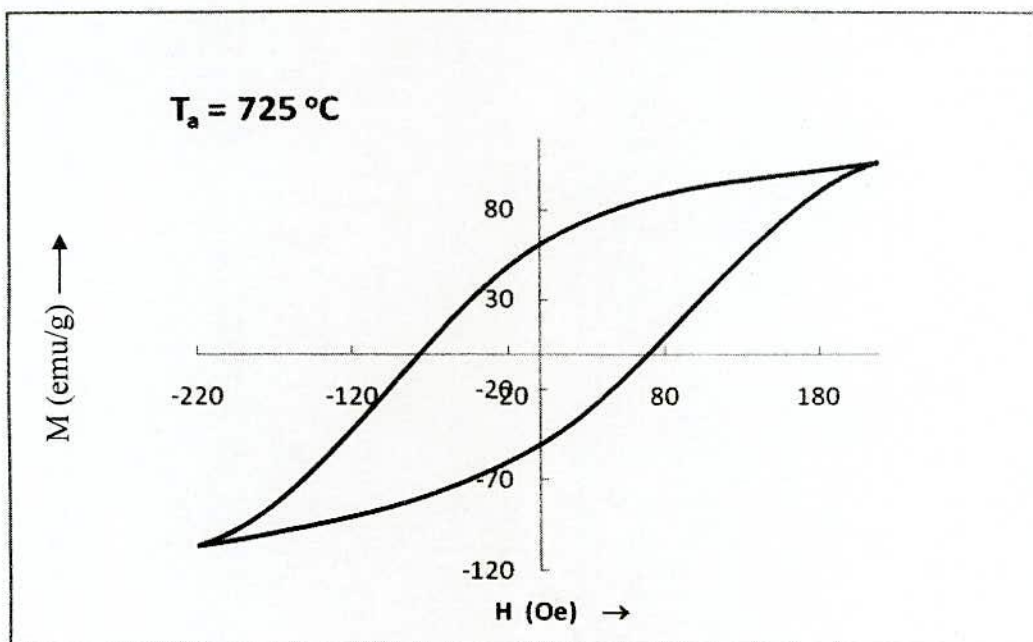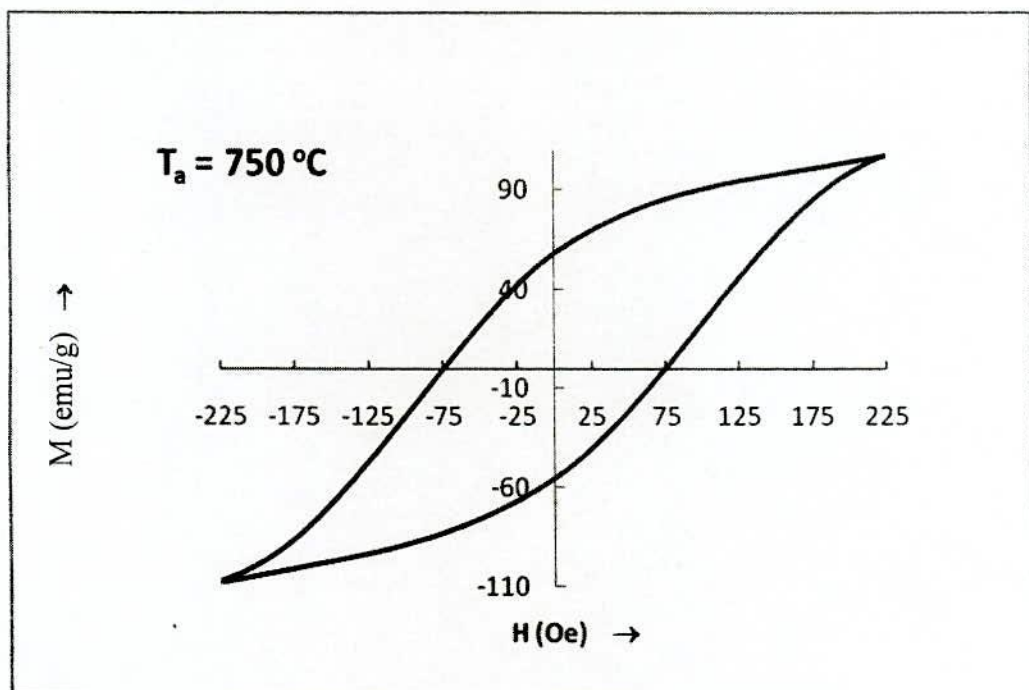Fig.-5.18(b)

Fig.-5.18(c)

Fig.-5.18(d)

Fig.-5.18(a, b, c, d)   Magnetic hysteresis of $(Fe_{0.95}Co_{0.05})_{73.5}Cu_1Nb_3Si_{13.5}B_9$ alloy at different annealing temperature for constant annealing time 30 minutes

CHAPTER - VI

Conclusions

Conclusions

6.0 Conclusions

Nanocrystalline amorphous ribbon of the FINEMET family with a nominal composition $(Fe_{0.95}Co_{0.05})_{73.5}Cu_1Nb_3Si_{13.5}B_9$ has been studied to find out the correlation between microstructural features and soft magnetic properties dependent on various stages of nanocrystalline during the isothermal annealing around the crystallization temperature of their amorphous precursors. These ribbons were produced by melt spinning technique with 20 – 25 µm thickness. Crystallization behavior and magnetic properties have been studied by DTA, XRD, LCR meter and VSM.

Crystallization behavior of the samples was investigated by DTA and XRD experiments. The frequency spectra of the annealed samples were performed by an LCR meter and specific magnetization of the annealed sample as a function of magnetic field were measured by a VSM. From the systematic investigation on the crystallization structural and magnetic properties, the following conclusions can be outlined:

(i)   DTA experiments was performed for five different heating rate 10, 20, 30, 40 and 50 ^{0}C/min in steps of 10 ^{0}C/min up to a temperature of 900 ^{0}C. DTA reveals the primary and secondary crystallization onset temperatures with the manifestation of two well-defined exothermic peaks corresponding to nanocrystalline FeCo(Si) and FeB and /or FeCoB phases respectively. The knowledge of crystallization temperatures has been fruitfully utilized during the isothermal annealing of these amorphous ribbons for nanocrystallization, which ultimately controls the magnetic properties of FINEMET alloys. For heating rates 10, 20, 30, 40 and 50 ^{0}C/min, the onset of the first crystalline (T_{x_1}) were found 528 ^{0}C, 529 ^{0}C, 533 ^{0}C, 528 ^{0}C, 541 ^{0}C and that of the second crystalline phase (T_{x_2}) were found 674 ^{0}C, 677 ^{0}C, 677 ^{0}C, 670 ^{0}C, 687 ^{0}C respectively.

(ii)   The activation energy values of the first crystalline phase α-FeCo(Si) and the second crystalline phase (FeB and /or FeCoB) calculated using Kissinger's plots were 2.40 and 4.31 eV respectively. The temperature difference between two crystallization peaks $\left(T_{P_2} - T_{P_1}\right)$ is found to exist around 137 ^{0}C. This peak separation temperature is important for the stability of primary crystallization phase FeCo(Si), against detrimental boride phases which is necessary for fabrication of high quality inductors.

(iii)   The amorphous stage of the as-cast ribbons has been confirmed by XRD. The evolution of nanocrystallites of α-FeCo(Si) and their sizes have been determined from the line broadening of fundamental peaks (110) from XRD pattern as affected by annealing around the crystallization temperatures. The grain size determined for the sample from 9 to 26 nm for the annealing temperature from 550 ^{0}C to 750 ^{0}C. The crystallization onset temperature for the sample is found between 500 ^{0}C to 550 ^{0}C which coincides well with the value obtained from DTA. The lattice parameter and Siat.% shows an inverse relationship indicating that Si diffuses in the crystalline phase at the initial stage of crystallization at 550 ^{0}C for which Siat.% increased with decrease in lattice parameter that continued up to 675 ^{0}C. Beyond 675 ^{0}C, Si at.% is found to decrease with increase in lattice parameter, that indicates diffusion of Si out of nanograin, indicating recrystallization i.e. formation of boride phases.

(iv)   Magnetic initial permeability of nanocrystalline /amorphous ribbon strongly depends on annealing temperature. The improvement in the soft magnetic properties can be ascribed to the much refined grain structure in the range of 9 to 26nm obtained at various temperatures during annealing. When alloys were annealed for 30 minutes at various temperatures, the maximum initial permeability (μ') were observed at T_a = 550 ^{0}C for $(Fe_{0.95}Co_{0.05})_{73.5}Cu_1Nb_3Si_{13.5}B_9$ alloy. The temperature corresponds to a maximum initial permeability and lowest losses. A sharp increase of initial permeability at this temperature indicates that μ' is related to structural relaxation. The high permeability is attributed to the drastic decrease of

effective anisotropy due to nanometric grain size effect and strong inter grain magnetic coupling sample showed magnetic hardening at 600 ^{0}C to 750 ^{0}C with very low value of μ' due to stress developed during the initiation of crystallization.

(v) The highest value ($\approx 5.8 \times 10^3$) of real part of initial permeability is achieved for the sample annealed at 550 ^{0}C, for which the least value of relative loss factor was found. So, 550 ^{0}C is the most suitable heat treatment temperature from the application point of view in case of the present alloy as a soft magnetic material.

(vi) For technological uses of nanocrystalline materials at elevated temperature and for magnetic stability it is important to look for this composition that give higher value of Curie temperature (T_c). The T_c is 422 ^{0}C for as-cast amorphous $(Fe_{0.95}Co_{0.05})_{73.5}Cu_1Nb_3Si_{13.5}B_9$ alloy. T_c of interfacial amorphous phase has been found to decrease for samples when annealed above crystallization temperatures due to the depletion of Fe and increase of relative amount of Nb in the residual amorphous phases.

(vii) The saturation magnetization for nanocrystalline samples has slightly increased for annealing at temperature around the onset crystallization when annealed at higher temperature at which complete crystallization takes place, magnetization decrease again.

There is much scope for further research in controlling the magnetic characteristics by changing composition and heat treatment certain important parameter like temperature dependence magnetization, anisotropy and magnetostriction can be study in detail for a better understanding of micro structure property relationship of FINEMET type alloys.

References

References

Chapter – I

[1.1] T. Kulik, A. Hernando, M. Vasquez; "Correlation between structure and the magnetic properties of amorphous and nanocrystalline $Fe_{73.5}Cu_1Nb_3Si_{22.5-x}B_x$ alloys"; J. Magn. Magn. Mater. (1994) 133, 310.

[1.2] Jing Zhi, Kai-Yuan He, Li-Zbi Cheng, Yu-jan Fu; "Influence of the elements Si/B on the structure and magnetic properties of Nanocrystalline $(Fe,Cu,Nb)_{77.5}Si_xB_{22.5-x}$ alloys"; J. Magn. Magn. Mater. (1996) 153, 315.

[1.3] S. N. Kane, S. Sarabhi, A. Gupta, L. K. Varga, T. Kulit; "Effect of quenching rate on crystallization in $Fe_{73.5}Si_{13.5}B_9Cu_1Nb_3$ alloy"; J. Magn. Magn. Mater. (2000) 215-216, 372.

[1.4] M. El Ghannami, T. Kulit, A. Hernando, L. Fermandez Barquin, J. C. Gomez Sal, P. Gorria, J. M. Barandarian; "Infulence of the Preparation Condition on the Magnetic Properties and Electrical resistivity of $Fe_{73.5}Cu_1Nb_3Si_{13.5}B_9$ Nanocrystalline alloys"; J. Magn. Magn. Mater. (1994) 133, 314.

[1.5] S. P. Mondal, Kazi Hanium Maria, S. S. Sikder, Shamima Choudhury, D. K. Saha and M. A. Hakim; "Influence of Annealing Conditions on Nanicrystalline and Ultra-Soft Magnetic Properties of $Fe_{75.5}Cu_1Nb_1Si_{13.5}B_9$ alloy"; J. Mater. Sci. Technol., 2012, 28(1), 21-26.

[1.6] M. Hassiak, J. Zbroszczyk, J. Olszewki, W. H. Ciuzynska, B. Wyslocki, A. Blachowicz; "Effect of cooling rate on Magnetic properties of Amorphous and Nanocrystalline $Fe_{73.5}Cu_1Nb_3Si_{15.5}B_7$ alloy"; J. Magn. Magn. Mater. (2000) 215-216, 410.

[1.7] Y. Yoshizawa, S. Oguma, K. Yamauchi; "New Fe-Based Soft Magnetic Alloys Composed of Ultra fine Grains Structure"; J. Appl. Phys. (1988) 64, 6044.

[1.8] Y. Yoshizawa and K. Yamauchi; IEEE Trans. Magn. 25(1989), p.3324; Abstract-INSPEC/order Document/ order Document/ Full Text via Cross Ref./ Abstract References in Scopus/ Cited by inscopus.

[1.9] Vacuum Schmelze Gmbh, Toridal Cores of VITROPERM, Data sheet PW-014 (1993)

[1.10] G. Herzer; "Grain size dependence of coercivity and permeability in nanocrystalline ferromagnets"; IEEE Trans. Magn. 26, 1397-1402 (1990).

[1.11] G. Herzer; "Magnetization Process in nanocrystalline Ferro magnets"; Mat. Sci. Eng. A133, 1(1991), 1-5.

[1.12] G. Herzer; "Nanocrystalline Soft Magnetic Alloys"; in Hand Book of Materials, Vol.10ed., K. H. J. Buchow, 1997, Elsevier Pub. Co.

[1.13] M. A. Hakim and S. M. Hoque; "Effect of Structural parameters on Soft Magnetic properties of two phase nanocrystalline alloy of $Fe_{73.5}Cu_1Ta_3Si_{13.5}B_9$"; J. Magn. Magn. Mater. (JMMM), 284(2004), p.395-402.

[1.14] D. K. Saha and M. A. Hakim; "Crystallization Behavior of $Fe_{73.5}Au_1Nb_3Si_{13.5}B_9$ Amorphous nanocrystalline soft magnetic alloy"; Bangladesh Academy of Science, Vol.30, No.2(2006), p.177-187.

[1.15] S. Manjura Hoque and M. A. Hakim; "Ultra-soft magnetic properties of dvitrified $Fe_{75.5}Cu_{0.6}Nb_{2.4}Si_{13}B_{8.5}$; J. Materials Chemistry and Physics, (2007) 101, 112-117.

[1.16] R. Alben, J. J. Becker, M. C. Chi; "Random anisotropy in amorphous ferromagnets"; J. Appl. Phys. 49, 1953(1978).

[1.17] O. Ohnuma, D. H. Pins, T. Abe, H. Onodera and K. Hono; "Optimazition of the microstructure and properties of Co-substituted Fe-Si-B-Nb-Cu nanocrystalline soft magnetic alloys"; J. Appl. Phys., Vol.93, No.11, 1 june 2003, p.1986-1994.

[1.18] K. Hono, A. Inoue, T. Sakurai; Appl. Phys. Lett. 1991; 58(19): 2180.

[1.19] K. Y. Kim, T. H. Noh, Y. H. Lee, I. K. Kang, T. Kang.; J. Appl. Phys. 1993; 73:6594.

[1.20] J. D. Ayers, V. G. Harris,. J. C. Sprague, W. T. Elam; Appl. Phys. Lett. 1994; 64:974.

[1.21] J. D. Ayers, V. G. Harries, J. C. Sprague, W. T. Elam, H. N. Jones; Acta Mater. 1998; 46:1861.

[1.22] Y. Yoshizawa and K. Yamachi; Fe-based soft magnetic alloys composed of ultra fine grain structure"; Mater. Trans. JIM (1990a) 31, 307.

[1.23] T. H. Noh, M. B. Lee, H. J. Kim, I. K. Kans; "Relationship between crystallization process and magnetic properties of Fe-(Cu-Nb)-Si-B amorphous alloys"; J. Appl. Phys. (1990) 67, 5568.

[1.24] Siba Pada Mondal, M. Phil. Thesis; Department of Physics, KUET, Khulna, November 2008.

[1.25] Kazi Hanium Maria, Siba P. Mondal, Shamima Choudhury, S. S. Sikder, M. A. Hakim and D. K. Saha; "Effect of Annealing Temperature on the Soft Magnetic Properties of $Fe_{75.5}Cu_1Nb_1Si_{13.5}B_9$ Amorphous Alloys"; Journal of Emerging Trends Sciences (JETEAS) 2(1): 102-108, 2011.

[1.26] Le Minh, Bach Thanh Cong, Tran Quoc and Nguyen Chau; Proceeding of the 2nd International Workshop on Material Science (IWOMS'95), Hanoi, Oct.(1995).

[1.27] E. Estevez Rams, J. Fidler, M. Dahlgren, R. Grossinger, M. Knobel, P. Tiberto, P. Alia and F. Vinal; J. Phys. D; Appl. Phys. (1996) 29, 848-854.

[1.28] Saroaut Noor, M. Phil. Thesis; Department of Physics, KUET, Khulna, March 2005.

[1.29] Saroaut Noor, S. S. Sikder, D. K. Saha and M. A. Hakim; "Time and Temperature Dependence of Nanocrystallization and Initial Permeability of FINEMET Alloy"; Nuclear Science and Applications, Vol.15, No.1, 9-13, 2006.

[1.30] M. Müller and N. Matern; J. Magn. Magn. Mater. (1994), Vol.136, p79.

[1.31] A. Inoue, K. Kobayshi, J. Kereria and T. Masumoto: Sci. Rep. Res. Inst. Tohoku Univ. (1981), Vol.A29, p.331.

[1.32] K. Suzuki, A. Makino, N. Kataoko, A. Inoue and T. Masumoto; J. Appl. Phys. (1991), Vol.70, p.6232.

[1.33] K. Suzuki, A. Makino, A. Inoue and T. Masumoto; J. Appl. Phys. (1993), Vol.74, p.3316.

[1.34] R. N. G. Dalpaddo and K. Shirac; J. Appl. Phys. (1981) Vol.52, p.1917.

[1.35] G. Buttino, A. Ceechetti, M. Poppi and G. Zini; J. Magn. Magn.Mater. (1984), Vol.41, p.205.

[1.36] G. Herzer; IEEE Trans. Magn., (1990), MAG-26, p.1397.

[1.37] V. Fernco, C. F. Conde, A. Conde, L. F. Kiss; J. Magn. Magn. Mater. (2000), Vol.215-216, p.400.

[1.38] C. Y. Um and M. E. McHenry; "Magnetic properties of Fe-Nb-Ta-Mo-B alloys"; IEEE Transactions on Magnetics, Vol.40, No.4, July 2004.

129

Chapter – II

[2.1] P. Duwez.; J. Am Inst. Metall Eng. 1951; 191:765.

[2.2] P. Duwez, R. H. Willens and W. Klement; 1960, J. Appl. Phys. 31, 1136.

[2.3] P. Duwez; Trans. Am SOC Met. 1967; 60:607.

[2.4] P. Duwez; Ann Rev. Mat. Sci. 1967; 6:83.

[2.5] S. Mader, Nowick As.; Appl. Phys. Lett. 1965; 7:57.

[2.6] C. C. Tsuei, P. Duwez; J. Appl. Phys. 1960; 37:435.

[2.7] T. Mizoguchi; IBM Research Report, (1976) RC 6054.

[2.8] R. Alben, J. J. Budnic and G. S. Gargill; α_{111} Metallic Glasses, "American SOC for metals" (1978) pp.304.

[2.9] Y. Yoshizawa and K. Yamauchi; "Fe-based soft magnetic alloys composed of ultra-fine grain structure"; Mater. Trans. (1990a) 31, 307.

[2.10] K. Hono and T. Sakuria; "Atom probe studies of nanostructured alloys"; Appl. Surf. Sci. (1995)87/88, 166.

[2.11] Kttono, K. Hiraga, Q. Wang, A. Inoue, T. Sakurai; "The Microstructure Evolution of $Fe_{73.5}Si_{13.5}B_9Nb_3Cu_1$ nanocrystalline soft magnetic material"; Acta Metal. Mater. (1992) 40, 2137.

[2.12] K. Hono, K. Higara, Q. Wang, A. Inoue and T. Sakurai; Acta Metall. Mater. 40 2137.

[2.13] J. D. Ayers, V. G. Harris, J. A. Sprague and W. T. Elan; 1994, Appl. Phys. Lett. 64, 974.

[2.14] U. Köster, U. Schonemann, M. Blank-Bewersdroff, S. Brauer, M. Sutton and G. B. Stephenson; 1991, Mat. Sci. Eng. A133, 611.

[2.15] G. Herzer; 1991, in:Proc. of Int. Synp. Nn3d-Transition – Semi Metal Thin Films Magnetism and Processing (Japan SOC. For Promotion of Science 131 Committee, Sendai, Japan), p.130.

[2.16] Y. Yoshizawa and K. Yamauchi; 1991a, Mater. Res. SOC. Symp. Proc. 232, 183.

[2.17] M. Sorescu, C. Y. Um, M. E. McHenry, L. Diamandescu; Journal of Non-Crystalline Solids 351 (2005) 663-667.

[2.18] T. Szumiata, M. Gawronski, K. Brzozka, B. Gorka, P. Sovak, G. Pavlik; NUKLEONIKA 2007; 52 (Supplement 1):S21-S28.

[2.19] A. Altube, A. R. Pierna; "Thermal and Electrochemical Properties of Cobalt Containing FINEMET type alloys"; Electrochemical Acta 49 (2004) 303-311.

[2.20] A. Makino, A. Inoue, T. Marumoto; Mat. Trans. JIM (!995) 36, 924.

[2.21] Turnbull; IEEE Trans. Magn. (1990) 26, 1397- 1402.

[2.22] JMD Coey and H. Sun; J. Magn. Magn. Mater. (1991) 87, L251.

[2.23] M. A. Asgar; Vol.1 (1984) Mechanical Engineering Research Bulletin (BUET) 1.

Chapter – III

[3.1] W. Heisenburg; Z. Phys. 619(1928).

[3.2] D. Turnbull; Contemp. Phys. (1969) 10, 473.

[3.3] W. L. Johnson, Progress in Materials Science, (1986) 30, pp.81 – 134.

[3.4] D. Louca, K. Ahn, V. Ponnanbalam and S. J. Poon; Mat. Res. SOC Proc. Vol.754, pp. cc7.7.6(2003).

[3.5] R. Harris , M. Plischke and M. J. Zuckerman ; 1973, Phys. Rev. Lett. 31, 160.

[3.6] M. H. Chohen and D. Turnbull.; Nature, (1961) 189, 131.

[3.7] A. E. Berkowitz, J. L. Watter, K. F. Wall; "Magnetic properties of amorphous particles produced by Spark Erosion"; Phys. Rev. Lett. (1981) 46, 1484.

[3.8] H. Jones, Rep. Prog. Phys., (1973) **36** 1425.

[3.9] D. Turnbull, J. dc physique, (1974) **35** C4-1.

[3.10] S. Takayama, J. Materials Sci., (1976) **11** 164.

[3.11] J. T. S. Irvine, E. Amano, A. Huanosta, R. Valenzuela, A. R. West; "Solid State should peak at T_c" Ionic (1990) **40/41** 220.

[3.12] M. H. Cohen and D. Turnbull; Nature, (1961) **189** 131.

[3.13] G. Gargil, III; J. Appl. Phys. (1970) **41** 2248.

[3.14] H. S. Chen, Acta Met. (1974) **22** 1505.

[3.15] S. R. Nagel and J. Taue, "Nearly-Free-Electron Approach to the theory of Metallic Glass Alloys" Phys. Rev. Lett., (1975) **35** 380.

[3.16] A. E. Berkowitz, J. L. Walter, K. F. Wall, " Magnetic Properties of amorphous particles produced by Spark Erosion" Phys. Rev. Lett. (1981) **46** 1484.

[3.17] P. Murray and J. White ; "Kinetics of the thermal dehydration of clays"; Trnas. Brit. Ceram. SOC. 48(1949) 187-206.

[3.18] P. Murray and J. White ; "Kinetics of thermal decomposition of clay 2, Isothermal decomposition of clay materials"; Trna. Brit. Ceram. SOC. 54 (1955) 151-187.

[3.19] P. Murray and J. White ; "Kinetics of thermal decomposition of clay 4, Interpretation of the differential thermal analysis of clays"; Trans. Brit. Ceram. SOC. 54 (1955) 204-237.

[3.20] E. C. Sewel ; "The consequences for differential thermal analysis of assuming a reaction to be first order"; Clay Minerals Bul. 2 (1955) 233-241.

[3.21] H. E. Kissinger ; "Reaction Kinetics in Differential Thermal Analysis"; Anal. Chem. 29(11) (1957) 1702-1706.

[3.22] F. G. Boswell ; "On the calculation of activation energies using a modified Kissinger method"; J. Therm. Anal. 18(2) 1980, 353-358.

[3.23] B. D. Cullity; "Elements of X-ray diffraction" Reading, M. A; Addisonwesley, (1978).\

[3.24] G. Herzer; "Grain Size Dependence of Coercivity and Permeability of Nanocrystalline ferromagnets" IEEE Trans, Magn. (1990) **MAG-26** 1397.

[3.25] R. Alben, J. J. Becker, M. C. Chi.; "Random Anisotropy in Amorphous Ferromagnets" J. Appl. Phy. (1978) **49** 1653-1658.

[3.26] G. Bertotti, E. Ferrara, F. Fiorillo, P. Tiberto; Mat. Sci. Eng. (1997) **A, 226-228** 603.

[3.27] JMD Coey; "Rare-earth iron permanent magnets",. Oxford; Oxford Science Publications, Clearendon Press, (1996).

[3.28] G. Herzer; "Nanocrystalline Soft Magnetic Materials" J. Magn. Magn. Mater. (1996) **157/158** 133.

[3.29] A. Hernando, M. Vazquez, T. Kulik and C. Prados; "Analysis of the dependence of Spin-Spin correlations on the thermal treatment of nanocrystalline materials" Phys. Rev. B (1995) **51** 3581.

[3.30] R. Grossinger, D. Holzer, C. Ksshach, H. Sassik, R. Stao Turtelli, J. P. Sinnecker, E. Witting; J. Magan. Magan. Mater. in press.

[3.31] A. Hernando, T. Kulik; "Exchange interactions through amorphous paramagnetic layers in ferromagnetic nanocrystals" Phys. Rev. B (1994) **49** 7064.

[3.32] R. Harris, M. Plisehke, M. J. Zuckorman; "New Model for Amorphous Magnetism" Phys. Rev. Lett. (1973) **31** 160.

[3.33] R. Bozorth; "Ferromagnetism", D. Van Nostrand, Princeton N. J.) (1951) **76**.

[3.34] J. S. Kouvel ; "Magnetism and Metallurgy"; eds. A. Berkowitz and E. Kneller (Academic Press, New York, 1969) Vol.2, p.523.

[3.35] K. Handrich; "Conditions for the Existence of Amorphous Ferromagnets" Phys. Stat. Sol.(b) (1972) **53** k17.

Chapter – IV

[4.1] H. Le Chatelier; Bull SOC. France Mineral, (1987) 10, 204.

[4.2] W. B. Pearson; "A Hand book of Lattice spacing and Structures of Metals and Alloys" (Oxford Pergamon) (1958).

[4.3] A. Arrott; "Criterion for Ferromagnetism from Observations of Magnetic Isotherms"; Phys. Rev. (1957) 108, 1394.

[4.4] K. P. Belov; Magnetic Transition, Consultants Bureau (New York) (1961).

[4.5] J. S. Kouvel and M. E. Fisher; "Detailed Magnetic Behavior of Nickel near its Curie point"; Phys. Rev. (1964) 136, A1626.

[4.6] M. A. Mazid and M. A. Chowdhury; "Design and Construction of Forner type Vibrating Sample Magnetometer"; AECD/MMD/1, June, 1986 (Bangladesh).

[4.7] Simon Forner; "Versatile and Sensitive Vibrating Sample Magnetometer"; Rev. Sci. Instr. 30 (1959) 160.

Chapter – V

[5.1] W. G. Clements and B. Canter; 1976, in Rapidly quenched metal, Section-I, (eds. N. J. Graut and B. C. Giessen) (MIT Press Cambridge, Mass) p-267.

[5.2] F. E. Luborsky; Material Sci. Engg.-28 (1977), p-139.

[5.3] McHenry M. E., Willard M. A. and Laughlin D. E.; Prog. Mat. Sci. 44, 29-433 (1999).

[5.4] S. Manjura Hoque, M. A. Hakim, F. A. Khan, N. Chau ; Mat. Chem. Phys. 101, 112-117 (2007).

[5.5] D. K. Saha and M. A. Hakim.; Journal of Bangladesh Academy of Sciences; Vol.30, No.2, 177-187 (2006).

[5.6] F. F. Marzo, A. R. Pierna, A. A. Altube; "Analysis of nanocrystallization of FINEMET type alloy by temperature modulated differential scanning calorimetry"; Journal of Non-crystalline solids, 287 (2001) 349-354.

[5.7] S. S. Sikder, Ph. D. Thesis, Department of Physics, BUET, Dhaka, July 1999.

[5.8] C. L. Chen and R. S. Hasegawa; ibid (1978) 49, 1721.

[5.9] K. Moorjan, S. K. Chatak, K. V. Rao, B. Kramer and H. S. Chen; Int. Conf. on liquid and amorphous metals, Grenomle, France (1980).

[5.10] G. Herzer; "Elsevier handbook of magnetic materials"; (1997) 10, 427.

[5.11] Y. Yoshizawa, S. Oguma, K. Yamauchi; "New Fe-based soft magnetic amorphous alloys composed of ultrfine grain structure"; J. Appl. Phys. 64(10) 1988, 6044-6046.

[5.12] N. Chau, N. X. Chein, N. Q. Hoa, P. Q. Niew, N. H. Luong, N. D. Tho, V. V. Hiep; J. Magn. Magn. Mater. 282, 174-179 (2004).

[5.13] H. E. Kissinger; J. Res. Nat. Bur. Stand, 57 (1956) 217.

[5.14] Y. Yoshizawa and K. Yamachi; "Fe-based soft magnetic alloys composed of ultrfine grain structure"; Mater. Trans. JIM 31 (1990a) 307.

[5.15] T. Liu, N. Chen., Z. X. Xu, R. Z. Ma; "The amorphous to nanocrystalline transformation in $Fe_{73.5}Cu_1Nb_3Si_{13.5}B_9$ studied by thermogravimetry analysis"; J. Magn. Magn. Mater. 152 (1996) 359-364.

[5.16] S. Noor; "Effects of two-step annealing on complex permeability of Fe-Cu-Nb-Si-B nanocrystalline soft magnetic materials"; M. Phil. Thesis, March 2005, KUET, p70-72.

[5.17] T. J. Papaioannu, P. Svee, D. Janickovic, C. S. Karagianni, F. Hristoforou; "Phase transformation of Co-enhanced FINEMET amorphous ribbons based on resistance temperature measurements"; J. Optoelect Adv. Mater. 10(5) (2008) 1048-1051.

[5.18] Bozorth; "Ferromagnetism"; D. Van Norstrand Company, Inc., Princeton, NJ, 1964, p.64.

[5.19] T. Szumiata, M. Gawronski, K. Brozka, B. Gorka, P. Sovak, G. Parli.; "The influence of Co and V substitution on structural properties of FINEMET type alloys"; NUKLEONIKA 2007, 52(Supplement 1) S21-S28.

[5.20] D. Szewieczek, T. Raszka; "Structure and magnetic properties of $Fe_{63.5}Co_{10} Cu_1 Nb_3Si_{13.5}B_9$ alloy"; J. Achiev. Mater. Manf. Eng. 18(1-2) 2006, 179-182.

[5.21] W. Z. Chen, P. L. Ryder; "X-ray and differential scanning calorimetry study of amorphous $Fe_{63.5}Co_{10} Cu_1 Nb_3Si_{13.5}B_9$ alloy"; Mater. Sci. Eng. B(34) 1995, 204-209.

[5.22] J. M. Borrego, C. F. Conde, A. Cond., J. M. Greneche.; "Crystallization of Co-containing FINEMET alloys"; J. Non. Crys. Solids, 287 (2001) 120-124.

[5.23] V. Franco, C. F. Conde, A. Conde; "Changes in magnetic anisotropy distribution during structural evolution of $Fe_{76}Si_{10.5}B_{9.5}Cu_1Nb_3$"; J. Magn. Magn. Mater. 185 (1998) 353-359.

[5.24] O. Kubaschewsky; "Iron-binary phase diagrams"; Springer Verlag, Berlin, Heidelberg, N. Y., Verlag Stableign mbh. Dusseldorf (1982).

[5.25] E. F. Kneller and F. E. Luborsky; "Particle size dependence of coercivity and remanence of single domain particle"; J. Appl. Phys. 34 (1963) 656.

[5.26] G. Herzer; "Grain Size Dependence of Coercivity and Permeability in Nanocrystalline Ferromagnets"; IEEE Trans. Magn. 26 (1990) 1337.

[5.27] B. D. Cullity; "Elements of X-ray Diffraction"; Adison-Wisley Publishing Company Inc., London, England, 1959, p.262.

[5.28] M. Rubinstein, V. G. Harris and P. Lubitz; "Ferromagnetic resonance in nanocrystalline $Fe_{73.5}Cu_1Nb_3Si_{13.5}B_9$ alloy"; J. Magn. Magn. Mater. 234 (2001) 306-312.

[5.29] W. A. PHILIPS; J. Low Temp. Phys., 7, 351, 1972.

[5.30] Siba Pada Mondal; "Study of Nanocrystalline formation in FINEMET Metallic Glasses and their Magnetic Properties"; M. Phil Thesis, November 2008, KUET, p 94-100.

[5.31] I. Skorvanek, J. Kovac, J. Kotzler; Phys. Stat. Solidi(b) 236, 303-309 (2003).

[5.32] I Skorvassek, J. Kovac, J. M. Greneche; J. Phys. Condens Mater. (2000) 12, 9085.

[5.33] L. K. Varga, K. V. Rao; Nano structured materials; (1999) 12, 1157-1160.

[5.34] V. Franco, C. F. Conde, A. Conde, L. F. Kiss L; "Super paramagnetic behavior in an $Fe_{76.5}Si_{10.5}B_{9.5}Cu_1Nb_3$ alloy"; J. Magn. Magn. Mater. 215-216 (2000) 400-403.

[5.35] G. Herzer; "Nanocrystalline soft magnetic materials"; Handbook of Magn. Mater., K. H. J. Buchow (ed.), 10(1997) 415-462.

[5.36] S. Mϕrup, P. H. Christensen and B. S. Clausen; "Magnetic hyperfine splitting in super paramagnetic particles in external magnetic fields"; J. Magn. Magn. Mater. 68(1987) 160-170.

[5.37] A. Inoue, T. Masumoto; Mater. Sci. Eng. 1993; 173A:1.

[5.38] C. Appino. and F. Florillo; J. Magn. Magn. Mater.; 133, 107, 1994.

[5.39] H. Knonmuller, N. Moser and T. Reininger; Anales de FisicaB 86(1), 1990.

[5.40] G. R. Aranda, J. Gonzalez, K. Kulakowski; J. Appl. Phys. (1998) 83:6341.

[5.41] A. Lovas, L. F. Kiss, L. Balong; "Saturation magnetization and amorphous Curie point changes during the early stage of amorphous nanocrystalline transformation of a FINEMET type alloy"; J. Magn. Magn. Mater. (2000) 215-216, 463.

[5.42] A. E. Berkowitz, J. L. Walter & K. F. Wall; "Magnetic properties by spark Frosion"; Phys. Rev. Lett. (19810 46, 1484.

Publication

"The Influence of Annealing Treatment on the Exothermic behavior and Structural Properties of $(Fe_{0.95}Co_{0.05})_{73.5}Cu_1Nb_3Si_{13.5}B_9$"

Ratan K. Howlader, S. S. Sikder, D. K. Saha. M. A. Gafur & H. N. Das.

National Conference on Physics for Technology development, 27-28 December 2012, AEC, Dhaka.